Available online at www.sciencedirect.com

ScienceDirect

Journal of Magnesium and Alloys 11 (2023) 4082–4127

www.elsevier.com/locate/jma

Review

Review on friction stir welding of dissimilar magnesium and aluminum alloys: Scientometric analysis and strategies for achieving high-quality joints

Mohamed M.Z. Ahmed[a,*], Mohamed M. El-Sayed Seleman[b], Dariusz Fydrych[c], Gürel ÇAM[d]

[a] *Department of Mechanical Engineering, College of Engineering at Al Kharj, Prince Sattam Bin Abdulaziz University, Al Kharj 11942, Saudi Arabia*
[b] *Department of Metallurgical and Materials Engineering, Faculty of Petroleum and Mining Engineering, Suez University, Suez 43512, Egypt*
[c] *Faculty of Mechanical Engineering and Ship Technology, Institute of Machines and Materials Technology, Gdańsk University of Technology, Gabriela Narutowicza Street 11/12, Gdańsk 80-233, Poland*
[d] *Department of Mechanical Engineering, Iskenderun Technical University, Iskenderun, Hatay 31200, Turkiye*

Received 30 June 2023; received in revised form 28 August 2023; accepted 18 September 2023
Available online 2 November 2023

Abstract

Magnesium and aluminum alloys continually attract interest as lightweight structural materials for transport applications. However, joining these dissimilar alloys is very challenging. The main obstacle that hinders progress in dissimilar Mg-Al joining is the formation of brittle intermetallic compounds (IMCs). As a solid-state joining technique, FSW is an excellent candidate to attenuate the deleterious IMC effects in dissimilar Al-Mg joining due to the inherent low heat inputs involved in the process. However, the IMCs, namely Al_3Mg_2 and $Al_{12}Mg_{17}$ phases, have also been reported to form during Al-Mg dissimilar FSW; their amount and thickness depend on the heat input involved; thus, the weld parameters used. Since the heat dissipated in the material during the welding process significantly affects the amount of IMCs, the heat input during FSW should be kept as low as possible to control and reduce the amount of IMCs. This review aims to critically discuss and evaluate the studies conducted in the dissimilar Al/Mg FSW through a scientometric analysis and also with a focus on the strategies recently applied to enhance joint quality. The scientometric analysis showed that the main research directions in Mg/Al FSW are the technological weldability of aluminum and magnesium during FSW, structural morphology, and mechanical properties of dissimilar welded joints. Considering the scope of application of the aforementioned joints, the low share of articles dealing with environmental degradation and operational cracking is surprising. This might be attributed to the need for well-developed strategies for obtaining high-quality and sustainable joints for applications. Thus, the second part of this review is conventional, focusing mainly on the new strategies for obtaining high-quality Mg/Al joints. It can be concluded that in addition to the necessity to optimum welding parameters to suppress the excessive heat to limit the amount and thickness of IMC formed and improve the overall joint quality, strategies such as using Zn interlayer, electric current assisted FSW(EAFSW), ultrasonic vibration FSW (UVaFSW), are considered effective in the elimination, reduction, and fragmentation of the brittle IMCs.

Keywords: Friction stir welding (FSW); Al-alloys; Mg-alloys; Dissimilar material welding; Intermetallics; Weld performance.

1. Introduction

In many industrial applications, especially in the transportation sector, welding of different materials is required due to its essential advantages, such as low production cost, design flexibility, and weight savings. Friction stir welding (FSW) [1] is a method with great potential to achieve defect-free and high-quality joints, particularly in dissimilar material systems with far different mechanical and physical properties that are impossible or difficult to join with conventional fusion welding methods [1–8]. The main problem in welding differ-

* Corresponding author.
E-mail address: Moh.ahmed@psau.edu.sa (M.M.Z. Ahmed).

https://doi.org/10.1016/j.jma.2023.09.039

Table 1
The main challenges of welding Mg to Al alloy [22].

Challenges	Possible negative effect	Technical solution
The chemical activity of base metal	Difficult wetting by brazing filler metal	Halide brazing fluxes or vacuum brazing
The fast growth of oxide film Low solidus of base metals	Changes in structure and the shape of brazed parts	Short holding time or low-temperature filler metals
The joining temperature is close to solidus. Formation of the intermetallic compounds of Mg/Al	Limited tensile strength of the joint	Choose the correct welding method, welding parameters, filler metal, and assisting strategy.

ent materials stems from the different physical, chemical, and mechanical properties of the materials on both sides of the joint interface, such as melting point, thermal conductivity, high-temperature strength, density, and fluidity [9–11] This situation causes the heat generation and material flow to be asymmetrical in the FSW process as well as the asymmetry in the material flow to be higher in the joining of dissimilar materials. Therefore, while the FSW process is easily applied in different material combinations with similar physical and mechanical properties (for example, joining of different Al-alloys with each other), it is more problematic to apply when welding materials with different properties, such as welding of Al-alloy with Mg-alloy [12–19] or Al-alloy with steel [20,21]. Friction stir welding of Al-alloys with steels is currently used in the mass production of automotive structural parts. The use of this welding method for joining other different materials, such as Al-alloy/Mg-alloy or Mg-alloy/steels will further save weight in transport systems. However, for the extensive use of the FSW method in welding different material combinations, the problems of intermetallic formation and corrosion must first be overcome. When FSW is used to weld Al/Ti or Al/Fe or Cu/Al and Mg/Al dissimilar alloys, the intermetallics (IMCs) formed are quite different under different welding temperatures, and even no obvious IMCs cannot be observed, which is mainly related to not only the temperature of IMCs formation but also the welding temperature [9–11]. The parameters affecting the FSW butt joint quality are wide, starting from the material features and characteristics, the type of FSW machine used, the type of FSW method, the tool geometry, the welding parameters applied, and the strategy that can be applied to assist the FSW process as illustrated in Fig. 1(a). On the other hand, the joint quality after FSW can be determined through different levels, starting from the thermomechanical cycle conditions, the top surface quality, transverse macrograph quality, mechanical properties, microstructure, and life cycle, as illustrated in Fig. 1(b). In recent years, intensive research has been conducted on the weldability of dissimilar Mg and Al by FSW to overcome the challenges of welding Mg/Al dissimilar alloys (Table 1). Although there are some very good overview manuscripts in the open literature on the topic, vigorous attempts have been made to develop and improve joint quality through various strategies, such as external cooling and ultrasonic vibration assistance, in the recent decade. Therefore, this review aims to analyze the already published research works on Mg/Al dissimilar FSW with a main focus on the new strategies to enhance joint quality in order to find the research gap for future research works. In achieving this objective, a scientometric analysis of literature in Mg/Al dissimilar FSW is conducted in this review to provide more realistic findings regarding the research gap. Furthermore, an insight into the leading sources, authors, keywords, and articles is provided to assist researchers in reviewing the existing literature in the dissimilar Mg/Al FSW. This is followed by a conventional review of the recent strategies for achieving high-quality Mg/Al dissimilar joints.

2. Scientometric review of Mg/Al dissimilar FSW

2.1. Methodology

A global literature survey on the exact subject of this review article using the Web of Science (WOS) indexing database was conducted. In order to collect as many relevant works as possible (mainly scientific articles and conference proceedings), the search of resources was carried out with the following three browser settings: the search was not limited in time, search terms: “FSW AND Al/Mg,” “friction stir welding AND magnesium AND dissimilar” and “friction stir welding AND magnesium AND aluminum” were used. This allowed to collect a set of thematically homogeneous publications in the number of 220, 225, and 321, respectively, (total: 767 works). The data set was saved and prepared for analysis: based on the content, their thematic correctness was verified, duplicate works were removed, two works in local languages and one retracted article. The analyses of the collected data (195 papers available on April 30, 2023 directly related to the subject of dissimilar FSW of aluminum-magnesium alloys) were carried out using the tools available in WOS, in VOSviewer 1.6.16 software [23,24]. In addition, web applications available at the following addresses: https://www.jasondavies.com/wordcloud/ and https://www.datawrapper.de/maps/choropleth-map were used, as well as a Microsoft Excel spreadsheet. Articles from the dataset under consideration were cited 5615 times in 2886 publications outside this dataset.

2.2. Literature

In accordance with the publication trend for the subject area under consideration, shown in Fig. 2, until 2003, no publications were indexed on WOS. This is understandable

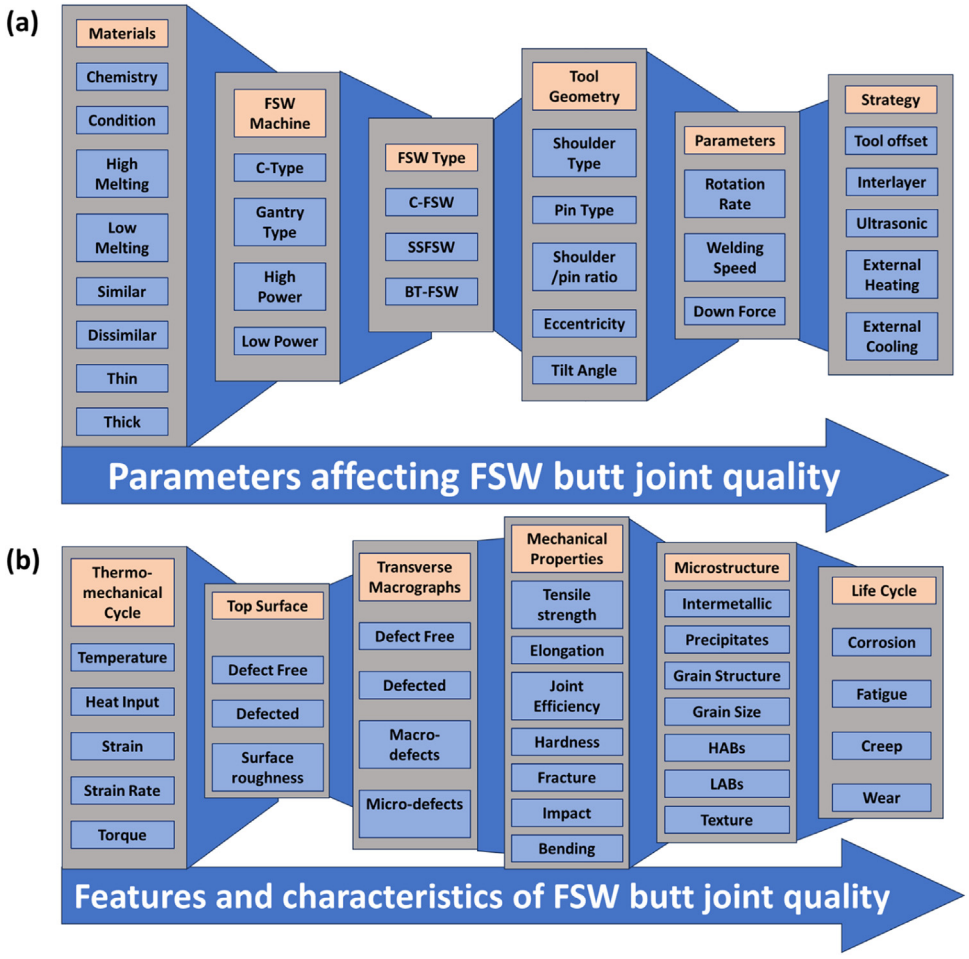

Fig. 1. Schematic flow chart of parameters affecting, features, and FSW butt joint quality characteristics. Note: C-FSW: conventional friction stir welding, SSFSW: stationary shoulder FSW, BT-FSW: bobbin tool FSW, HABs: High angle boundaries, LABs: low angle boundaries.

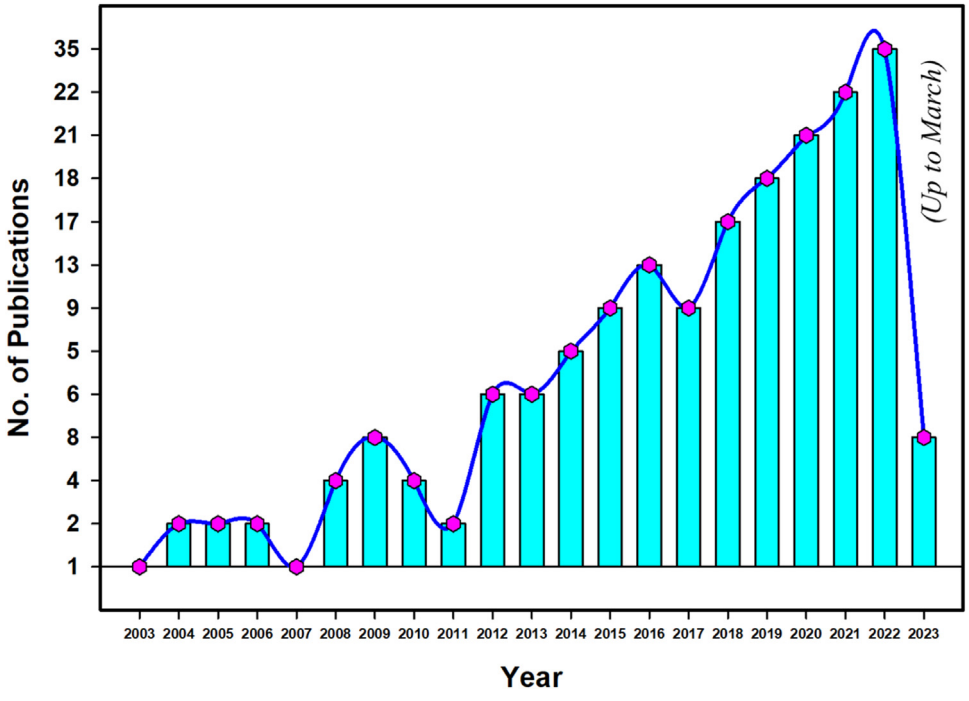

Fig. 2. Publication trend of dissimilar FSW of aluminum-magnesium alloys literature (WOS).

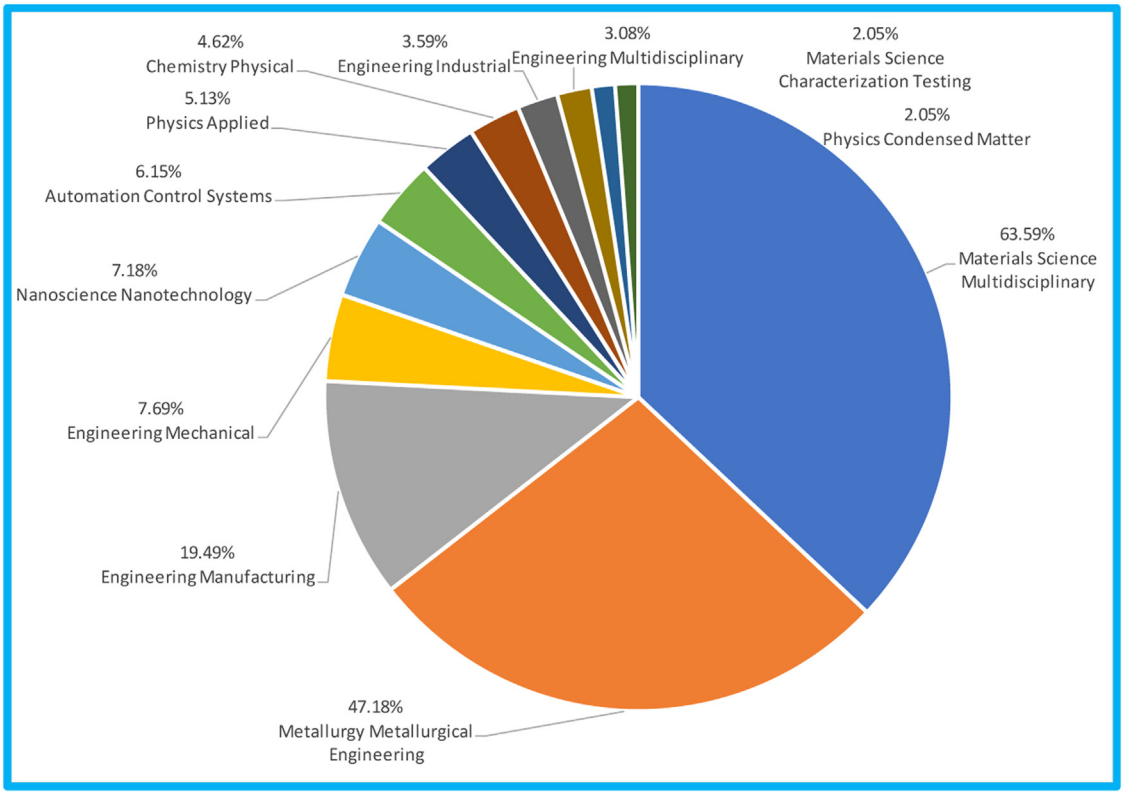

Fig. 3. Subject areas of dissimilar FSW of aluminum-magnesium alloys literature (WOS).

Table 2
Types of publications (WOS).

Publication type	publications	% of 195 publications
Article	161	82.564
Proceeding Paper	24	12.308
Review Article	14	7.179
Early Access	5	2.564

Table 3
Publication access types (WOS).

Open Acces type	publications	% of 195 publications
All Open Access	48	24.615
Gold	31	15.897
Gold-Hybrid	5	2.564
Free to Read	8	4.103
Green Published	9	4.615
Green Accepted	1	0.513
Green Submitted	7	3.59
Not specified	147	75.385

considering the novelty of the FSW subject (first patent granted in 1991). In the following years, the number of published works increased rapidly in the last five years.

Tables 2 and 3 contain a summary - information on the type and mode of access to the analyzed works listed. About 85% of the works are regular research articles. The lack of publications in the datasets type is noticeable, which can be considered as a certain limitation in the possibility of using multidimensional methods (inter alia: Data Mining techniques) for the analysis and development of the dissimilar FSW of aluminum-magnesium alloys process. Subject areas were determined based on WOS categories (Fig. 3). Since each article can be included in more than one category, percentages of categories do not add up to 100%. For better visibility, categories with less than 2% of work each (10% in total) have been omitted from the chart. Most of the publications fall into one of three categories: Materials Science Multidisciplinary (63.59%), Metallurgy Metallurgical Engineering (47.18%), and Engineering Manufacturing (19.49%). This analysis is supplemented by a bibliometric analysis of keywords in the analyzed set of publications, shown in Fig. 4. As can be seen on the word cloud (Fig. 4a), the most important keywords are arranged in the term: “dissimilar friction stir welding of aluminum and magnesium”. On the other hand, the analysis of the maps generated in VOSviewer shows that, apart from the name of the process, significant terms are related to the directions of testing welded joints: „process parameters”, „microstructure”, „tensile properties,” and „intermetallics compounds”.

2.3. Sources

The total number of journals and conference proceedings in which the analyzed papers were published is 75. The citation network is shown in Fig. 5a, while the density of relationships between each individual journal is presented in Fig. 4b. The largest numerical share have journals published by Elsevier (45.6%), Springer Nature (19.4%) and

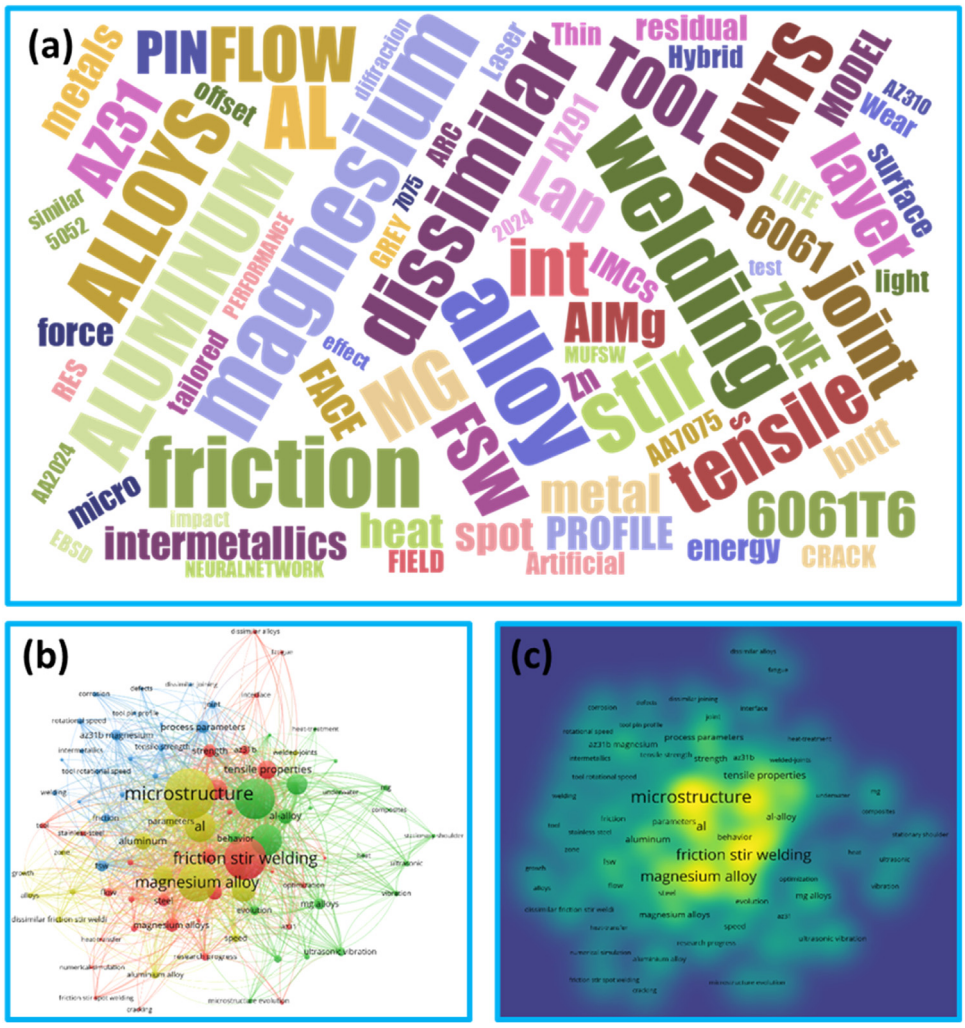

Fig. 4. Bibliometric analysis of the publications keywords: (a) wordcloud (https://www.jasondavies.com/wordcloud/), (b) keywords network (VOSviewer), (c) keywords density (VOSviewer).

Taylor&Francis (8.2%) publishing houses: Journal of Manufacturing Processes (6.6%), International Journal of Advanced Manufacturing Technology (5.6%), Materials Today Proceedings (5.6%), Science and Technology of Welding and Joining (5.1%). Table 4 contains the results of the bibliographic analysis of the most frequently selected sources in which at least three works from the examined set of 195 articles were published. These are reputable journals publishing articles on materials science, manufacturing, and processing, some strongly focused on welding technologies.

2.4. Author, organizations and countries

Out of 602 co-authors of 195 works, 17 scientists were selected who published at least 4 publications on the considered subject (Table 5 and Fig. 6) . Among the most active authors are: CS Wu, SD Ji, XC Meng, A Gerlich, L Shi and H Su. The above-average active participation of these scientists in publishing their research achievements determines the results of subsequent analyses: leading organizations, leading countries, and financing of research projects (Tables 6–9, Figs. 7–10). The leaders among authors' affiliations are organizations from China, India, Iran, USA, Canada, Germany and Japan. A map showing all 34 countries from which the authors of the papers come is shown in Fig. 9. From this group, authors from 20 countries participated at least once in international research projects. China and India are leading in this respect, which is shown in Fig. 10c.

The ten most frequently cited articles from the presented group are listed in Table 9. The paper by Sato et al. has the largest number of citations, but the review article authored by Heidarzadeh et al. has the highest citation dynamics. The interrelationships between all the articles are shown in the maps presenting the network and density of citations (Fig. 11).

2.5. Concluding remarks

Summing up the bibliometric analyzes as a technical approach, not burdened with a subjective view, it should be emphasized that the upward trend in the number of papers published in the subject of dissimilar FSW of

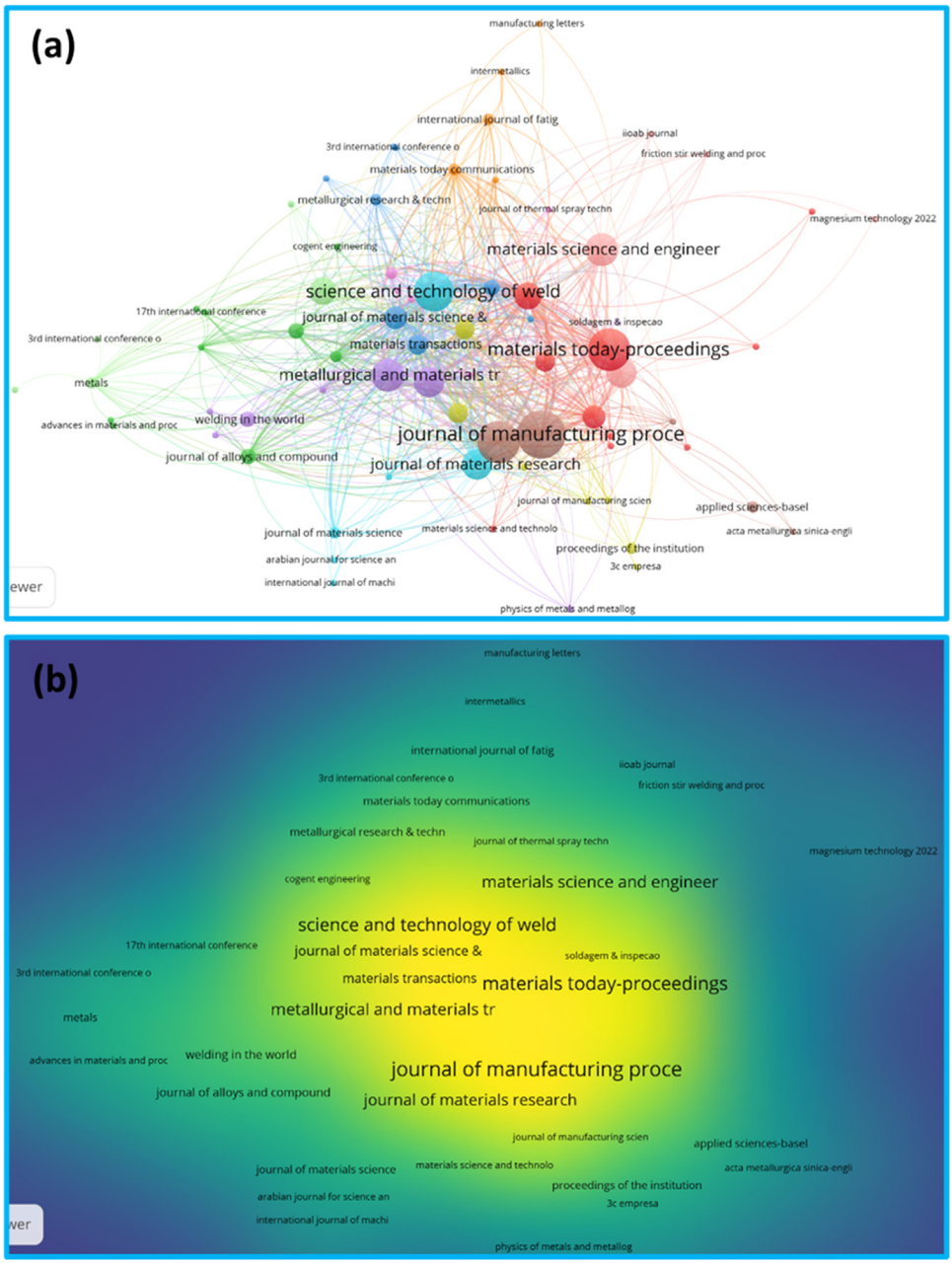

Fig. 5. Bibliometric analysis of sources of dissimilar FSW of aluminum-magnesium alloys literature: (a) sources network, (b) sources density (VOSviewer).

aluminum-magnesium alloys is strongly noticeable. The presented results of the analyzes show that the studies are performed in many countries, but several research centers obtain funding for conducting systematic and consistent research, resulting in the publication of papers in various reputable journals.

The main directions of research determined by the analysis of keywords are the research on the technological weldability of aluminum and magnesium during FSW, structural morphology and mechanical properties of dissimilar welded joints. Taking into account the scope of application of the aforementioned joints, the low share of articles dealing with environmental degradation (this applies in particular to corrosion tests) and operational cracking (this applies in particular to fatigue tests) is surprising.

The presented data show that the development of this research topic can be accelerated by intensifying efforts to conduct international projects, which favors the synergy effect.

The subject of dissimilar FSW of aluminum-magnesium alloys is very popular among authors of publications from other thematic areas. The interdisciplinary topics covered in the articles from the analyzed set may be evidenced by the fact that they are cited in works belonging to a wide spectrum of fields: materials science, metallurgy, physics, chemistry, transportation, optics, and computer science, among others.

Table 4
Leading sources of dissimilar FSW of aluminum-magnesium alloys literature (WOS).

Publication Titles	Publications	% of 195	Citations	Publisher
JOURNAL OF MANUFACTURING PROCESSES	13	6.667	253	Elsevier
INTERNATIONAL JOURNAL OF ADVANCED MANUFACTURING TECHNOLOGY	11	5.641	345	Springer Nature
MATERIALS TODAY PROCEEDINGS	11	5.641	96	Elsevier
SCIENCE AND TECHNOLOGY OF WELDING AND JOINING	10	5.128	453	Taylor&Francis
MATERIALS SCIENCE AND ENGINEERING A	8	4.103	424	Elsevier
METALLURGICAL AND MATERIALS TRANSACTIONS A	8	4.103	449	Springer Nature
JOURNAL OF MATERIALS PROCESSING TECHNOLOGY	7	3.59	365	Elsevier
JOURNAL OF MATERIALS RESEARCH AND TECHNOLOGY	7	3.59	141	Elsevier
MATERIALS DESIGN	7	3.59	626	Elsevier
JOURNAL OF MAGNESIUM AND ALLOYS	6	3.077	72	Elsevier
SCRIPTA MATERIALIA	6	3.077	246	Elsevier
JOURNAL OF MATERIALS SCIENCE TECHNOLOGY	5	2.564	122	Elsevier
TRANSACTIONS OF NONFERROUS METALS SOCIETY OF CHINA	5	2.564	86	Elsevier
JOURNAL OF MATERIALS ENGINEERING AND PERFORMANCE	4	2.051	69	Springer Nature
MATERIALS	4	2.051	23	MDPI
MATERIALS LETTERS	4	2.051	286	Elsevier
MATERIALS TRANSACTIONS	4	2.051	220	J-STAGE
JOURNAL OF ALLOYS AND COMPOUNDS	3	1.538	164	Elsevier
MATERIALS CHARACTERIZATION	3	1.538	403	Elsevier
MATERIALS RESEARCH EXPRESS	3	1.538	34	IOP Publishing
WELDING IN THE WORLD	3	1.538	5	Springer Nature

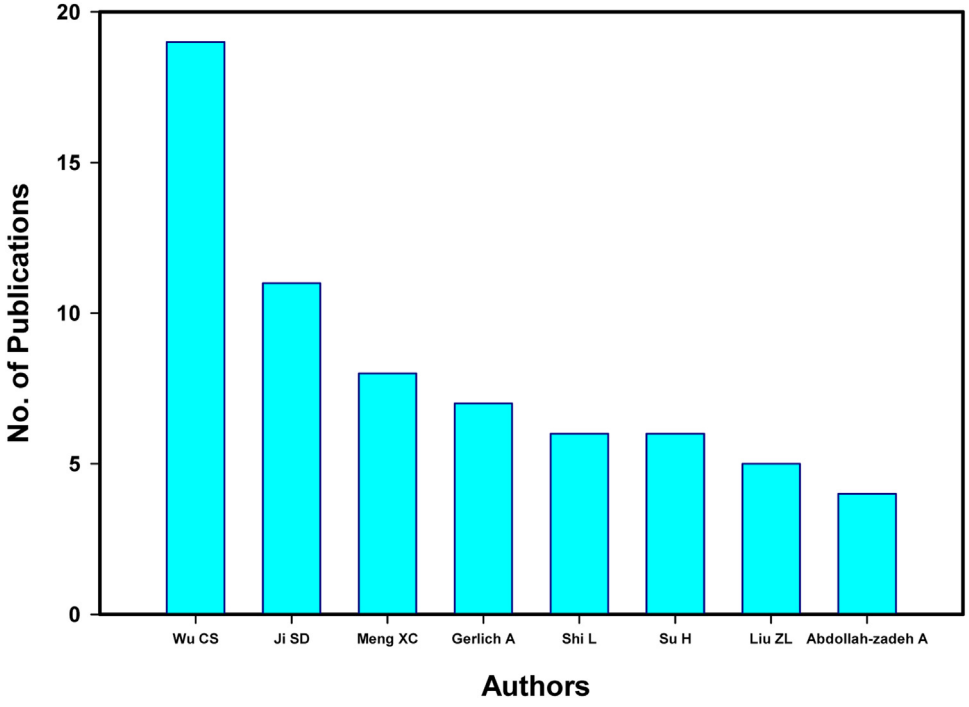

Fig. 6. Contribution of some leading authors in Al/Mg FSW literature.

3. Microstructure evolution of FSWed magnesium and aluminum alloys

3.1. Similar and dissimilar FSWed magnesium alloys

FSW of magnesium alloys results in the formation of the typical FSW characteristic features in terms of nugget zone (NG), thermo-mechanically affected zone (TMAZ), and heat affected zone (HAZ) [25–27]. The NG zone experiences a thermomechanical cycle that allows the dynamic recrystallization process to occur, which results in the formation of a new fine-grained structure [28–31]. The TMAZ also experiences a thermomechanical cycle, but it does not allow the recrystallization to occur and only results in geometrically distorted grains, mainly due to the passage of the tool with a high density of substructures [30,25]. The HAZ only experiences a thermal cycle that affects the existing precipitates based on the temper condition [30,25]. Numerous studies have investigated

Table 5
Leading authors of dissimilar FSW of aluminum-magnesium alloys literature (WOS).

Authors	Publications	% of 195	Citations
Wu CS	19	9.744	355
Ji SD	11	5.641	439
Meng XC	8	4.103	478
Gerlich A	7	3.589	793
Shi L	6	3.077	32
Su H	6	3.077	42
Liu ZL	5	2.564	240
Abdollah-zadeh A	4	2.051	380
Balasubramanian V	4	2.051	213
Kumar S	4	2.051	74
Li ZW	4	2.051	393
Reddy GPK	4	2.051	132
Sunil BR	4	2.051	132
Wagner G	4	2.051	44
Yan K	4	2.051	191
Zhao JJ	4	2.051	39
Zhao Y	4	2.051	191

the microstructure evolution during and after FSW of magnesium alloys [26,28–38]. The typical transverse macrograph of the FSWed magnesium is shown in Fig. 12. In terms of microstructure evolution during FSW, Mengran et al. [38] investigated the quasi-*in-situ* microstructure evolution during FSW of pure Mg mainly along the real flow path. They divided the FSW into five stages, stage 1 where forward compression occur after plunging and initial start of traverse, during this stage (10–12) twins and LABs, stage 2 where temperature increases and start of recovery and recrystallization occur, stage 3 and stage 4 where severe material flow and shearing occur and both continuous (CDRX) and discontinues dynamic recrystallization (DDRX) contribute in the new grain structure formation, stage 5 after the stop of material flow the annealing process took place and static recrystallization occur that results in grain growth [38]. Fig. 13 schematically illustrates the various stages they reported to occur during FSW of pure Mg and causes the microstructure evolution [38]. Mironov et al. [30] investigated the microstructure evolution during FSW of AZ31 at different rotation rates from 300 to 3000 rpm that corresponds to a range of temperatures from 0.57Tm to 0.85Tm(where Tm is the melting point of the alloy), respectively. They investigated the grain structure evolution a head of the tool from the NG to the BM as presented in Fig. 14 and their results confirmed the model proposed by Mengran et al. [38] for the microstructure evolution and schematically presented in Fig. 13. They also, reported that after FSW in the NG zone new grain structure was formed with the grains not completely delineated by a continuous HABs perimeter and the grain size found to increase by the increase of the tool rotation rate as can be seen from the grain boundary maps in Fig. 15.

The FSW of dissimilar magnesium alloys was also investigated through a number of studies [33,40,26]. Xie et al. [33] investigated the microstructure evolution of FSWed magnesium alloys ZK60 and ATZ511 of 4 mm thickness using a rotation rate of 1500 rpm and welding speed of 75 mm/min with tool pin offset to the AS by 0.15 mm. They also examined the alloy positions exchange at AS/RS, ZK60/ATZ511 joint, and the ATZ511/ZK60 joint. They observed bottom-up spiral mixing of the two dissimilar alloys by the rotating tool pin threads forming three regions within the SZ, namely SZ1, S2, and SZ3. They noted that the metal from the RS moves into the SZ1, the metal from the AS flows into the SZ2, and the two metals seem to be mixed within the SZ3. Fig. 16 shows the horizontal plane cross-section at a depth of 1.2 mm around the keyhole in (a), (b) and the transverse cross-section macrographs in (c), (d)

Table 6
Leading organizations of dissimilar FSW of aluminum-magnesium alloys literature (WOS).

No	Affiliations	Publications	% of 195	Citations
1	SHANDONG UNIVERSITY	20	10.256	411
2	NATIONAL INSTITUTE OF TECHNOLOGY NIT SYSTEM	14	7.179	289
3	SHENYANG AEROSPACE UNIVERSITY	11	5.641	439
4	HARBIN INSTITUTE OF TECHNOLOGY	9	4.615	453
5	INDIAN INSTITUTE OF TECHNOLOGY SYSTEM IIT SYSTEM	6	3.077	38
6	ISLAMIC AZAD UNIVERSITY	6	3.077	351
7	UNIVERSITY OF WATERLOO	6	3.077	698
8	AMIRKABIR UNIVERSITY OF TECHNOLOGY	5	2.564	195
9	CHONGQING UNIVERSITY	5	2.564	72
10	NANJING UNIVERSITY OF AERONAUTICS ASTRONAUTICS	5	2.564	20
11	ANNA UNIVERSITY	4	2.051	15
12	ANNAMALAI UNIVERSITY	4	2.051	213
13	HITACHI LIMITED	4	2.051	166
14	JIANGSU UNIVERSITY OF SCIENCE TECHNOLOGY	4	2.051	191
15	OSAKA UNIVERSITY	4	2.051	346
16	PANDIT DEENDAYAL ENERGY UNIVERSITY	4	2.051	123
17	RAJIV GANDHI UNIV KNOWLEDGE TECHNOL AP IIIT	4	2.051	132
18	SHANGHAI JIAO TONG UNIVERSITY	4	2.051	189
19	TARBIAT MODARES UNIVERSITY	4	2.051	380
20	UNIVERSITY OF TEHRAN	4	2.051	418
21	VIGNANA BHARATHI INST TECHNOL	4	2.051	132

Table 7
Leading countries of dissimilar FSW of aluminum-magnesium alloys literature (WOS).

Countries/Regions	Record Count	% of 195	Citations	Citations per publication
CHINA	70	35.897	2007	28.7
INDIA	50	25.641	852	17.0
IRAN	20	10.256	1307	65.4
USA	19	9.744	1296	68.2
CANADA	12	6.154	1057	88.1
GERMANY	9	4.615	415	46.1
JAPAN	9	4.615	971	107.9
ITALY	7	3.59	253	36.1
SOUTH KOREA	7	3.59	468	66.9
TURKEY	6	3.077	439	73.2
ENGLAND	4	2.051	321	80.3
RUSSIA	4	2.051	402	100.5
MALAYSIA	3	1.538	123	41.0
QATAR	3	1.538	90	30.0
SPAIN	3	1.538	108	36.0

Table 8
Leading funding agencies of dissimilar FSW of aluminum-magnesium alloys literature (WOS).

Funding Agencies	Publications	% of 195
National Natural Science Foundation Of China	46	23.59
Natural Sciences And Engineering Research Council Of Canada	6	3.077
Aeronautical Science Foundation Of China	5	2.564
Natural Science Foundation Of Liaoning Province	5	2.564
China Postdoctoral Science Foundation	4	2.051
United States Department Of Energy Doe	4	2.051
Graduate Innovation Base Laboratory Open Fund Of Nanjing University Of Aeronautics And Astronautics	3	1.538
Key R D Program Of Shandong Province In China	3	1.538
National Key Research And Development Plan	3	1.538
National Science Foundation	3	1.538
University Of Alabama	3	1.538
Wisconsin Alumni Research Foundation Warf Of The University Of Wisconsin Madison	3	1.538

Table 9
Leading documents of dissimilar FSW of aluminum-magnesium alloys literature (WOS).

Author	Title	Source	Year	Citations	Citations per year
Sato	Constitutional liquation during dissimilar friction stir welding of Al and Mg alloys	Scripta Materialia	2004	323	17.0
Heidarzadeh	Friction stir welding/processing of metals and alloys: A comprehensive review on microstructural evolution	Progress in Materials Science	2021	291	145.5
Chen	Friction stir lap joining aluminum and magnesium alloys	Scripta Materialia	2008	212	14.1
Somasekharan	Microstructure in friction-stir welded dissimiliar magnesium alloys to 6061-T6 aluminum alloy	Materials Characterization	2004	189	9.9
Zhao	Effect of Zn alloy interlayer on interface microstructure and strength of diffusion-bonded Mg-Al joints	Scripta Materialia	2008	180	12.0
Yan	Microstructure characteristics and performance of dissimilar welds between magnesium alloy and aluminum formed by friction stirring	Scripta Materialia	2005	178	9.9
Firouzdor	Al-to-Mg Friction Stir Welding: Effect of Material Position, Travel Speed, and Rotation Speed	Metallurgical and Materials Transactions A	2010	160	12.3
Kostka	Microstructure of friction stir welding of aluminium alloy to magnesium alloy	Scripta Materialia	2009	160	11.4
Fu	Friction stir welding process of dissimilar metals of 6061-T6 aluminum alloy to AZ31B magnesium alloy	Journal of Materials Processing Technology	2015	144	18.0
Kwon	Dissimilar friction stir welding between magnesium and aluminum alloys	Materials Letters	2008	144	9.6

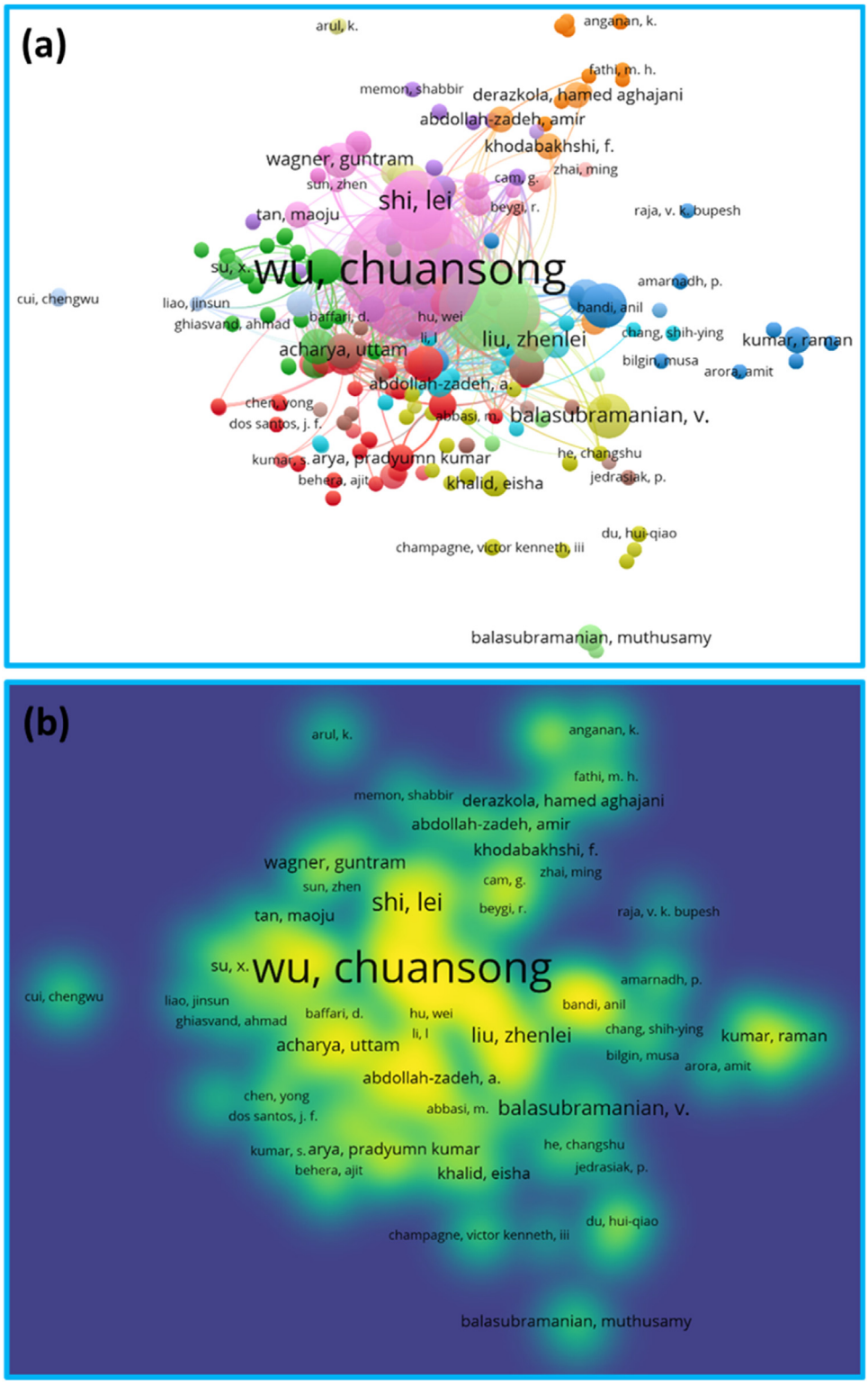

Fig. 7. Bibliometric analysis of authors of dissimilar FSW of aluminum-magnesium alloys literature: (a) authors network, (b) authors density (VOSviewer).

of the joints ZK60/ATZ511 and ATZ511/ZK60, respectively. In terms of grain structure, the starting BM average grain size was 6.36 μm and 21.53 μm for Zk60 and ATZ511, respectively. This grain size was found to be slightly increased in the case of ZK60 and significantly decreased in the case of ATZ511to be as follows for each region and joint. Joint ZK60/ATZ51, SZ1=10.67 μm, SZ2= 8.43 μm and SZ3= 6.81 μm; joint ATZ511/ZK60, SZ1=9.63 μm, SZ2= 10.82 μm and SZ3= 6.35 μm. Fig. 17 shows the optical microstructure for both joints at each subregion [33]. Similarly, Zhang

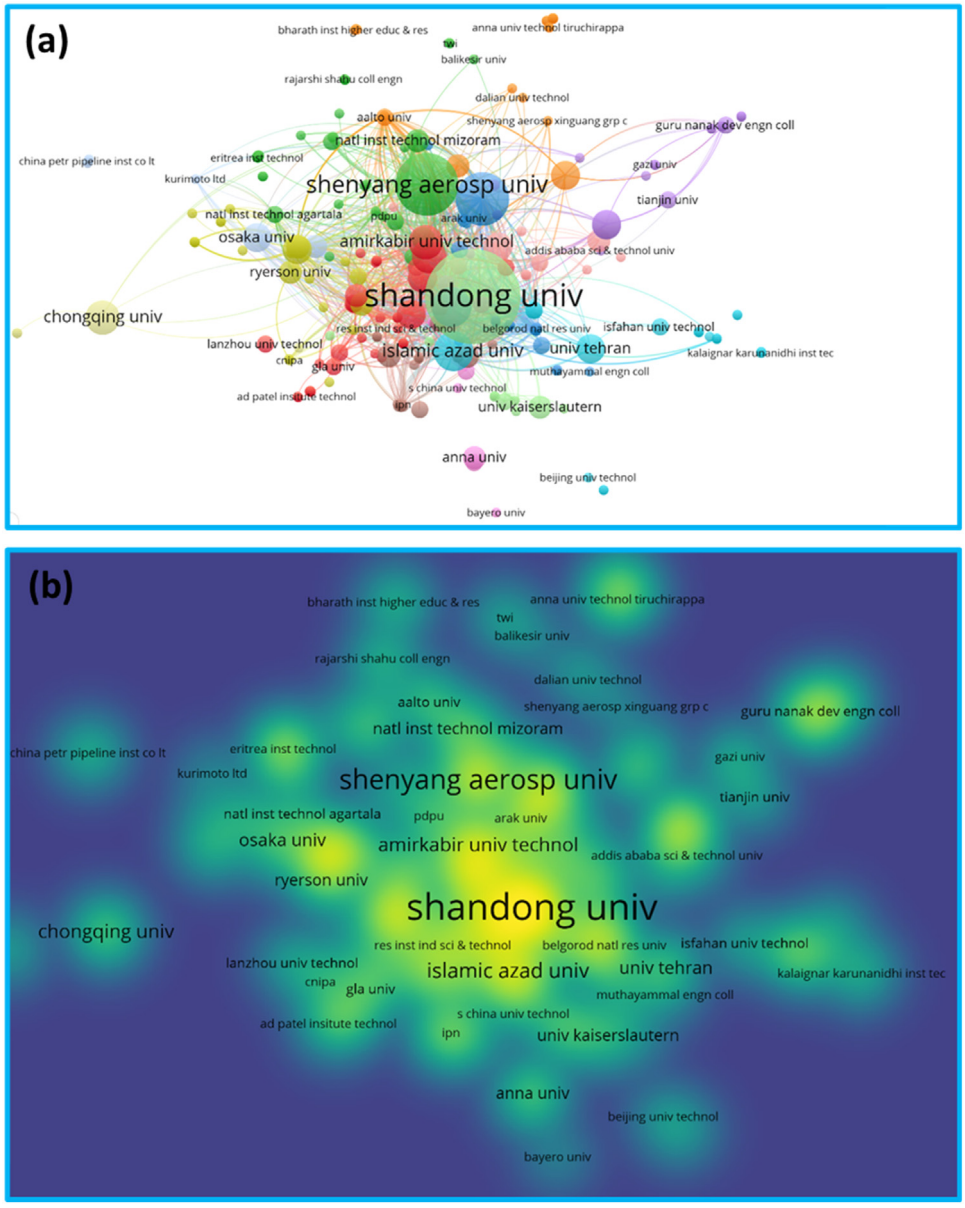

Fig. 8. Bibliometric analysis of organizations of dissimilar FSW of aluminum-magnesium alloys literature: (a) organizations network, (b) organizations density (VOSviewer).

et al. [40] investigated the microstructure evolution of dissimilar AZ31/AM60 after double-sided and stationary shoulder FSW. They also reported grain refining in the NG zone after both processes. Thus it can be concluded that the main mechanism of grain refining during FSW of similar and dissimilar magnesium alloys is the dynamic recrystallization that is driven by the severe plastic deformation at high temperatures due to the FSW tool stirring and shearing of the material. Also, the mixing of dissimilar materials can result in different subregions with different grain sizes inside the SZ.

3.2. Similar and dissimilar FSWed aluminum alloys

Two typical weld cross-sectional views are encountered in FSW of similar materials, as seen in Fig. 18. In the first of these, the weld region consists of three different zones, namely A: the onion-ring-shaped stir zone (SZ), also called the dynamic recrystallization zone (DRX), B: the thermo-mechanically affected zone (TMAZ) and C: the heat-affected zone (HAZ), Fig. 18 a) [41–46]. In this type of weld cross-section, the nugget zone (NZ) or stir zone (SZ) comprises two regions, namely the thermo-mechanically affected zone (TMAZ) and the dynamically recrystallized zone (DRX). This three-zone weld cross-section is typically formed in FSW of materials with a low recrystallization rate, such as Al-alloys. In the second weld section type given in Fig. 18(b), the weld zone consists of only two different zones, the stir zone (SZ), also called the nugget zone (NG), and the heat-affected zone (HAZ). This type of weld cross section is usually observed in FSW of materials with a high recrystallization rate. Fig. 19a

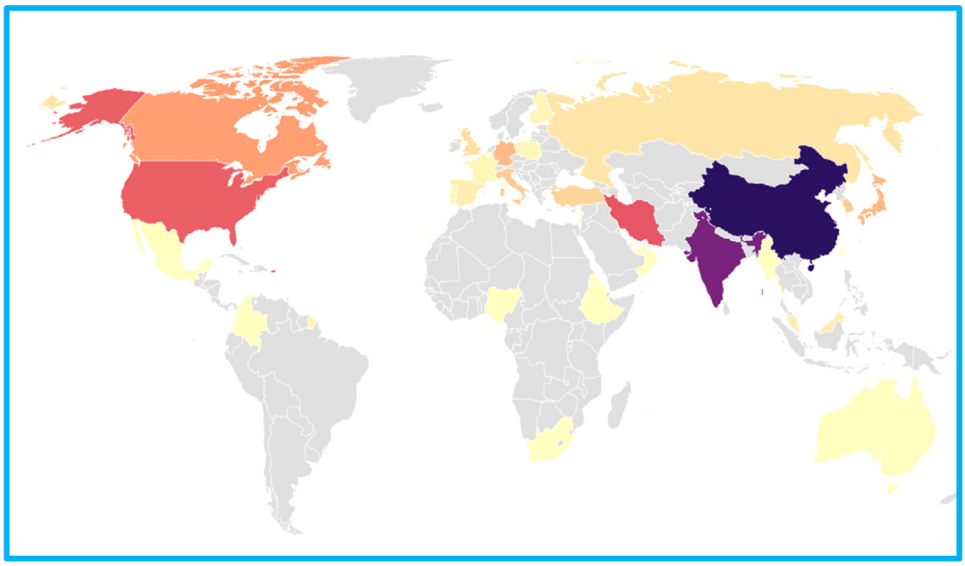

Fig. 9. Countries of dissimilar FSW of aluminum-magnesium alloys literature.

shows the typical transverse cross-section macrographs obtained after FSW of aluminum alloys with the different zones are indicated, and a longitudinal FSW macrograph obtained after stop-action FSW is shown in Fig. 19b with the temperature distribution is indicated [39]. Yazdipour et al. [47] proposed a microstructural model for microstructural evolution in AA5083, shown schematically in Fig. 20. In their microstructural model, the starting AA5083 was assumed to have coarse grains labeled 1 in Fig. 20; when it experiences hot severe plastic deformation during FSW/FSP, it starts to recover dynamically, which results in the formation of subgrain structure with a high misorientation angle labeled 2 in Fig. 20. Then, based on the temperature gradient and the second-phase particle precipitation, continuous dynamic recrystallization occurs, which results in a relatively fine and uniform grain labeled 3 in Fig. 20. Also, particle coarsening occurs in the heat affected (HAZ) labeled 4 in Fig. 20, and finally, the metadynamic recovery(MDRV) proposed to appear in the NG after leaving the FSW tool deformation zone and that results in different size grain structure based on the cooling rate labled 5 in Fig. 20. Fig. 19 shows the OIM maps across the interface of friction stir welded AA5083 welded at 400 rpm tool rotation rate and 60 mm/min welding speed showing the HAZ, TMAZ, and the NG. (a) IPF map and (b) grain boundary map with high-angle grain boundaries (HAGBs) >15 in black lines and low-angle grain boundaries (LAGBs) <15 in red lines. This microstructural evolution OIM map obtained using 0.6μm step size at the interface of FSWed AA5083 agrees well with the proposed microstructural model in terms of the grain structure of the different zones as can be noted.

Complex material movements occur in dissimilar FSW depending on the welding conditions and parameters, resulting in the formation of a complicated microstructure in the SZ. The microstructure evolving in the SZ may vary from lamellar structure [48] to complex intercalated lamellar structure (vortex-like cell structure or onion ring structure as seen in Fig. 21) with single or double cell appearance provided that a sufficient intermixing of both base materials is achieved [48–53]. When the intermixing of abutting BMs is good, then macrostructure with clearly distinguishable zones typical of similar aluminum alloy welds is obtained. In contrast, more asymmetric weld regions are observed if the intermixing is insufficient. Thus, since material flow is more critical in FSW of different materials than in the welding of similar materials, the formation of microstructure in the weld zone depends on the welding variables [54]. Guo et al. [51] investigated the effect of process parameters on the dissimilar FSW of AA7075 and AA6060. They mainly investigated the effect of welding speed (180 mm/min and 300 mm/min) and the position of different alloys at the advancing and retreating sides on the material flow and properties at a constant tool rotation rate of 1200 rpm. Fig. 22 shows the transverse cross-section macrographs where Fig. 22 (a, b) AA6061 was fixed at the RS and Fig. 22 (c,d) AA6061 was fixed at the AS. They concluded that the material mixing was much more effective when AA6061 alloy was located on the advancing side and multiple vortex centers formed vertically in the nugget. Fig. 23 shows the complex materials flow patterns (onion rings) on the top AS and RS: (a and b), and the multiple vortexes in the nugget center (c,d).

If the welding parameters are inconvenient, the base materials' intermixing is insufficient, as seen in Fig. 22a,b. On the other hand, if all welding parameters are appropriately chosen, it ensures a perfect intermixing of both base materials, and a defect-free and more symmetrical weld seam is obtained, as shown in Fig. 22c,d.

4. Microstructural evolution and properties of FSWed dissimilar Mg/Al alloys

4.1. Microstructural evolution

As mentioned before, many problems such as the formation of coarse-grained structure, brittle intermetallic com-

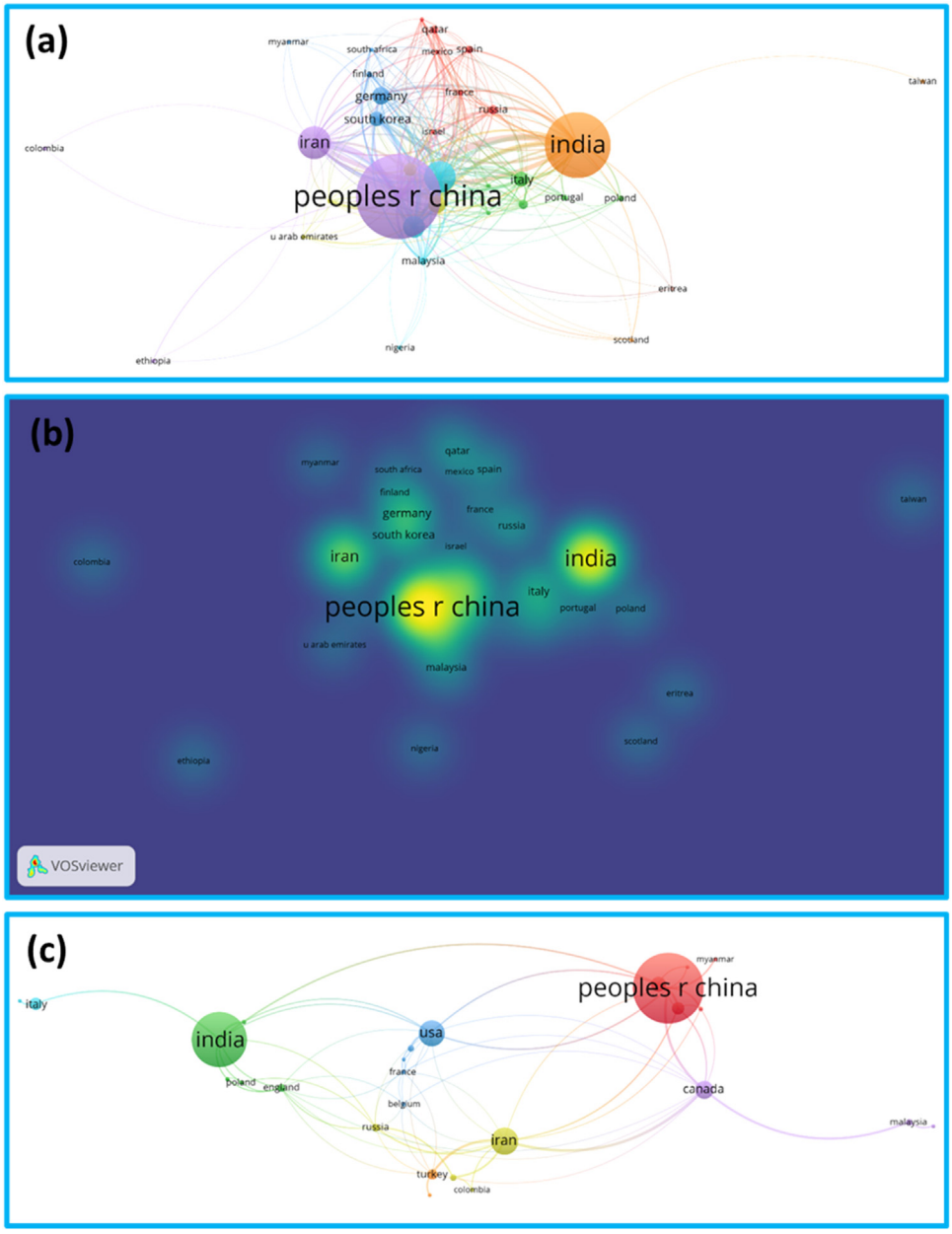

Fig. 10. Bibliometric analysis of countries of dissimilar FSW of aluminum-magnesium alloys literature: (a) countries network, (b) countries density, (c) co-authorship network (VOSviewer).

pounds and large HAZ, solidification cracks, porosity, and evaporation of alloying elements are encountered in conventional fusion welding of these two different materials [4,6,7,55–59]. The most important among these problems is the formation of brittle intermetallic compounds, which adversely affect the mechanical properties of the welded joint due to the very low solubility of these two metals in each other at room temperature [60,61]. Al_3Mg_2 and $Al_{12}Mg_{17}$ intermetallic phases (IMCs) are formed in the FSW of dissimilar Al- and Mg-alloys, and the amount and thickness of these compounds vary depending on the heat input experienced by the base materials during welding, and thus, the welding parameters used [55–57,62–69].

The FSW method, which is a solid-state welding process and therefore has a very low heat input transferred to the welded material, is a suitable welding technique to reduce and control the harmful effects of intermetallics formed in the weld zone during the welding of dissimilar Al-alloys and Mg-alloys. However, in order to keep the amount of intermetallic formed sufficiently low, welding parameters should be selected so that the heat input is as low as possible during FSW [60,70,71].

The heat input transferred to the materials in FSW of different materials depends on the welding parameters, namely the position of the plates to be welded, the diameter of the stirring tool and shoulder, the plunging location of the stirring

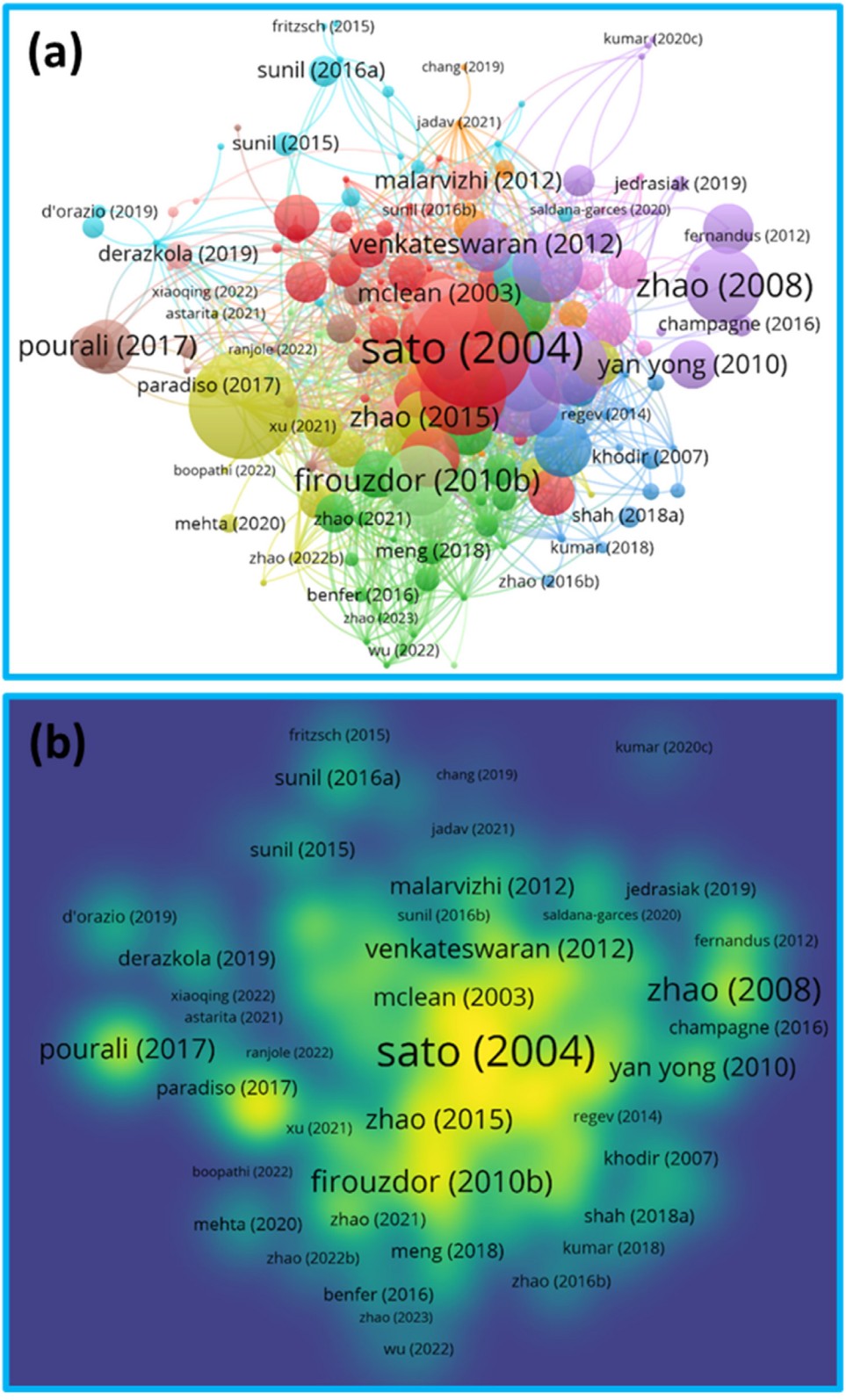

Fig. 11. Bibliometric analysis of documents of dissimilar FSW of aluminum-magnesium alloys literature: (a) documents network, (b) documents density (VOSviewer).

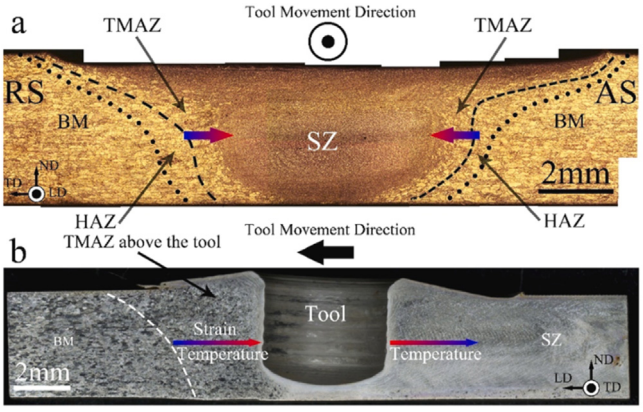

Fig. 12. (a) A typical optical cross-section of FSWed AZ31 showing SZ, TMAZ, HAZ and BM. Dotted and dashed lines show outer boundaries of TMAZ and HAZ. Colored arrows indicate gradients of temperature, strain and strain rate from low (purple) to high (red) values. (b) Optical metallograph of a longitudinal cross-section was obtained using the "stop-action" technique (pin was moving from left to right). The dotted line indicates the outer boundary of TMAZ. Colored arrows indicate gradients of temperature, strain, and strain rate from low (purple) to high (red) values [39].

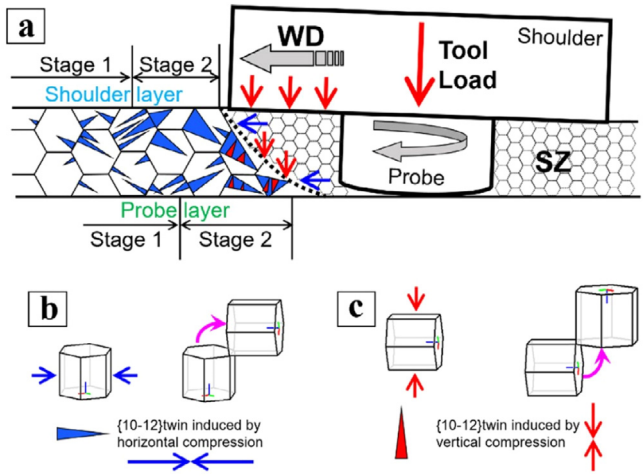

Fig. 13. (a) schematic illustration of microstructure evolution during FSW of pure Mg indicating the difference in compression stress and stages of mechanical twins formation due to (b) horizontal compression and (c) vertical compression [38].

tool with respect to the plates welded, the rotation rate, the tool traverse speed and the tool traverse speed/rotation rate, which in turn determine the Al-Mg welding interface and the weld performance. It is emphasized that FSW of unlike materials is more feasible when the harder material is placed on the advancing side. Thus, a better intermixing of the two materials is achieved in the weld zone when the Al-alloy, which generally has higher formability in FSW, is placed on the advancing side (AS) prior to welding. However, placing Al on the AS in a butt joint configuration will develop a higher heat input leading to the possibility of the formation of IMCs in the stir zone.

Thus, the heat input transferred to the materials in Al-Mg FSW can be increased by placing the Mg-alloy which has lower formability on the trailing side, and plunging the stirring tool more into the Al-alloy rather than equally sinking into the two materials. For example, Firouzdor and Kou

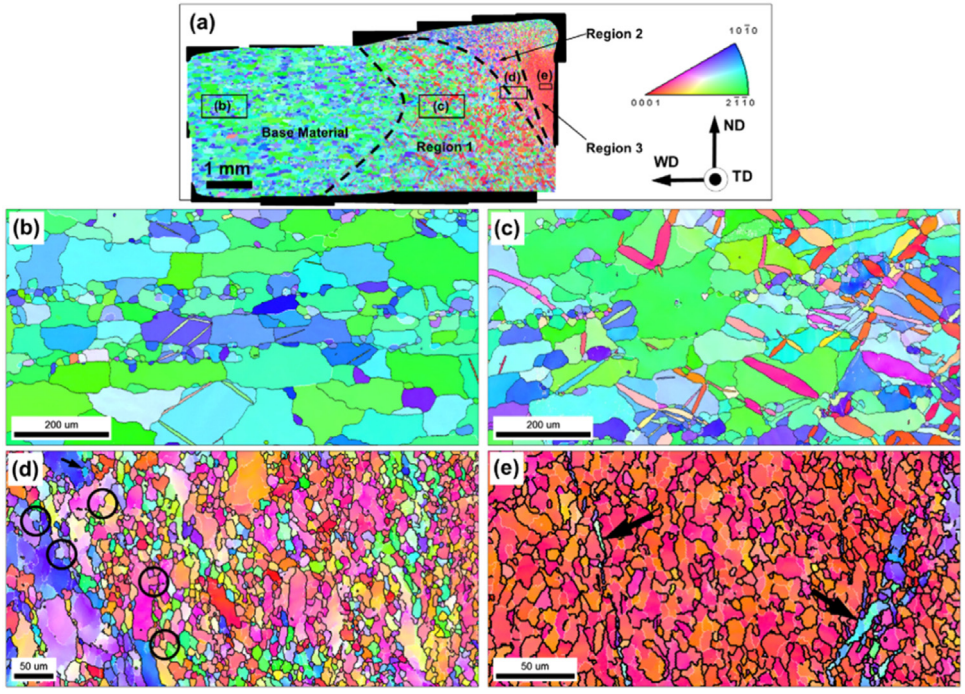

Fig. 14. Microstructure evolution at relatively high welding temperature: (a) the composite EBSD map showing grain structure developed ahead of the welding tool in the stop-action experiment with selected areas shown at higher magnifications in (b)–(e). In the map, individual grains are colored according to their crystallographic orientation relative to the WD; In (b)–(e), LABs and HABs are depicted as white and black lines, respectively. Note difference in scales [30].

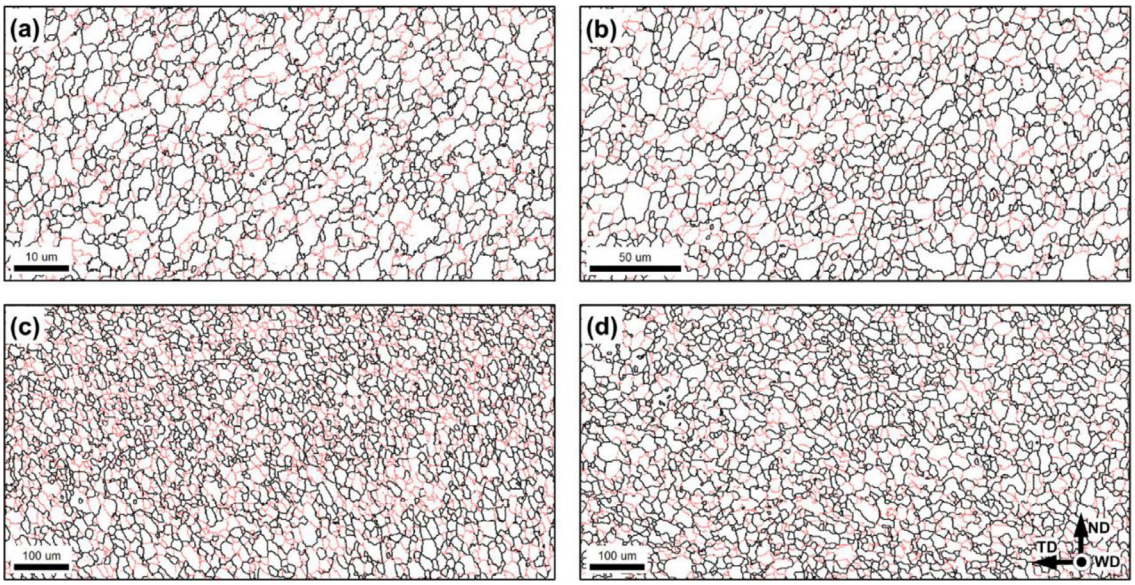

Fig. 15. EBSD grain-boundary maps with LABs in red and HABs in black lines, taken from the center of the NG zone of FSWed AZ31 at different tool rotational speeds of (a) 300 rpm (0.57Tm), (b) 1000 rpm (0.75Tm), (c) 2000 rpm (0.84Tm) and (d) 3000 rpm (0.85Tm). In the maps, respectively. Note the difference in scales [30].

[72] reported that a higher peak temperature was reached by placing the Al-alloy on the advancing side prior to FSW and penetrating the stirring tool more into the Al-alloy. Fu et al. [57] also stated that as the plunging position of the stirring tool is shifted from the interface to the Al-alloy side, the heat generated during welding increases and most of the heat generated is in the Al-alloy. However, high heat generation may lead to more intermetallic formation in the stir zone, which diminishes the joint quality. In contrast, Fu et al. [57] obtained defect-free joints by placing the Mg-alloy on the advancing side and using a tool offset on the Mg-alloy side. In this case, sufficient heat generation should be achieved by employing optimum weld parameters such as rotational rate and traverse speed. However, it should be noted that the use of more complex shaped stirring tools and shoulder profiles in FSW will facilitate material flow and thus improve the intermixing of the base materials and subsequent joint quality. As a matter of fact, stirring tools with threaded tips are often preferred to increase welding efficiency as they provide better material flow. In addition, higher rotational speed and lower tool feed rate will increase the heat input, thus ensuring defect-free joints with higher mechanical properties. Moreover, it should also be taken into account that the use of excessively high rotational rate/traverse speed ratios (also called cold welding) results in low maximum temperature and insufficient material flow, while extremely low ratios (i.e. hot welding) result in undesired material flow and more liquation, and subsequently lead to the growth and increase of the detrimental intermetallic layer within stir zone [60].

For instance, Shah et al. [60] suggested that welding parameters also affect the cross-sectional macrograph of the weld area obtained by joining Al and Mg alloys by FSW, and that the generally encountered cross-section macrographs can be divided into three groups. The cross-sectional macrographs of these different joint interfaces (Fig. 24) are called the interface with a distinct boundary (interface), also called the inclined curvilinear interface (Type I), the lamellar structure with distinct boundary, also known as the interpenetrating interface (Type II), and the complex intercalated lamellar structure also called as the interpenetrating interface with onion rings (Type III). Using unsuitable welding parameters

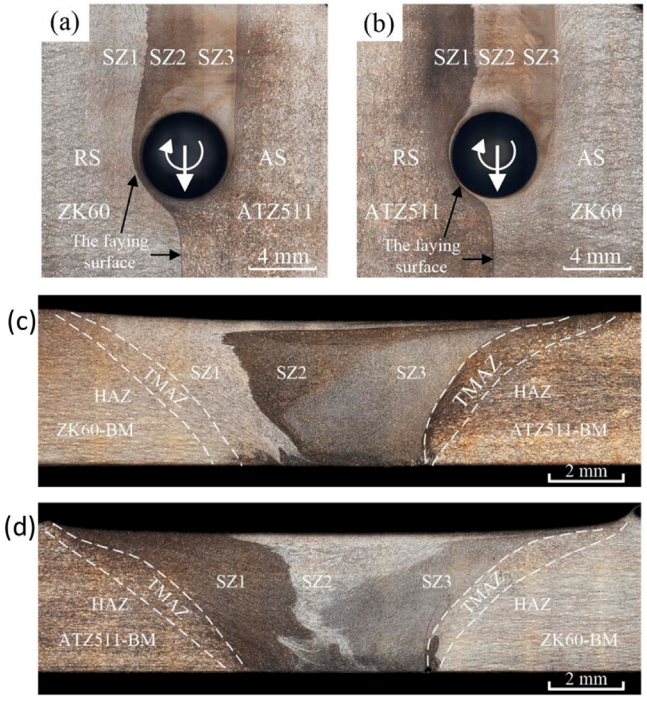

Fig. 16. (a), (b) horizontal plane cross section at a depth of 1.2 mm around the keyhole, and (c), (d) transverse cross section macrographs of the joints ZK60/ATZ511 and ATZ511/ZK60, respectively [33].

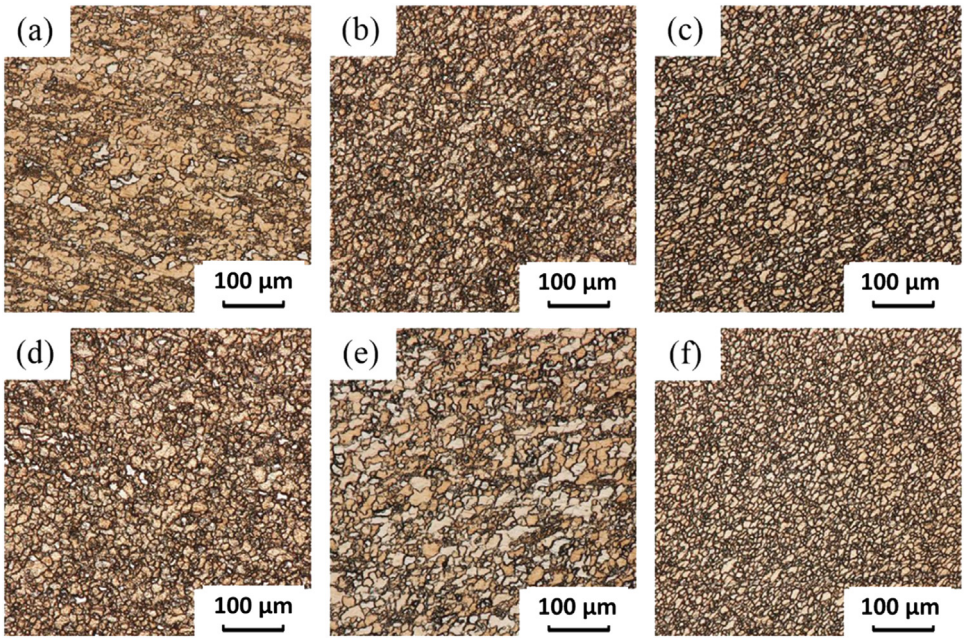

Fig. 17. Optical micrographs in various stirring sub-zones of the two welded joints:(a) SZ1, (b) SZ2, (c) SZ3 of the ZK60/ATZ511 joint; (d) SZ1, (e) SZ2, (f) SZ3 of the ATZ511/ZK60 joint [33].

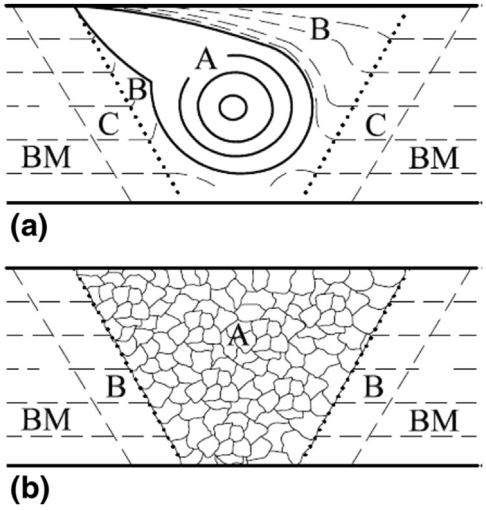

Fig. 18. Schematic representation of different weld cross-sections obtained in FSW: (a) in metals with a low recrystallization rate (eg. Al-alloys) and (b) in metals with a high recrystallization rate (for example, austenitic stainless steels or Ti-alloys). A: stir zone (SZ), B: thermo-mechanically affected zone (TMAZ), C: heat affected zone (HAZ) and BM: unaffected base material [41].

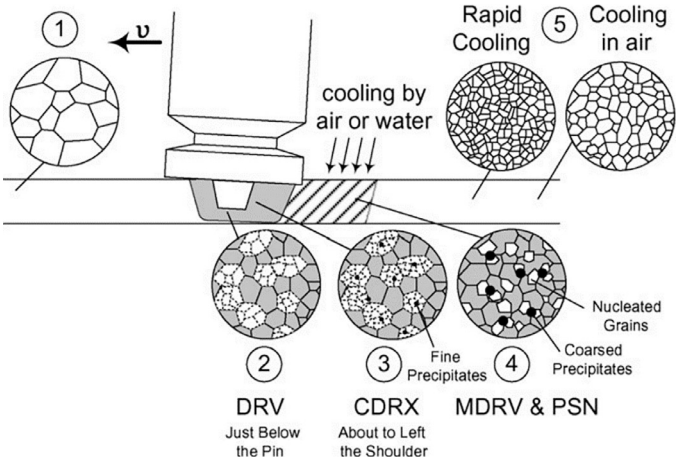

Fig. 19. Schematic of a microstructural evolution model during FSP/FSW of a coarse-grained aluminum alloy AA5083 [47].

leads to insufficient heat input, thus forming type I interfaces and a very small mixture of Al and Mg at the interface. In Al-Mg alloy joints exhibiting such an interface, fracture occurs along the joint line due to the brittle intermetallic phase density at the interface [73–76]. Among these three different cross-section structures, type III is the most preferred in terms of welding performance. This complex interface structure shows greater resistance to crack propagation than the one with a distinct boundary (Type I). As a matter of fact, Venkateswaran and Reynolds [69] conducted a detailed study of the weld cross-sectional macrostructure encountered in dissimilar FSW of Al-alloys and Mg-alloys. They also observed that three different types of weld cross-section macrostructure occur in the weld interface, such as the interface with a distinct boundary, the interpenetrating interface with a distinct boundary resembling a shape of the kidney and the interpenetrating interface with onion rings as depicted in Fig. 25.

4.2. Intermetallics formation

Intermetallics (IMCs) formation is a critical issue in the dissimilar FSW of Mg and Al alloys as it controls the joint quality and strength. Fig. 26 shows the Al-Mg binary phase

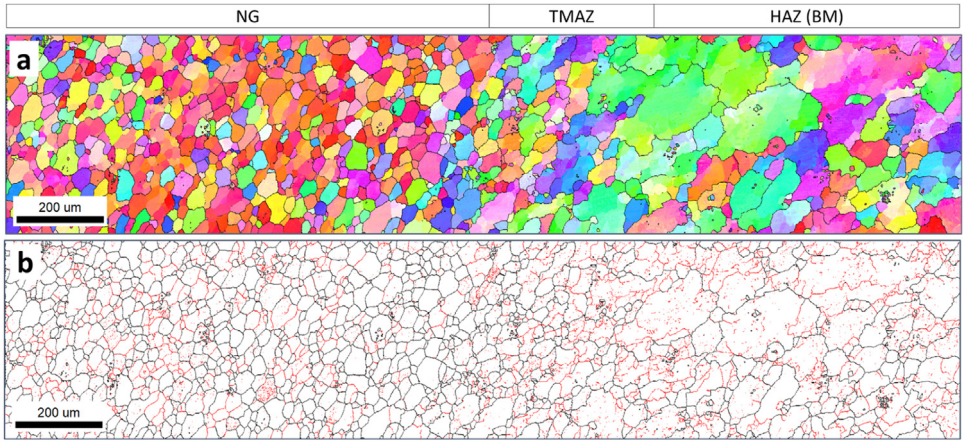

Fig. 20. OIM maps across the interface of friction stir welded AA5083 welded at 400 rpm tool rotation rate and 60 mm/min welding speed, showing the HAZ, TMAZ, and the NG. (a) IPF map and (b) grain boundary map with high-angle grain boundaries (HAGBs) >15° in black lines and low-angle grain boundaries (LAGBs) <15° in red lines.

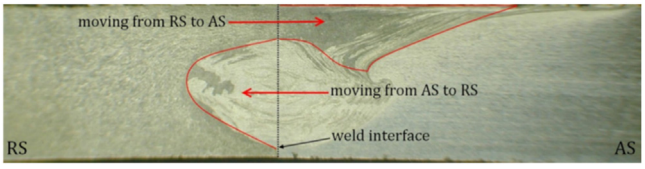

Fig. 21. Cross-sectional view of the weld zone of the dissimilar AA6061-AA7075 joint friction stir welded while the low strength AA6061 Al-alloy is on the advancing side, showing that the mixing zone is mainly composed of AA6061 alloy [48].

diagram. According to the phase diagram, two IMCs phases of Al_3Mg_2 and $Al_{12}Mg_{17}$ exist near Al and Mg, respectively. The $Al_{12}Mg_{17}$ is formed due to an eutectic reaction between Mg and $Al_{12}Mg_{17}$ at 67% Mg and at an eutectic temperature of 437 °C. This is more likely responsible for the formation of this IMCs inside the NG zone of the FSWed Mg-Al dissimilar joints [77]. Mclean et al. [77] detected the existence of $Al_{12}Mg_{17}$ IMCs with a thickness of 2.5 μm inside the NG of the FSWed AZ31B and AA5083 of 12 mm thickness. They reported that its planar shape implies that it was formed due to a divorced eutectic between $Al_{12}Mg_{17}$ and Mg. They explained that by the heat generated during FSW resulted in a temperature enough for melting and this eutectic reaction to occur [77]. They recommend avoiding the formation of these IMCs by maintaining a lower temperature below 437 °C during FSW or by using interlayer material between Mg and Al [77]. This melting might occur due to the high heat input during FSW of Mg and Al, Sato et al. [56], in their investigation of FSWed AZ31 and AA1050 they reported that constitutional liquation occurs as a result of mutual diffusion when the material is constantly held very close to the melting temperature which resulted in the formation of $Al_{12}Mg_{17}$ with large volume. Also, Kostka et al. [78] in their study of FSWed AZ31 and AA6040 of 1.5 mm thickness, they reported that IMCs layer of 1μm thickness was formed that mainly consists of fine-grained $Al_{12}Mg_{17}$ and nano-size grained Al_3Mg_2, as can be seen from Fig. 27. The crystallographic informa-

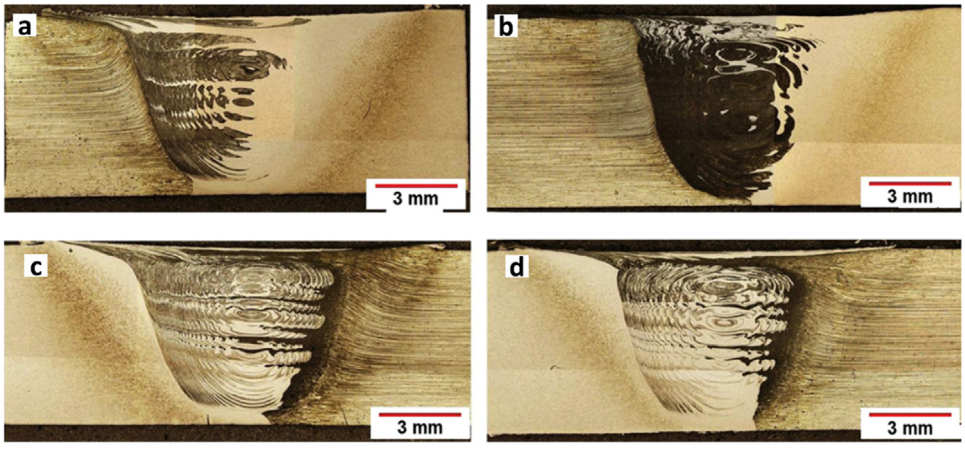

Fig. 22. Macro-graphs showing the weld cross-sections of the dissimilar AA6061/AA7075 joints produced at 1200 rpm and under different conditions: (a) AA6061 alloy is on the trailing side and the welding speed is 3 mm/s, (b) AA6061 alloy is on the trailing side and the welding speed is 5 mm/s, (c) AA7075 alloy is on the trailing side and the welding speed is 3 mm/s, and (d) AA7075 alloy is on the trailing side and the welding speed is 5 mm/s [51].

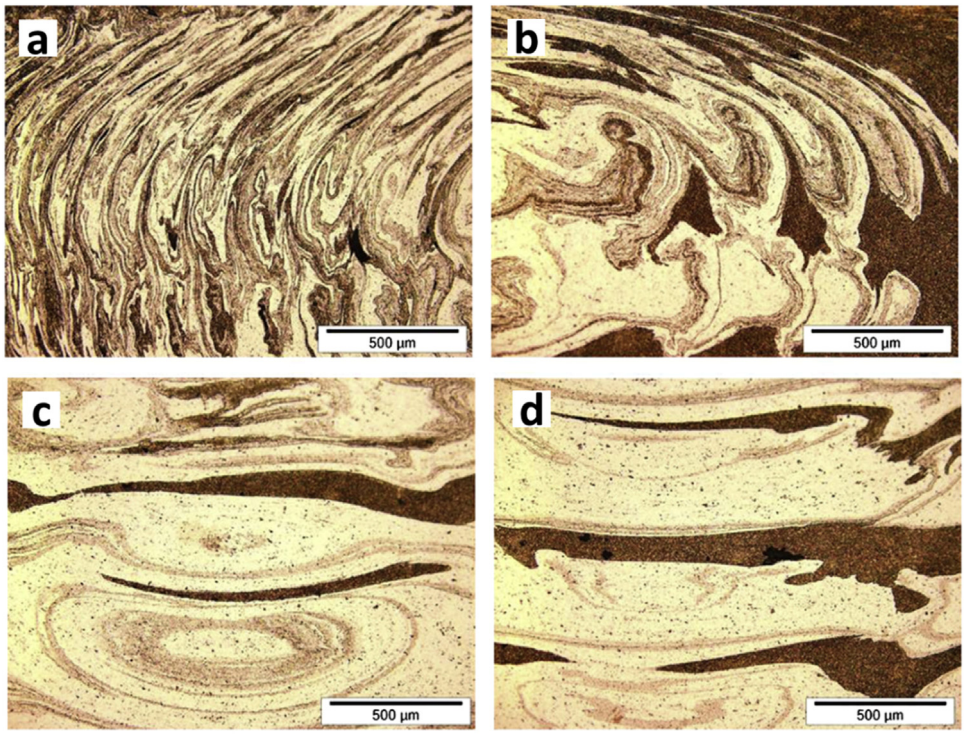

Fig. 23. Images show the complex materials flow patterns (onion rings) on the top advancing and retreating sides: (a and b), and the multiple vortexes in the nugget center: (c and d) [51].

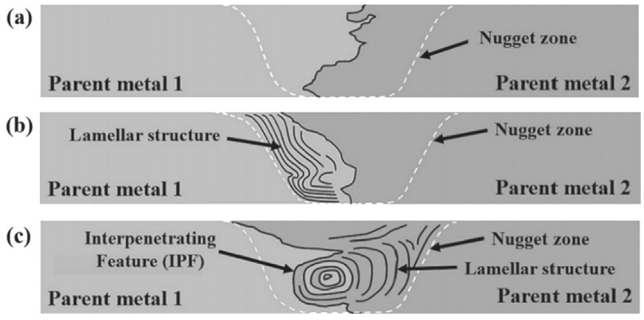

Fig. 24. Schematic illustration of the three characteristic joint macrostructures observed in the dissimilar Al-Mg joints: (a) Type I, distinct boundary, (b) Type II, lamellar structure with distinct boundary, and (c) Type III, complex intercalated lamellar structure [60].

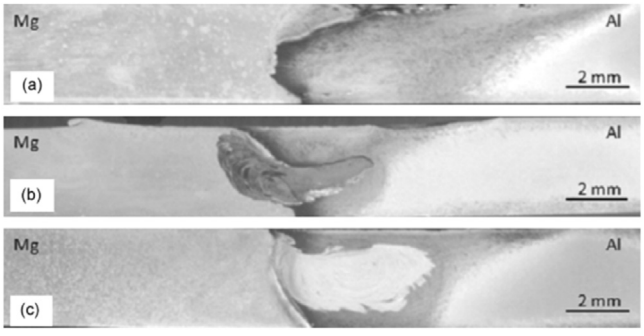

Fig. 25. Weld cross-sectional macrographs observed in FSWed AA6063/AZ31B joints: (a) the interface with a distinct boundary, (b) the interpenetrating interface with a distinct boundary resembling the shape of the kidney, and (c) the interpenetrating interface with onion rings [60].

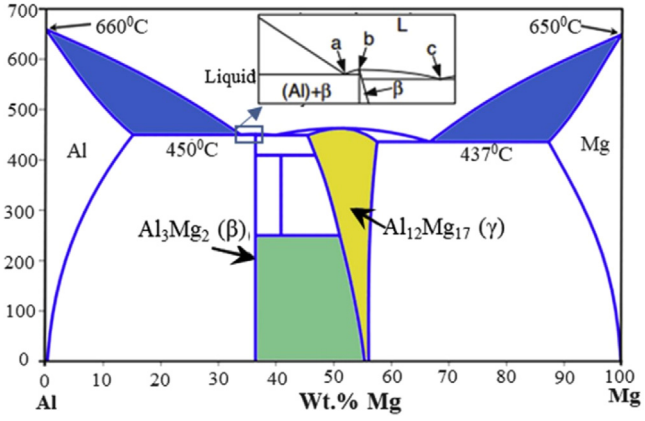

Fig. 26. Typical Al-Mg binary phase diagram [81].

tion of the Al/Mg intermetallics is given in Table 10. Also Yan et al. [79] in their investigation of FSWed AZ31 and AA1060 of 4 mm thickness, they reported the existence of both Al_3Mg_2 and $Al_{12}Mg_{17}$ IMCs in the NG and attributed the crack of the joints upon FSW to these IMCs. Recently, Xu et al. [80] tried to reduce the IMCs layer thickness during FSW of AZ31B/5A06 by using an innovative tool design to enhance the mechanical interlocking. They reported that the IMC thickness was reduced to 10 µm while they obtained a relatively low tensile strength of 32MPa maximum. This, indicates the deteriorative effect of the thick IMCs on the strength of Mg/Al joints. Thus advanced steratiges are needed to enhance the tensile strength and joint quality.

Table 10
Crystallographic information on Al/Mg intermetallic phases [78].

	Al	Mg	Al_3Mg_2	$Al_{12}Mg_{17}$
Crystal Structure	FCC	HCP	FCC	BCC
Lattice Parameters (°A)	a: 4.05	a= 3.209 c= 5.211	a= 28.23	a= 10.54

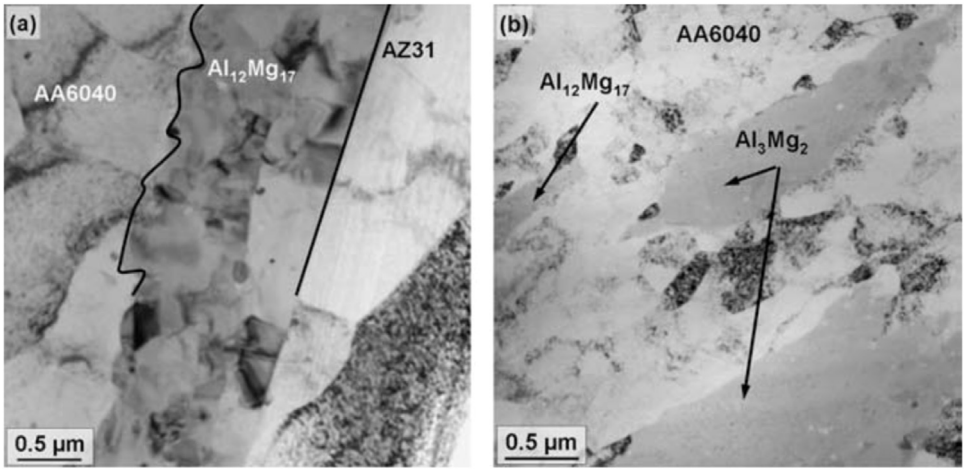

Fig. 27. TEM microstructure of inside the NG of FSWed AZ31 and AA6040 at the interface region: (a) fine-grained $Al_{12}Mg_{17}$ IMCs compound separates the AA6040 Al alloy (left) from AZ31 Mg alloy and (b) small nanosize-grained inclusions of the Al_3Mg_2 phase adjacent to the $Al_{12}Mg_{17}$ [78].

4.3. Effect of welding parameters on the properties and quality of FSWed Mg/Al joints

FSW parameters such as tool rotation rate, welding speed, and tool geometry are key parameters in the FSW process as they control the heat generated and affect the material plastic flow and mixing during the process. Especially in welding dissimilar materials, FSW parameters are more significant and crucial due to the critical issue of brittle intermetallic layers that formed between far different metallic alloys. Among dissimilar FSW of Al-alloys with other metallic materials, joining Al-alloys with Mg-alloys is easiest as several mechanical and physical properties of Al and Mg, such as hardness, melting point, etc. are similar. In the FSW of these two dissimilar alloys, tool wear is not a significant problem, so the conventional stirring tools developed for FSW of Al-alloys made of tool steels or hot worked steels (i.e. H13) can be used. However, optimum weld parameters should be employed to successfully join these dissimilar metals. In addition, several measures should be practiced to achieve a good intermixing of both base materials in the stir zone, thus obtaining a defect-free joint with acceptable properties. These precautions include the positioning of the base plates before joining and the plunging position of the stirring tool with respect to the base plates (i.e., tool offset). Numerous studies have been conducted to determine the effect of welding parameters on the quality of dissimilar Al-Mg friction stir welded joints [57,62,76,82,88]. For example, Paradiso et al. [84] observed that weld defects such as hot cracking occur in joints made with inappropriate welding parameters. On the other hand, no weld defects were observed in the AA2024 Al-alloy/ZE41Mg-alloy joints fabricated by placing the Al-alloy on the trailing side and plunging of stirring tool more into the Mg-side and employing a rotational rate of 1200 rpm and a traverse speed of 20 mm/min. Similarly, Fu et al. [57] reported that AA6061 Al-alloy and AZ31 Mg-alloy can be defect-free joined by the FSW method by placing the Mg-alloy on the advancing side and plunging the stirring tool more into the Mg-alloy, and using a rotational rate of 600–800 rpm and a weld speed of 30–60 mm/min. In addition, it was also stated that $Al_{12}Mg_{17}$ and Al_3Mg_2 intermetallic phases were formed in the stir zone, and the tensile strength of the welded joint was around 70% of the strength of the lower-strength Mg-alloy base plate. As a matter of fact, Fu et al. [57] suggested that moderate heat input values are more suitable for proper intermixing of Al and Mg-alloys and to obtain high weld quality. Yan et al. [85] also suggested that AA5052 Al-alloy and AZ31 Mg-alloy can be defect-free joined by conducting FSW at 600 rpm rotation speed and 40 mm/min tool feed rate.

Similarly, Samir and Anil [86] determined that AA6082 Al-alloy and AZ91 Mg-alloy could be defect-free welded by FSW at a rotational rate of 560 rpm and a traverse speed of 36 mm/min by placing the Al-alloy on the trailing side. It was also reported that the tensile strength of the welded joint obtained was around 72% of the strength of the AZ91 Mg-alloy base material. Masoudian et al. [87] also investigated the effects of weld parameters of AA6061 Al-alloy and AZ31 Mg-alloy on the weld quality in FSW. For this purpose, Mg-alloy was placed on the trailing side, and rotational rates of 600–1400 rpm and traverse speeds of 20–60 mm/min were used. Among these welding parameters, it was determined that a 1000 rpm rotational rate and 40 mm/min traverse speed gave

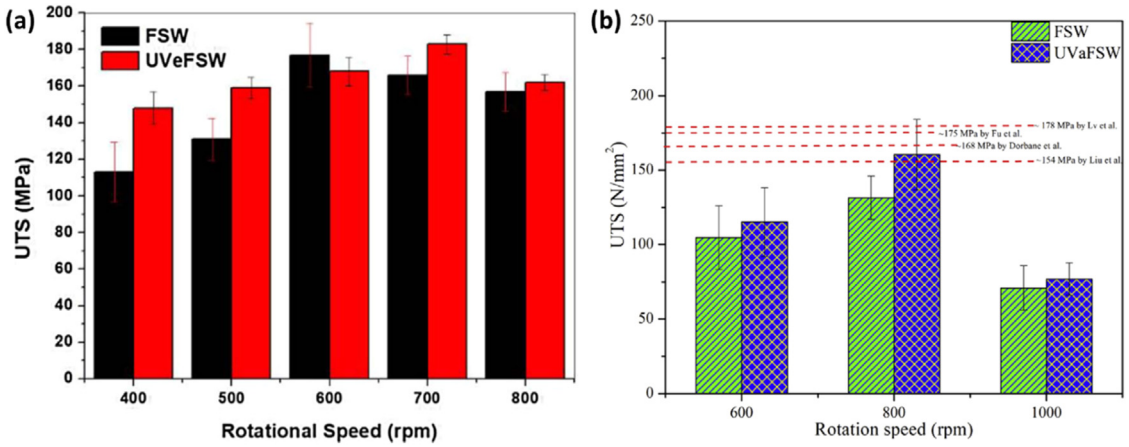

Fig. 28. (a) Tensile strengths at rotation speed range 400–800 rpm at constant welding speed of 50 mm/min of dissimilar FSWed and UVeFSWed AZ31B/AA6061-T4 joints [90] (b) Tensile strengths at rotation speed range 400–800 rpm at constant welding speed of 100 mm/min of dissimilar FSWed and UVeFSWed AZ31B/AA6061-T6 joints [81].

the best results in terms of material mixing and joint quality. In addition, grain refining and a vortex-like intercalated lamellar structure were observed in the stir zone. The highest tensile strength obtained from welded joints is 76% of the strength of the AZ31 Mg-alloy plate.

On the other hand, Malarvizhi and Balasubramanian [88] examined the effect of shoulder diameter/plate thickness ratio on the weld quality of FSWed AA6061-AZ31 dissimilar joints obtained while Al-alloy was on the trailing side at 300 rpm rotational rate and 20 mm/min traverse speed. This study revealed that while the optimum shoulder diameter/plate thickness ratio in FSW of similar materials is 3, this ratio should be 3.5 for FSW of dissimilar Al-alloy and Mg-alloy plates. This is because different materials require higher heat generation to provide the proper material intermixing in the FSW. The maximum tensile strength obtained from the welded joints fabricated by considering these conditions is 192 MPa, which corresponds to 89% of the tensile strength of the Mg-alloy base plate. Also, Simoncini and Forcellese [74] examined the effect of tool configuration using a tool with a pin and a pinless tool on the FSW of the dissimilar AA5754 and AZ31 thin sheets. They reported that the use of the pinless is critical, and sound joints using a tool were obtained, especially when placing Al in the AS and Mg in the RS. This will be discussed further in Section 4.3.3.

4.3.1. Effect of tool rotation rate

Tool rotation rate is one of the primary FSW parameters that is responsible on materials heating, flow, and mixing. Thus, it is directly affecting the joint properties and quality. It is more important to be optimized specifically in the dissimilar Mg/Al FSW. Liang et al. [89] investigated the effect of tool rotation from 600 rpm to 1000 rpm at 100 mm/nin welding speed on the dissimilar welded Mg/Al alloys. They observed that the tensile strength of the joints increases by the increase of the tool rotation rate with highest tensile of 166 MPa obtained at 1000 rpm. Also, Lv et al. [90] investigated the effect of tool rotation rate ranging from 400 to 800 rpm at a constant welding speed of 50 mm/min on the tensile properties of AZ31B/AA6061-T4 of 3 mm thickness with and without ultrasonic assistance. Fig. 28(a) shows their tensile results for the different joints. In the case of FSW, it can be noted that tensile strength increases from 110 MPa to 173 MPa by increasing the rotation speed from 400 rpm up to 600 rpm and further increase in the rotation rate to 700 and 800 rpm reduces the tensile strength again. This can be attributed to the thermal cycle experienced during the FSW process as the heat generated increases by the tool rotation rate increase, which has two effects. One is the improvement in the material flow and mixing of dissimilar materials, which enhances the tensile strength. The second one is the interdiffusion process that increases the thickness of the IMCs layer, thus reducing the tensile strength. Based on their results, it can be mentioned that the optimum FSW parameters for enhanced material mixing and minimum IMCs thickness is 600 rpm with 50 mm/min speed. Increasing the rotation rate above 600 rpm results in an enhanced interdiffusion that results in increasing the thickness of the IMCs layer. These results were confirmed by the finding of Kumar et al. [81] as they obtained almost similar results where the increase of the rotation rate from 400 rpm to 800 rpm at 100 mm/min speed increased the tensile strength from about 105 MPa up to 130 MPa in case of FSW and decreased to about 63 MPa by the increase of rotation rate to 1000 rpm Fig. 28(b). This reduction is mainly due to the increase in the IMCs layer thickness as they measured the IMCs thickness at each rotation rate and found a significant increase in the IMCs layer thickness by the increase of the rotation rate. It should be noted here that the difference in the welding speed 50 mm/min in the case of Lv et al. [90] study and 100 mm/min in the case of Kumar et al. [81] study has resulted in the increase of the optimum rotation rate to 800 rpm due to the faster welding speed. In terms of the effect of the rotation rate with the existence of ultrasonic vibration (UVaFSW) a similar trend can be noted with more increase in the tensile strength with ultrasonic vibration application. Due to the effect of UVaFSW

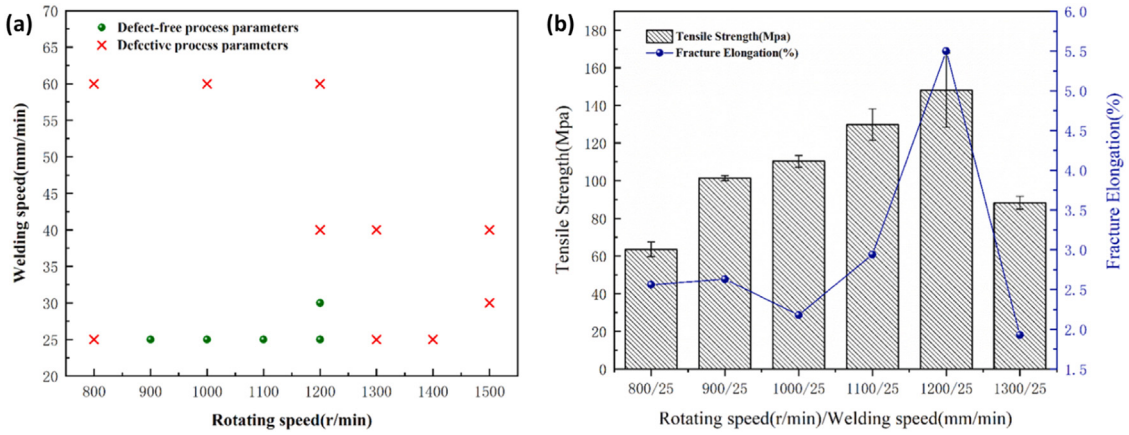

Fig. 29. (a) Conventional FSW parameters window for joining the dissimilar Mg/Al, (b) Effect of tool rotation speed on the tensile strength and elongation of the conventional FSWed dissimilar Mg/Al [91].

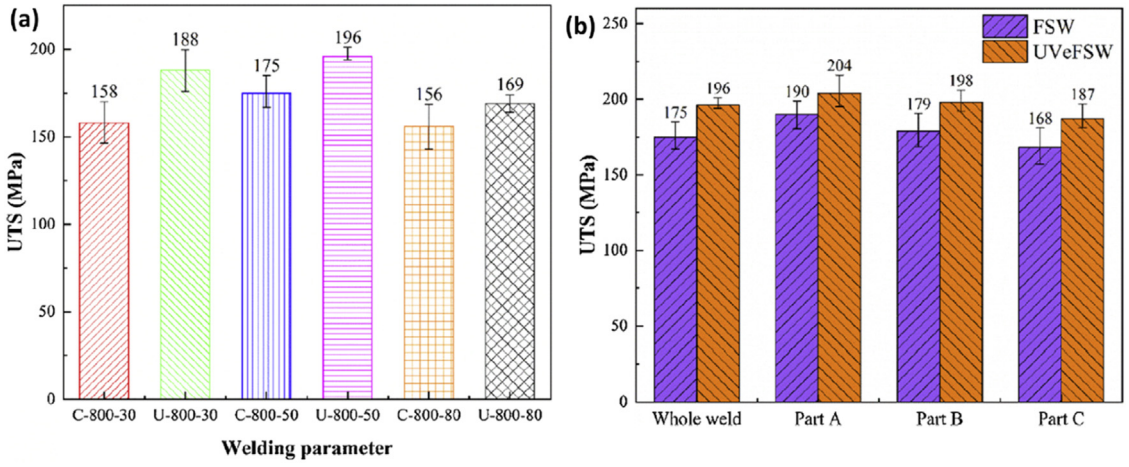

Fig. 30. Tensile strength of FSW and UVaFSW AZ31B-H24/AA6061-T6 at a constant tool rotation speed of 800 rpm at (a) different welding speeds, (b) Upper part (Part A), Middle part (Part B), lower part (Part C) for the joint 800 rpm-50 mm/min [92].

in IMCs fragmentation and reduction of thickness, the maximum tensile obtained at 700 rpm in the case of Lv et al. study [90]. Recently, Xiaoqing et al. [91] investigated the effect of a combination of FSW welding parameters on obtaining free defect joints between AZ31B/AA6061 and found that a low speed of 25 mm/min was favored at a range of rotation rates (Fig. 29a). In terms of the effect of tool rotation rate at a constant welding speed of 25 mm/min on the tensile strength and elongation, they reported that increasing the tool rotation rate up to 1200 rpm increases the tensile strength up to 162 MPa and elongation up to 5.5%, then both decreased again at 1300 rpm (Fig. 29b). It can be concluded that the tool rotation rate is one of the primary parameters that need to be optimized precisely to achieve the highest tensile strength and best joint quality.

4.3.2. Effect of welding speed

In terms of the effect of welding speed at a constant rotation rate as investigated by Zhao et al. [92]. They investigated the effect of welding speeds from 30 mm/min to 80 mm/min at a constant rotation rate of 800 rpm, and their tensile results are shown in Fig. 30. In terms of FSW, increasing the welding speed from 30 mm/min to 50 mm/min improved the tensile strength from 158 MPa to 175 MPa, then increasing from 50 mm/min to 80 mm/min has reduced the tensile strength again to 156 MPa. This can be explained by the excessive heat that resulted from the slow speed FSW, which can increase the interdiffusion and increase the thickness of the IMCs. However, increasing the speed to 80 mm/min affects the material mixing and reduces the tensile strength. In terms of the application of ultrasonic vibration, a similar trend can be noted, with a significant increase in the tensile strength in all cases relative to the FSW process. They reported that the optimum welding speed for both FSW and UVaFSW was 50 mm/min, which obtained the highest tensile strength of 175 MPa and 196 MPa, respectively, as can be observed from Fig. 30(a), and the upper part of the joint gave the highest tensile strength of 190 MPa and 204 MPa, respectively, as can be observed from Fig. 30(b). This indicates that the best effect of the ultrasonic vibration near the top surface of the joint and then the effect decreases [92]. Similarly, Kumar et al. [93] investigated the effect of the welding speed range

Table 11
Summary of materials, FSW parameters, and mechanical properties of FSWed Mg/Al alloys.

Alloys (Mg/Al), thickness (mm)	FSW parameters 1. Rotation rate, rpm 2. Welding Speed, mm/min 3. Mg Position 4. Strategy	Properties (Strategy Vs No strategy) Hardness, HV Tensile strength MPa, % Elongation	Comments	Refs.
AZ61/AA6061-T6, 3.	1. 1000, 2. 25, 3. RS 4. Zn interlayer 0.1 mm	I. 132 vs 177 II. 194 vs 148 III. 5.24 vs 2.29	Using Zn interlayer has inhibited the formation of the brittle Al-Mg IMCs and promoted the formation of MgZn and $MgZn_2$.	[108]
AZ31B/AA2024, 3	1. 700 2. 40 3. RS 4. Non**	I. NA* II. NA III. NA	Very thick layers of IMCs, Al_3Mg_2, $Al_{12}Mg_{17}$ were formed.	[18]
AZ31B-H24/AA6061-T6, 3	1. 800 2. 30–80 3. AS with 0.3 offset 4. Ultrasonic	I. NA II. NA III. NA	The use ultrasonic filed improved the degree of recrystallization	[109]
AZ31/AA6061-T6, 5	1. 550 – 600 650 2. 25 – 35 3. AS 4. Zn Interlayer 0.3 mm	I. NA II. 175 vs 140 III. 1.9 vs 0.7	The highest tensile was obtained using 600 rpm and 35 mm/min.	[110]
AZ31/AA6061-T6, 4	1. 1000 2. 250 3. RS 4. Zn interlayer 0.14 mm	I. NA II. 102 vs 80 III. NA	Al-Mg brittle IMC replaced by Mg-Zn IMCs	[111]
AZ31/ AA7075, 3	1. 1300 2. 20 3. RS, offset 0.45 to AS. 4. Cd interlayer 0.3 mm	I. 216 vs NA II. 129 vs NA III. 3.4 vs NA	Cd interlayer enhanced Tensile properties compared to similar joints without Cd in the literature.	[112]
AZ31B/AA6061-T6, 4	1. **750** 2. 20 3. AS, offset 0.3 to RS. 4. Ni interlayer 0.3 mm	I. 173 vs 153 II. 73 vs 65 III. 1 vs 0.7	Ni interlayer dose not inhibit the formation of Al-Mg brittle IMCs, 0.3 mm thickness Ni was best tensile but higher hardness.	[113]
AZ31B./AA6061-T6, 6	1. 600 2. 30, 45, 60 3. RS 4. None	I. NA II. 143 III. 0.55	The maximum tensile was obtained at speed of 45 mm/min. Complex mixing between Al and Mg was noted in all cases.	[114]
AZ31B / 5A06 Al, 20 mm	1. 375 2. 23.5 3. RS with offset 0.5 to AS. 4. Assisted external heating (220 °C)	I. 289 II. NA III. NA	The maximum hardness was 289 HV, which was on the IMC layer of the Mg side interface.	[115]
AZ31B./AA6061-T6, 6	1. 600–800 2. 8–12 3. RS 4. None	I. NA II. 104 III. NA	Optimized parameters of 600 rpm and 8 mm/min obtained the max tensile of 104 MPa.	[94]
AZ31/AA1060, 4	1. 315 2. 30 3. RS 4. Offset 4 mm to RS	I. NA II. 82.4 vs 8 III. NA	An offset of 4 mm into Mg was much more useful than into Al. Without offset, weld cracks immediately.	[72]

(*continued on next page*)

Table 11 (*continued*)

Alloys (Mg/Al), thickness (mm)	FSW parameters 1. Rotation rate, rpm 2. Welding Speed, mm/min 3. Mg Position 4. Strategy	Properties (Strategy Vs No strategy) Hardness, HV Tensile strength MPa, % Elongation	Comments	Refs.
AZ31B/AA6061, 6	1. 800 2. 70 3. AS 4. Submerged with offset of 1.1 mm to AS	I. NA II. 171 III. NA	SFSW has reduced the thickness of the IMCs and enhanced tensile strength.	[116]
AZ31B/AA6061, 3	1. 1200 2. 40 3. AS 4. SSFSW	I. 132 vs NA II. 66 vs 37 III. NA	The IMCs caused a brittle fracture to occur easily and appear at the intercalated structures.	[117]
AZ31B/ A5052-H, 3	1. 800 – 1600 2. 100 – 400 3. AS 4. None	I. 70 II. 147 III. 3.4	The best tensile was obtained at 1000 rpm and 200 mm/min with a joint efficiency of 61%.	[73]
AZ31B/AA6061, 3	1. 800 – 1500 2. 25 – 60 3. AS 4. EAFSW	I. 120 vs 160 II. 215 vs 162 III. 5 vs 2	The highest tensile of 162 MPa was obtained at 1200 rpm in FSW, and the highest tensile of 215 MPa was obtained at 900MPa and 25 mm/min in the case of EAFSW.	[91]

* NA: Not avialable,
** None: No steratgey used.

from 50 mm/min to 250 mm/min at different welding speeds. Their results showed that at the low rotation rates (400 – 600 rpm), low welding speed is required to obtain an acceptable joint; however, at high rotation rates (800 – 1200 rpm), higher welding speeds (100–150 mm/min) are required to obtain acceptable joints. This implies that both parameters are required to be optimized for the best plastic flow and mixing of dissimilar materials and, on the other hand, to keep minimum IMCs layer thickness [93,94]. Similarly, Kumara and Balasubramanian [94] investigated both rotation rate and welding speed in dissimilar FSW of AZ31 and AA6061and reached the same conclusion where at low rotation rate, low welding speed is required, and at high rotation rates, high welding speed can be used.

To summarize, two occurring effects during FSW are controlling the dissimilar Mg/Al FSWed joint quality. First is the IMCs formation and second is the material flow and mixing. Increasing the welding speed will reduce the heat input and thus reduce the interdiffusion rate and at the same time, will reduce the intermixing and material flow. This can reduce the thickness of the IMCs but also result in internal defects due to the lack of proper mixing. In contrast, reducing the welding speed will enhance the material flow and mixing; however, this will increase the heat input, raise the temperature inside the NG, and increase the IMCs layer thickness. Thus, at a constant tool rotation rate, the welding speed needs to be optimized so the proper mixing of the dissimilar materials occurs with minimum IMCs layer thickness formation. Table 11 summarizes the welded materials, FSW parameters, and the obtained mechanical properties from the literature for the dissimilar FSWed Mg/Al alloys with and without assistant strategies.

4.3.3. Effect of materials position and tool offset

Due to the difference in the physical and mechanical behavior of the dissimilar materials, their position relative to the FSW tool will affect the flow behavior, mixing of the two materials, and the heat generated. The two materials can be placed on the advancing side (AS: the side in which the tool rotation and direction of movement are similar) or on the retreating side (RS: the side where the tool rotation and direction of tool movement are opposite). Also, the FSW tool can be plunged at the centerline or offset to the AS or to the RS. Yan et al. [79] investigated the three modes of FSW tool plunging, at the centerline, 4 mm offset to the AS, and 4 mm offset to the RS during FSW of AZ31Mg/AA1060 of 4 mm thickness at a wide range of FSW parameters. They reported that regardless of the material position, the tool offset to the AS or RS has resulted in avoiding the IMCs formation and no cracks in the joint during FSW. However, having the tool at the centerline has resulted in the formation of IMCs and caused joint cracking upon FSW. They attributed this to the low heat input and temperature to a level below the eutectic reaction when using the tool offset [79]. Based on their results, the highest joint strength of 82.4 MPa (67% of AA1060 and 30% of AZ31) was obtained with the tool offset of 4 mm into Mg at the RS.

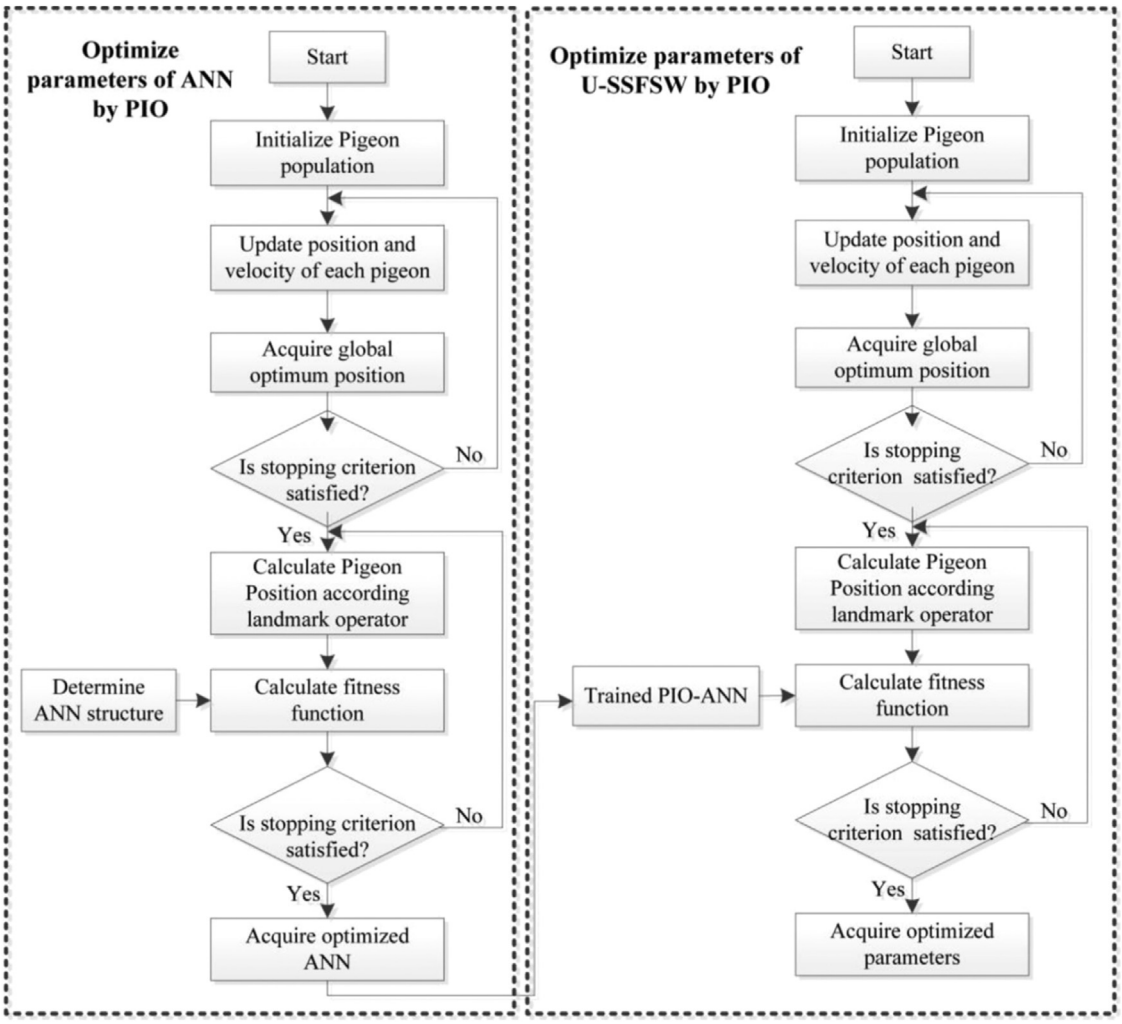

Fig. 31. Flow chart of optimization process [98].

Liang et al. [89] investigated in detail the effect of the tool offset on the weld quality of FSWed dissimilar Al-Mg joints. Their study revealed that when the Mg alloy is placed on the advancing side, a higher quality weld is obtained since lower heat input is generated, and therefore, the formation of brittle intermetallics is limited. However, it was observed that the best joint performance was exhibited by the joint obtained by plunging the stirring tool equally into the two materials with a rotational rate of 900 rpm. On the other hand, Regev et al. [95] investigated the weldability of AA6061 Al-alloy and AZ31 Mg-alloy with FSW and reported that optimum welding parameters are as follows: rotational rate 800 rpm, traverse speed 5 mm/min, plate positioning: Mg-alloy on the advancing side and tool offset on the Mg-side. Similarly, Azizieh et al. [96] conducted a recent study also demonstrated that better results were achieved in the FSW of AA1100 Al-alloy and AZ31 Mg-alloy with a tool offset on the Mg-side. It has been observed that the best tensile strength values were exhibited by the joint obtained using a rotation/feed rate ratio of 28.5 with Mg alloy placed on the advancing side. It has been suggested that the reason for this is that these welding parameters generate a maximum temperature within the eutectic reaction temperature range (430–460 °C).

To summarize the effect of the plate position and the tool offset on the welding quality, higher heat is generated during FSW when the joint is fabricated by placing the Al-alloy on the advancing side, and the tool offset on the Al side. In this case, measures should be taken to reduce the heat produced. Otherwise, more intermetallics will be formed in the stir zone, diminishing joint quality. On the other hand, when the Mg alloy is placed on the advancing side, and a tool offset on the Mg side is used, lower heat will be generated. In this case, optimum welding parameters should be used to ensure that the heat generation is sufficiently high to avoid the formation of weld defects in the stir zone. With these considerations in mind, dissimilar Al and Mg alloys can be successfully welded by FSW, using both plate positioning and with different tool offsets and without tool offsets.

4.3.4. FSW parameters optimization and properties prediction

Several machine learning algorithms can be used to optimize FSW parameters and predict FSW joint properties

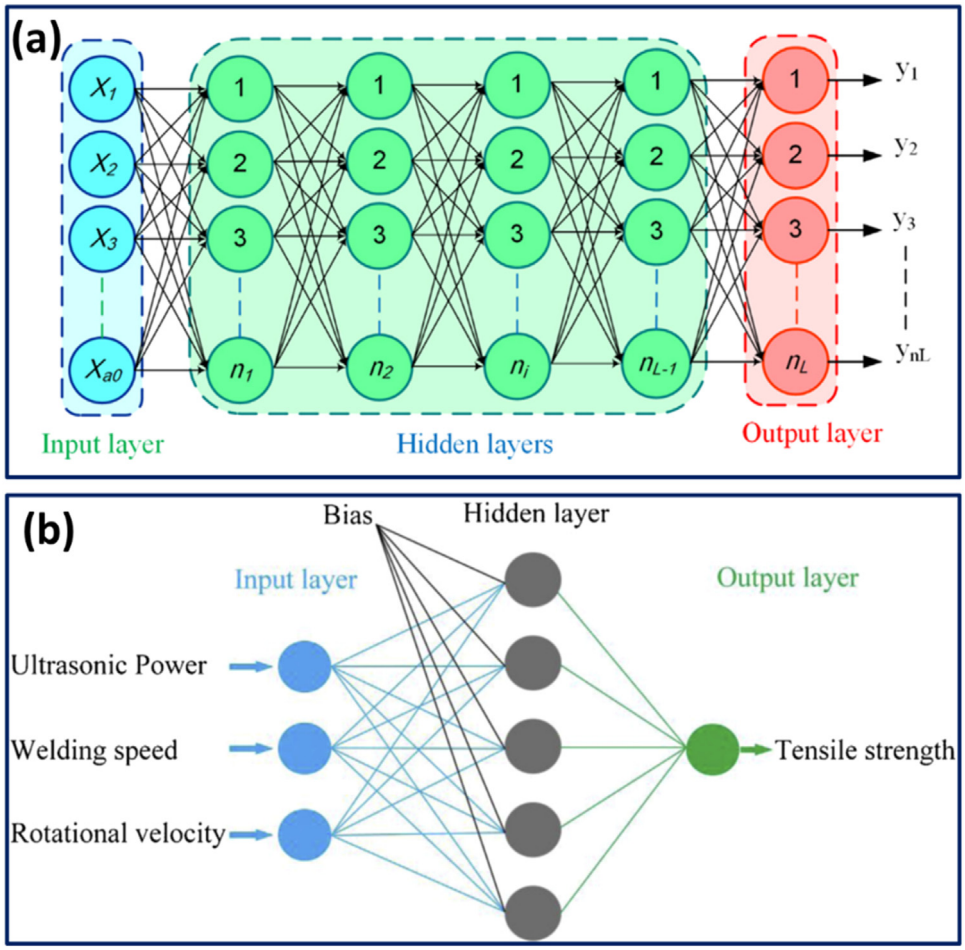

Fig. 32. (a) General structure of the ANN model [97] and (b) PIO-ANN model established [98].

[97–102]. Elsheikh [97] summarized them and briefly explained the following methods: multi-linear regression (MLR), K-nearest neighbor (KNN), random forest algorithm(RFA), Gaussian process regression(GPR), artificial neural network (RNN), support vector machine (SVM), radial basis function neural network(RBFNN), fuzzy logic (FL), adaptive neuro-fuzzy inference system(ANFIS), random vector functional link (RVFL). Several studies have used one or more of these algorithms to optimize FSW parameters and predict the FSW joint properties. Hu et al. [98] established a pigeon-inspired optimization (PIO) optimized artificial neural network (PIO-ANN) model to acquire the relationships between the inputs and output of the Al/Mg welding process by the U-SSFSW technique. Pigeon-inspired optimization (PIO) is a swarm-intelligent optimization algorithm proposed in mathematical modeling and process optimization by artificial intelligence. The flow chart of the optimization process they followed is shown in Fig. 31. For the inputs, they used the tool rotation rate, welding speed, and ultrasonic power to obtain their relation with the output, which is the tensile strength of the joints (Fig. 32). They used 80% and 20% of a wide range of data (27 sort of data) to train and test their model, respectively. The parameters covered were tool rotation (900 – 1100 rpm), welding speed (30–80 mm/min), and ultrasonic power (600–1800 W). They found the optimum input parameters from the PIO algorithm of rotation rate, welding speed, and ultrasonic power are 997 rpm, 63 mm/min, and 1426 W, respectively. The obtained joint resulted in a tensile strength of 161 MPa, the highest compared to that reported in the literature [98]. The results of the optimized U-FSWed condition are presented in Fig. 33, which clearly shows the significance of the optimization techniques in obtaining high tensile results and high-quality joints. Similarly, Dharmalingam et al. [99] optimized the FSW process parameters for welding dissimilar AZ31B /AA801 alloys using a hybrid method called an artificial neural network-based genetic algorithm (ANN-GA). They confirmed that the results obtained using the optimized parameters are highly reliable, which exhibits the optimal features of this hybrid method [99]. Similarly, Song et al. [103] have used the radial basis function neural network (RBFNN) to model the relationships between welding speed, rotating speed, and ultrasonic power as inputs and the ultimate tensile strength (UTS) as output during the ultrasonic vibration stationary shoulder FSW (U-SSFSW) of AZ31B/AA6061-T6. Also, they used the grey wolf optimization (GWO) algorithm to explore the maximum UTS and the corresponding optimal process parameters. The maximum UTS reached 158 MPa under the RBFNN-GWO system optimized process parameters, weld-

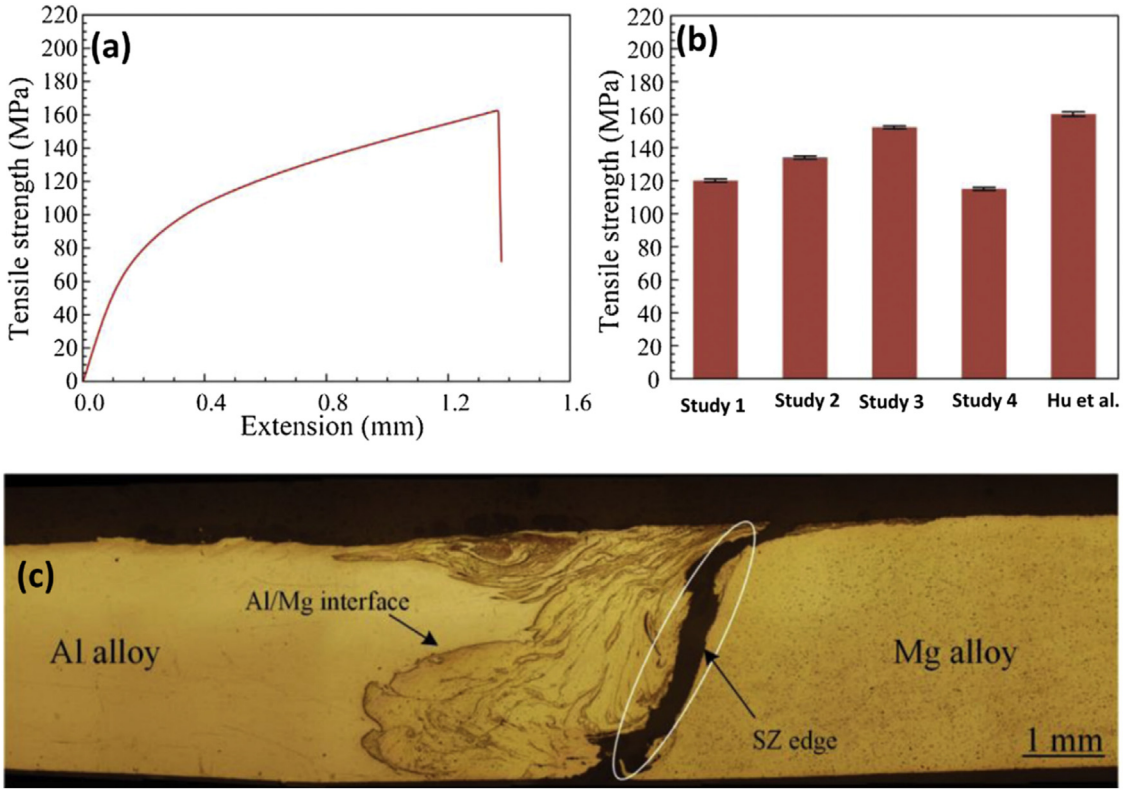

Fig. 33. (a) Tensile curve of U-SSFSWed ZA31/ AA6061-T6, (b) Comparison of Hu et al. [98] results with that reported in the literature. Study 1 [104], study 2 [105], study 3 [106], study 4 [107], and (c) transverse macrograph showing fracture location [98].

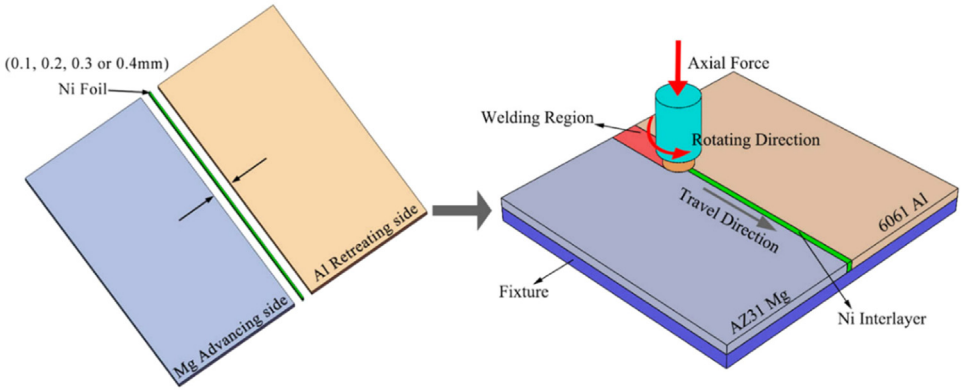

Fig. 34. A schematic diagram of FSW process with the introduction of Ni interlayer [113].

ing speed of 60.3 mm/min, rotating speed of 915.9 rpm, and ultrasonic power of 1485.1 W. Based on the summarized results, the machine learning optimization techniques showed a promising potential in optimizing the FSW parameters of similar and dissimilar Mg and Al alloys joining and predicting the FSW joint properties. Thus, ML optimization techniques can be used to improve the quality of the FSWed Mg/Al joints.

5. Recent strategies for improving joint quality

As aforementioned, most of the studies reported in the open literature on FSW of dissimilar Al and Mg focused on the determination of the effect of weld parameters on the joint quality [57,62,76,79,82–88,114,118–128] and these works have been well reviewed and discussed in detail by excellent overview papers [3,6,39,58–60]. Therefore, in this section, studies aiming to improve the joint quality of dissimilar Al-Mg welds by various welding strategies, which were the main focus of the research in the last decade, will be discussed.

Apart from the plate positioning, tool offset, and controlling of other weld parameters, other welding strategies have also been recently introduced to achieve successful results in dissimilar Al-Mg FSW. These measures are implemented for different reasons. For example, some of these measures are applied to prevent or reduce the formation of intermetallics

in the stir zone, while others are aimed at increasing the heat produced in order to provide better intermixing of base metals and improve weld quality. The others are employed to reduce heat production in case of excessive heat generation, thus minimizing intermetallic formation. The most common of these strategies include the use of interlayer and inclusion of nano-powders, provision of external heat, controlling heat generation (i.e., use of the stationary shoulder, pulsed current assisted FSW, external cooling and underwater welding), and ultrasonic vibration assistance. These strategies can be applied individually or in combination to improve the dissimilar Mg/Al joint quality, such as using a stationary shoulder in conjunction with ultrasonic vibration assistance (i.e. hybrid welding).

5.1. The use of interlayer and inclusion of nano-particles

One of the measures that can be taken to prevent or minimize the formation of intermetallic in the stir zone of FSWed different Al-Mg joints is the use of interlayer, schematically illustrated in Fig. 34. Using a metallic interlayer may prevent the diffusion of Al and Mg. This interlayer might act as a barrier to restrict the mixing of Al and Mg atoms. As a result, intermetallic formation may be eliminated or reduced, leading to increased joint performance. For instance, regardless of the weld parameters, the use of Ni interlayer eliminates the hazardous IMCs formation in FSW of AA6061-T6 Al-alloy and AZ31B Mg-alloy by serving as a barrier to limit the intermixing of Al and Mg alloys in the stir zone [129]. Similarly, Abdollahzadeh et al. [110] examined the effect of using Zn interlayer in FSW of AA6061 Al-alloy and AZ31 Mg-alloy and observed that the use of interlayer increases weld quality. The welded joints obtained at 600 rpm rotational rate and 35 mm/min traverse speed using the interlayer displayed a higher tensile strength of 35 MPa higher than the joint produced without using the interlayer.

Recently, Kumar et al. [108] investigated the effect of Zn interlayer on the mechanical strength of FSWed AZ61 mag-

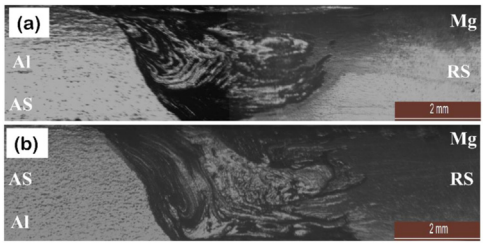

Fig. 35. Macrograph of cross-sectional views of (a) Al-Mg joint without Zn interlayered and (b) Al-Mg Zn interlayered joint [108].

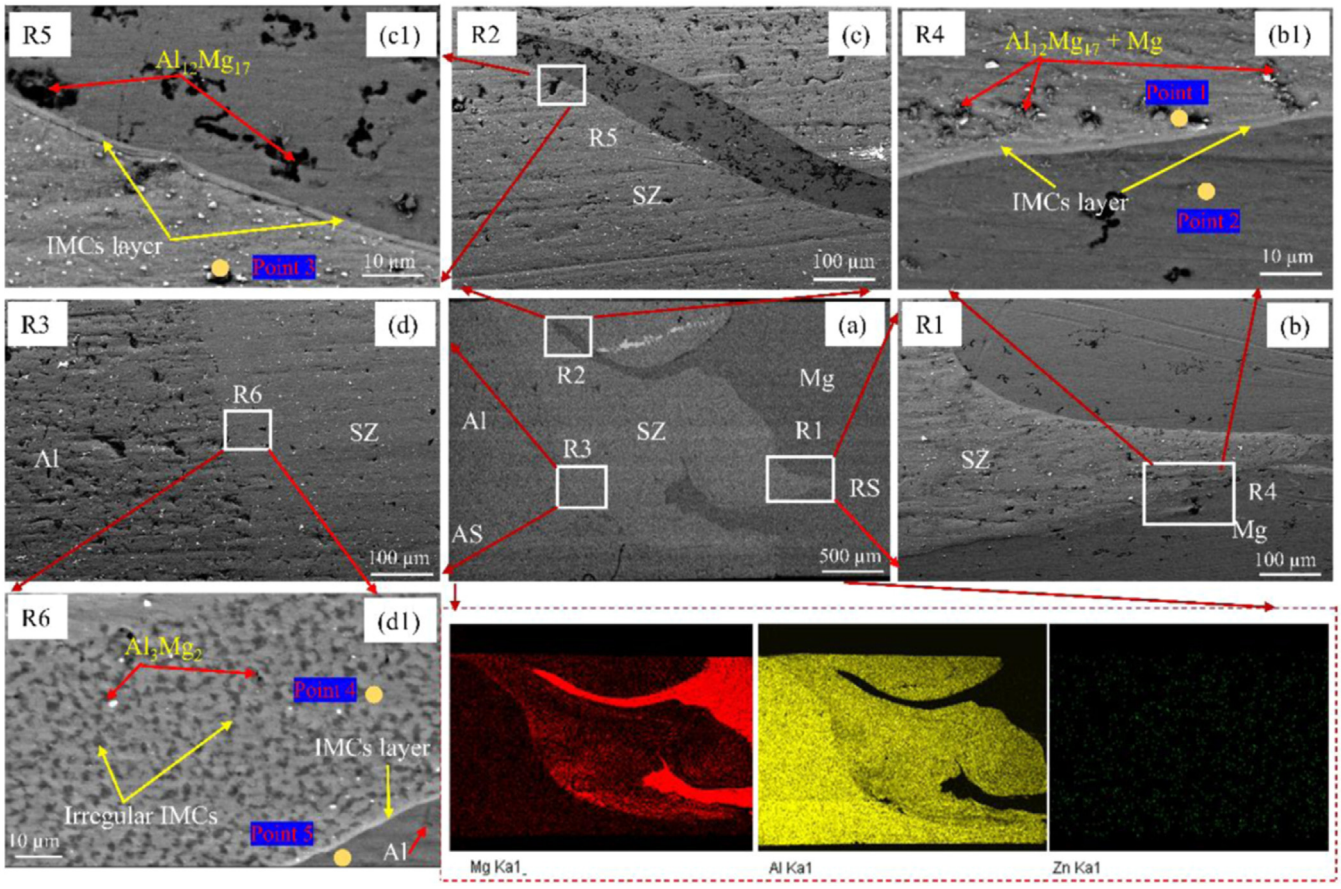

Fig. 36. SEM microstructures of Al/Mg without Zn interlayered joints and the results of the elemental mapping of SZ. (a) An overview of the SZ, (b–d) an enlarged view of R1, R2, and R3, and (b1-d1) an enlarged perspective of the marked area in (b–d) [108].

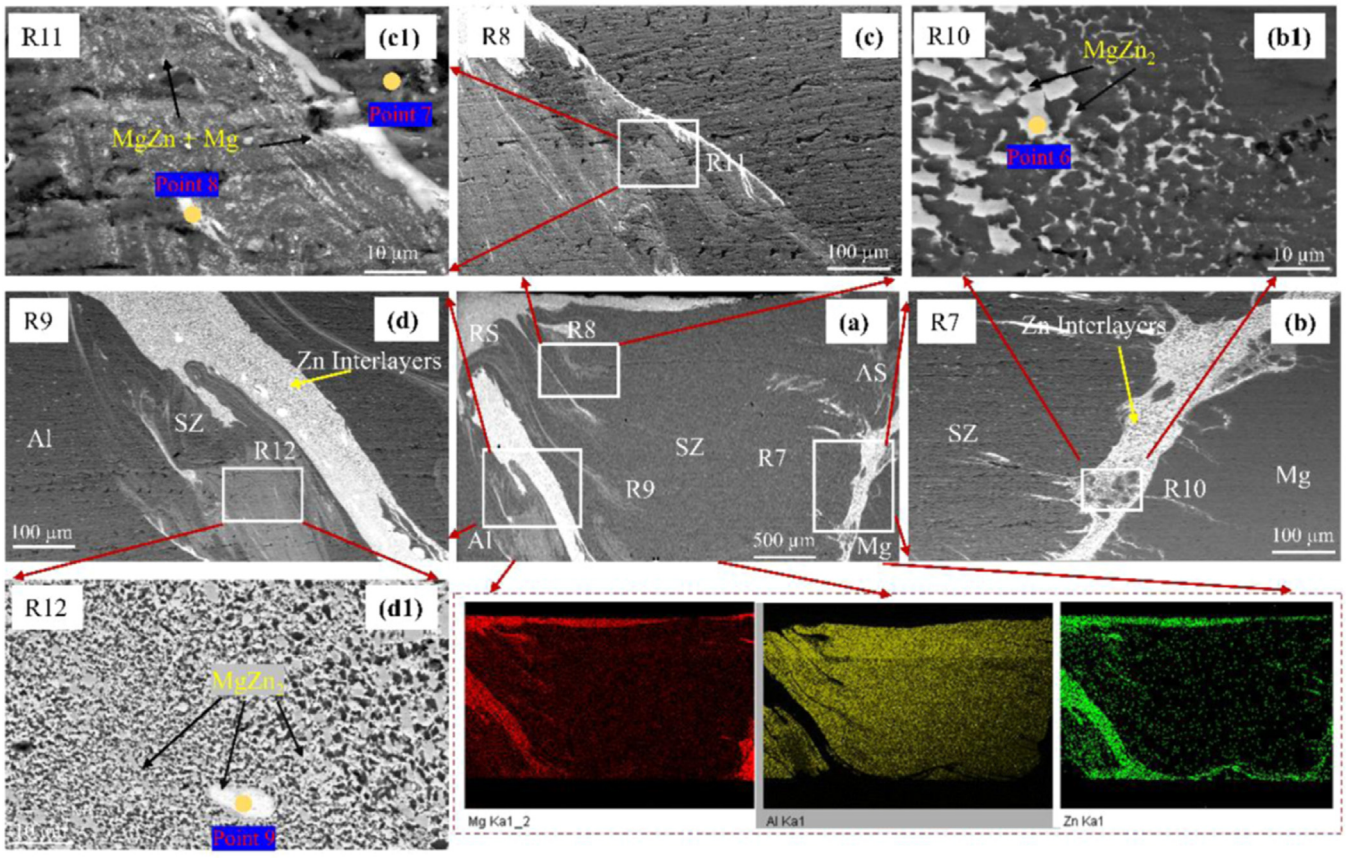

Fig. 37. SEM microstructures of Al/Mg joints with Zn, as well as the outcomes of elemental mapping of SZ. (a) An overview of the SZ, (b–d) a magnified view of R7, R8, and R9, and (b1-d1) an enlarged perspective of the marked area in (b–d) [108].

nesium alloy and AA6061-T6. Fig. 35 shows the transverse cross-section macrographs for the joint produced without (a) and with (b) Zn interlayer. They conducted a detailed investigation and identification of the IMCs for joints produced without and with Zn interlayer. For the joint produced without Zn interlayer, they noted that a multilayered structure of IMCs $Al_{12}Mg_{17}$ exists on the Mg-rich side and Al_3Mg_2 IMCs exist on the Al-rich side, as can be seen from the SEM and EDS analysis on Fig. 36. In Zn containing FSWed joint, they observed a finer and better distributed Mg-Zn IMCs formed in replacement of the brittle Al-Mg IMCs in the Zn-free FSWed joint, as can be noted in their SEM and EDS analysis in Fig. 37. Similarly, Zhong et al. [111] reported the replacement of the Al-Mg brittle IMCs with the Mg-Zn IMCs. This has significantly improved tensile strength to 198.85 MPa, with an increase of about 34% compared to without using the Zn interlayer. Similar results were obtained by other researchers through the use of Zn interlayer [130,110,111]. Also, the percent elongation increased to about 5.24% compared with 2.29% without Zn interlayer [108]. Kumar et al. [108] also used the TEM to confirm the existence of the IMCs at the interface of the FSWed Mg alloy AZ61 and Al alloys AA6061-T6 without (Fig. 38a–f) and with Zn interlayer (Fig. 38g, h). The IMCs in the weld without Zn interlayer showed the multilayered structure of (IMC +Al + IMC + Mg + IMC), which can indicate the mechanism of IMCs formation of thicker Al_3Mg_2 near Al side and $Al_{12}Mg_{17}$ near the Mg side, these IMCs are also confirmed through the diffraction pattern. These IMCs are not formed in the FSWed joint with the Zn interlayer instead Mg_2Zn is detected and confirmed using the diffraction pattern.

These results imply that the use of the Zn interlayer is significantly effective in enhancing the dissimilar Mg/Al joint quality through the prevention of Mg/Al interdiffusion, which reduces the formation of the brittle intermetallics (Al_3Mg_2 and $Al_{12}Mg_{17}$) and instead forming the less harmful Mg_2Zn IMCs. This has effectively improved the tensile strength of the joints produced using Zn interlayer to an average value of 194 MPa compared to 143 MPa for joints without using Zn interlayer (Fig. 39c). Also, the fracture position of the tensile samples has changed from the center (without Zn interlayer) of the NG zone to the interface (with Zn interlayer) between NG and TMAZ (Fig. 39a,b), with a significant increase in the elongation to about 5% from 2% (Fig. 39c). Furthermore, a considerable reduction of the microhardness distribution (Fig. 39d) has occurred through the use of the Zn interlayer, which confirms the suppression of the brittle intermetallic formation.

Other interlayer metallic elements have been used to improve the joint quality of Mg/Al FSWed joints, such as Cd interlayer [112], Ni interlayer [113]. Dewangan et al.

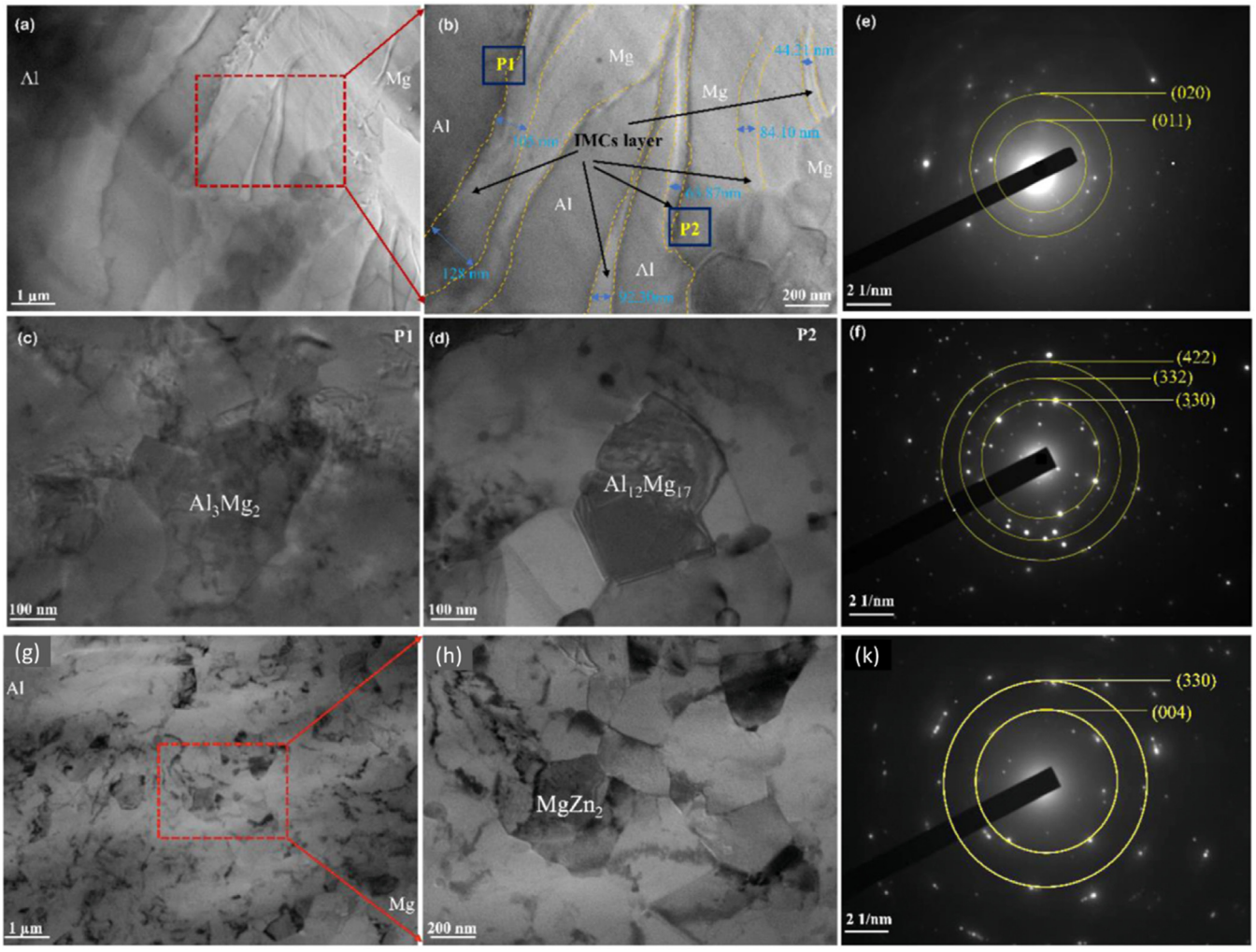

Fig. 38. TEM-SAED patterns outcomes of the Al/Mg FSW joint (a) bright-field TEM image, (b) magnification of the area spotted by red dotted box in (a), (c, d) a magnified view of P1 and P2 region marked in (b). (e, f) are SAED pattern of Fig.s (c and d). TEM-SAED patterns of the Al/Mg with Zn FSW joint: (g) bright field images of the interface, (h) showing MgZn2 phase with Zn rich area in Mg matrix, (k) SAED pattern of Fig. (b) [108].

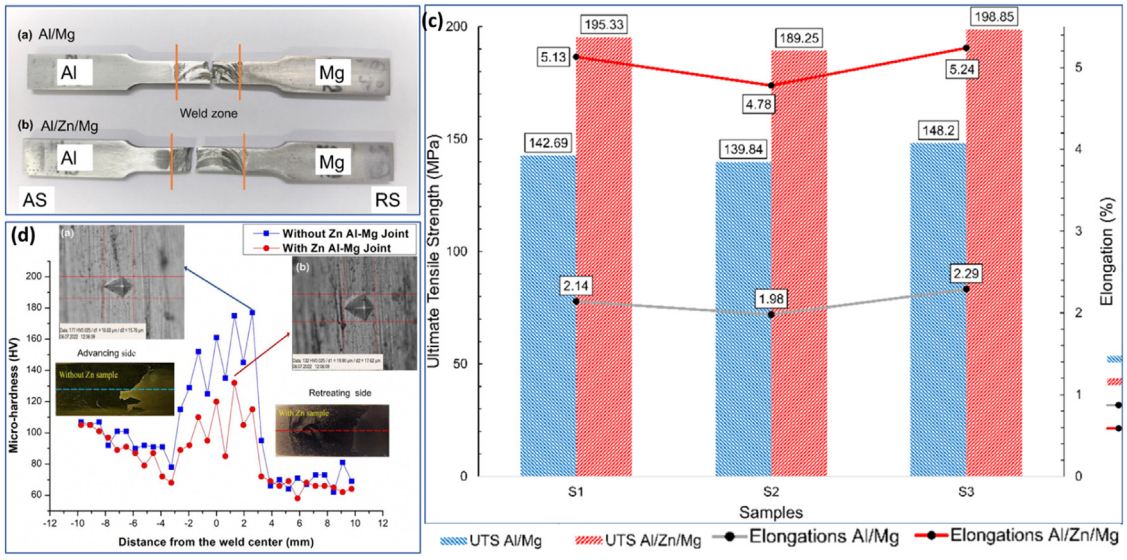

Fig. 39. (a, b) Fractured tensile specimens (a) without Zn and (b) with a Zn interlayer. (c) Tensile strength and Elongation profile for Al/Mg joints with and without Zn interlayer, (d) Distribution of hardness profile from AS(Al) to RS(Mg) for Al/Mg with and without Zn interlayered joints [108].

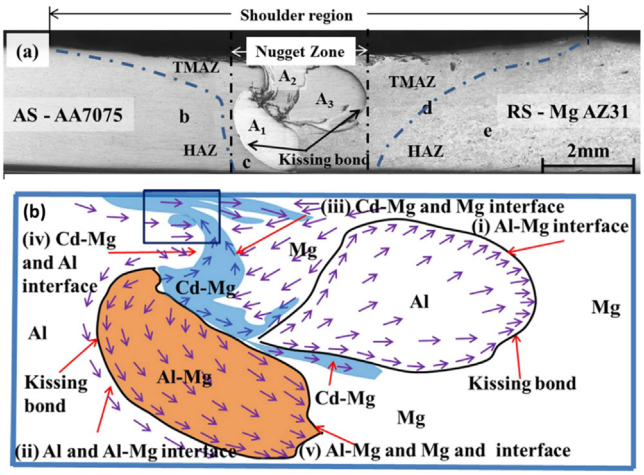

Fig. 40. (a) Transverse cross section macrograph of FSWed AZ31/AA7075 with Cd interlayer and (b) schematic of the nugget zone with indication the flow and different areas formed [112].

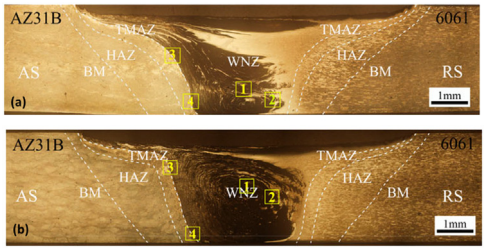

Fig. 41. Transverse cross section macrographs of FSWed AZ31B/AA6061 (a) without Ni interlayer and (b) with 0.3 mm thickness Ni interlayer [113].

[112] investigated the flow behavior and mechanical properties of FSWed AZ31 and AA7075 using Cd interlayer. Fig. 40 (a) Transverse cross-section macrograph of FSWed AZ31/AA7075 with Cd interlayer and (b) schematic of the nugget zone with an indication of the flow and different areas formed. They reported that the Cd reacted with Mg only and mainly formed CdMg and $CdMg_3$ IMCs near the MG side, and at the Al side, a supersaturated solid solution (SSSS) was formed with extrusion of Al into Mg. At the same time, thin layers of the brittle IMCs (Al_3Mg_2 and $Al_{12}Mg_{17}$) were observed. Overall, they reported an enhancement in the tensile strength of the joint compared with similar joints in the literature with Cd interlayer with a maximum tensile of 129 MPa achieved [112].

Dong et al. [113] investigated the effect of using Ni interlayer on the microstructure and properties of FSWed AZ31B and AA6061 compared with Ni-free FSWed joint. Fig. 41 transverse cross-section macrographs of FSWed AZ31B/AA6061 (a) without Ni interlayer and (b) with 0.3mm thickness Ni interlayer. They observed that in the FSWed joint without Ni interlayer, the materials near the bottom of the NG mixed in a vortex-like shape, and near the top, a banded structure was formed Fig. 41(a). On the other hand, the NG zone of the joint produced with Ni interlayer showed a typical onion ring structure with the materials alternately to form a complex banded interlayer Fig. 41 (b). They conducted SEM and EDS analysis at the points indicated on the macrographs for both joints. Fig. 42 shows SEM microstructure for the joint without Ni interlayer, and they observed the multilayered structure of Al+IMC+Mg+IMCs with the Al_3Mg_2 and $Al_{12}Mg_{17}$ are the two main IMCs. Fig. 43 shows SEM microstructure for the joint with 0.3 mm thick Ni interlayer. They observed that the use of the Ni interlayer does not inhibit the formation of the Al-Mg brittle IMCs, but rather, another Mg_2Ni IMCs was formed in addition to the existence of elemental Ni [113]. This has resulted in a tensile strength higher by 13% for the use of Ni interlayer, slightly higher ductility of 1% elongation relative 0.7%, and a higher hardness in the Ni interlayer containing joint as can be seen from Fig. 44, where the fracture path occurred at Mg/NG side interface in both joints.

Based on the above-summarized results of FSW joints with the use of different types of metallic interlayers Zn, Cd, and Ni interlayers, it can be emphasized that the use of the Zn interlayer due to its dissolution and mixing within the NG zone, has resulted in the suppression of brittle Al_Mg IMCs multilayered structure formation and replaced by Mg-Zn distributed IMCs particles through the enhancement of elemental distribution inside the NG [108]. This has improved strength, ductility, and corrosion resistance [108]. In contrast, the use of either Cd interlayer or Ni interlayer allows the formation of the brittle Al-Mg IMCs in addition to Mg_2Ni in the case of Ni interlayer, elemental areas, as well as solid solutions inside the NG zone. This has only slightly improved the tensile strength relative to the interlayer-free joints but still hardness is higher, and ductility is very limited [112] [113]. Thus, we believe using the Zn interlayer is a promising strategy for enhancing the quality of Mg/Al dissimilar FSW joints.

Also, nano-particle feeding during welding can be used to enhance the quality of Mg/Al FSW joints [131–133]. Nano-powder feeding increases grain refinement by the pinning effect in the stir zone, thus improving joint strength [131]. Tabasi et al. [132] reported that a fine microstructure with an average grain size of 4.3 μm at the stir zone was obtained in dissimilar FSW of AA7075 Al-alloy and AZ31 Mg-alloy by embedding nano SiC particles as well as controlling the process parameters (i.e., rotational speed of 560 rpm and traverse speed of 22.4 mm/min) [132]. Similarly, Abdollahzadeh et al. [133] also studied the effect of SiC nanoparticle embedding on the joint performance of dissimilar AA6061-T6 Al-alloy and AZ31 Mg-alloy joints. The joint fabricated at 35 mm/min and 650 rpm with SiC nanoparticle embedding improved by 28% in tensile strength and enhancement about three times in elongation compared to the joint fabricated without nanoparticles. Including the nanoparticles in the butt, FSW is not straightforward and hence needs special friction stir processing(FSP) step, as described by Abdollahzadeh et al. [133] which adds more complexity to the process and increases its cost.

5.2. External heat assistance

The concept of auxiliary energy assistance FSW is mainly developed to overcome the high load requirements on the tool

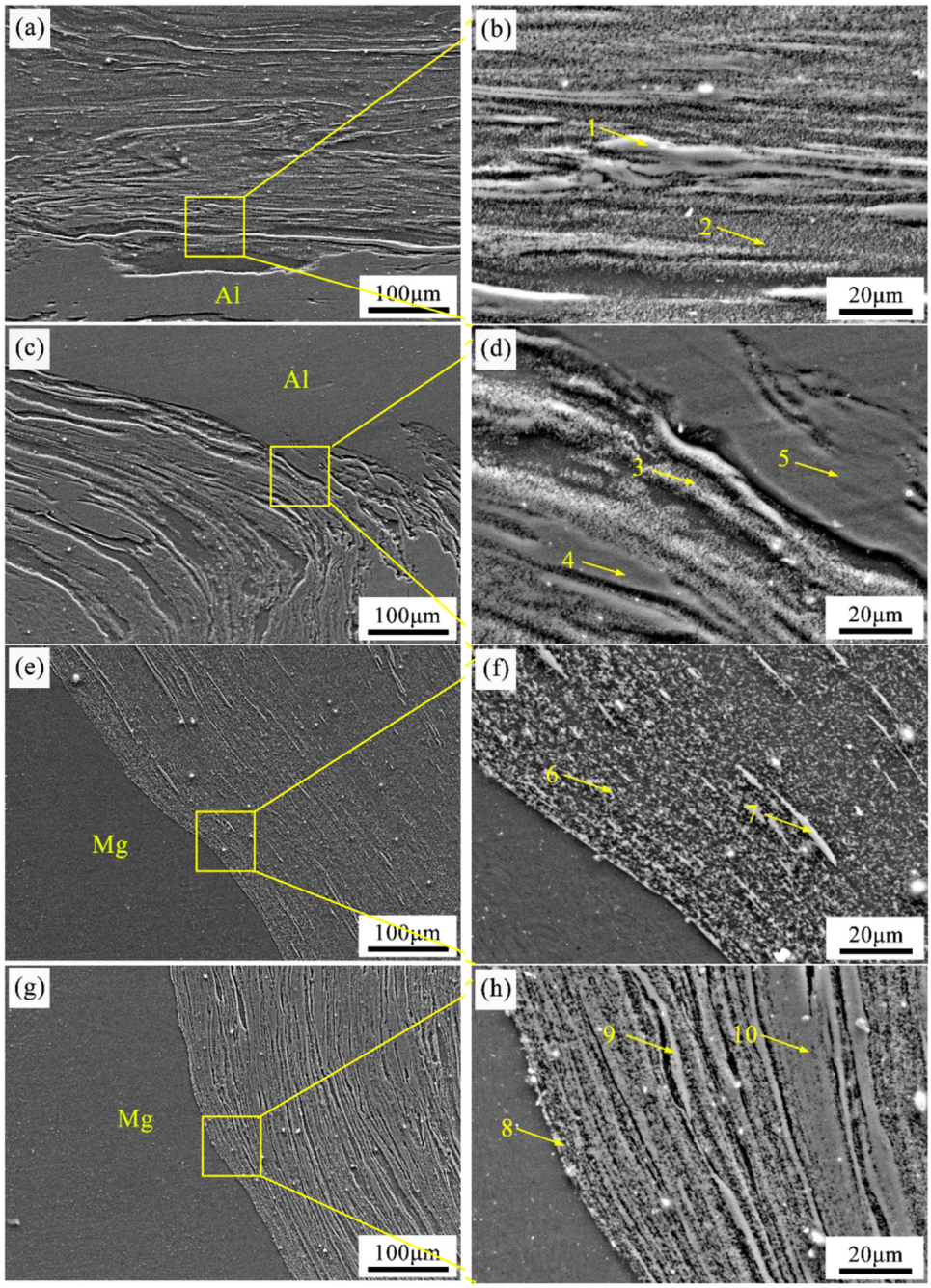

Fig. 42. Microstructures at different positions in the WNZ of sample 1: (a), (c), (e) and (g) are enlarged views of 1, 2, 3 and 4 of the marked areas in Fig. 41 [113].

during FSW of hard materials. This can generate additional softening during or before FSW, improving the tool performance, tool life, FSW window, welding efficiency, and joint quality [134]. Padhy et al. [134] have reviewed the auxiliary energy assistance FSW variants, including electrically assisted FSW (EAFSW), induction assisted FSW (IAFSW) process, laser-assisted FSW (LAFSW) process, arc-assisted FSW (AAFSW) and gas torch assisted FSW (GTAFSW), mainly focusing on the experimental setup and requirement as well as the advantages of each process compared to the conventional FSW process. The application of these processes to the joining of dissimilar Mg/Al has been quite limited. A few studies on the use of LAFSW are available, such as Change et al. [135], which investigated the use of LAFSW with Ni interlayer on the strength of dissimilar welded AZ31/AA6061 and they conducted the FSW process at 800 rpm rotational rate and 35 mm/min traverse speed while Al-alloy is placed on the advancing side. According to the results of this study, the joints produced by FSW using Ni interlayer with external heat-supply by laser exhibited higher tensile strength (i.e. 66% of the Mg-alloy base plate tensile strength) than the joints obtained without heat assistance with or without inter-

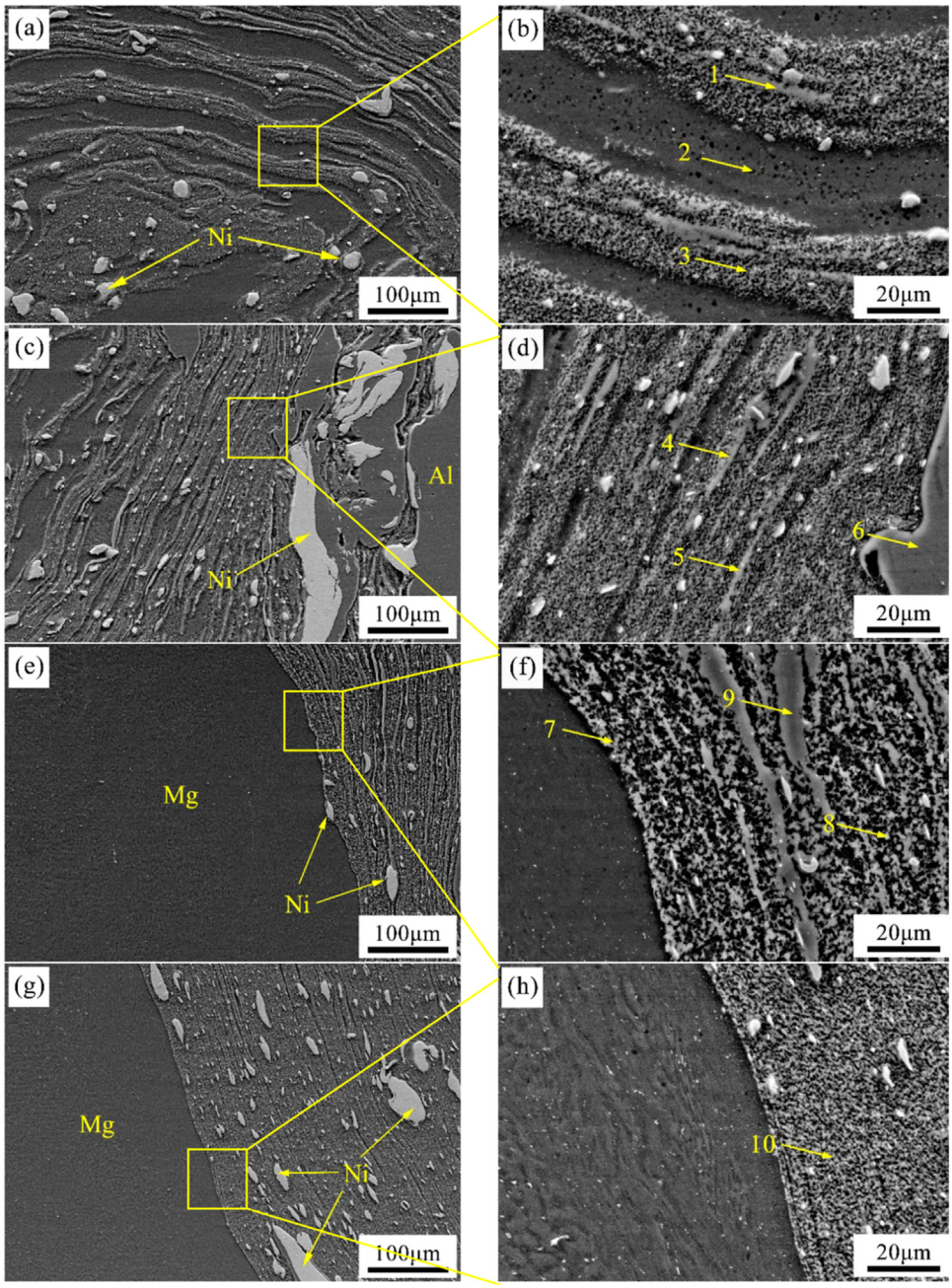

Fig. 43. Microstructures at different locations in the WNZ of sample 4: (a), (c), (e) and (g) are enlarged views of 1, 2, 3 and 4 of the marked areas in Fig. 41 [113].

layer. They proposed that this is due to the formation of a less brittle Ni_3Al intermetallic phase instead of a more brittle $Al_{12}Mg_{17}$ IMC in the joints produced by heat-assisted FSW. However, it should not be overlooked that the weld parameters (i.e., rotational rate, weld speed, shoulder geometry diameter, etc.) that will not cause excessive heat generation should be used in the case of external heat-assisted FSW.

Another heat-assisted FSW process that was applied to joining dissimilar Mg/Al alloys is the EAFSW, schematically illustrated in Fig. 45. In EAFSW, electric current is supplied directly to the workpieces or via the tool. This electric current provides assistance by producing resistance heating and electro-plastic effect [134]. Also, few studies are available to apply EAFSW for joining dissimilar Mg/Al alloys. For example, Xiaoqing et al. [91] employed EAFSW to join dissimilar AA6061 Al-alloy and AZ31B Mg-alloy. They examined rotation rates of 800 rpm and 900 rpm at 25 mm/min at three different pulse current ampers of 0, 300, and 500. They reported that increasing the pulse current has eliminated the NG zone defects (Fig. 46) and reduced the IMCs banded structure area compared to the conventional FSW. Thus, the tensile strength has gradually increased to 167 MPa at 800 rpm and

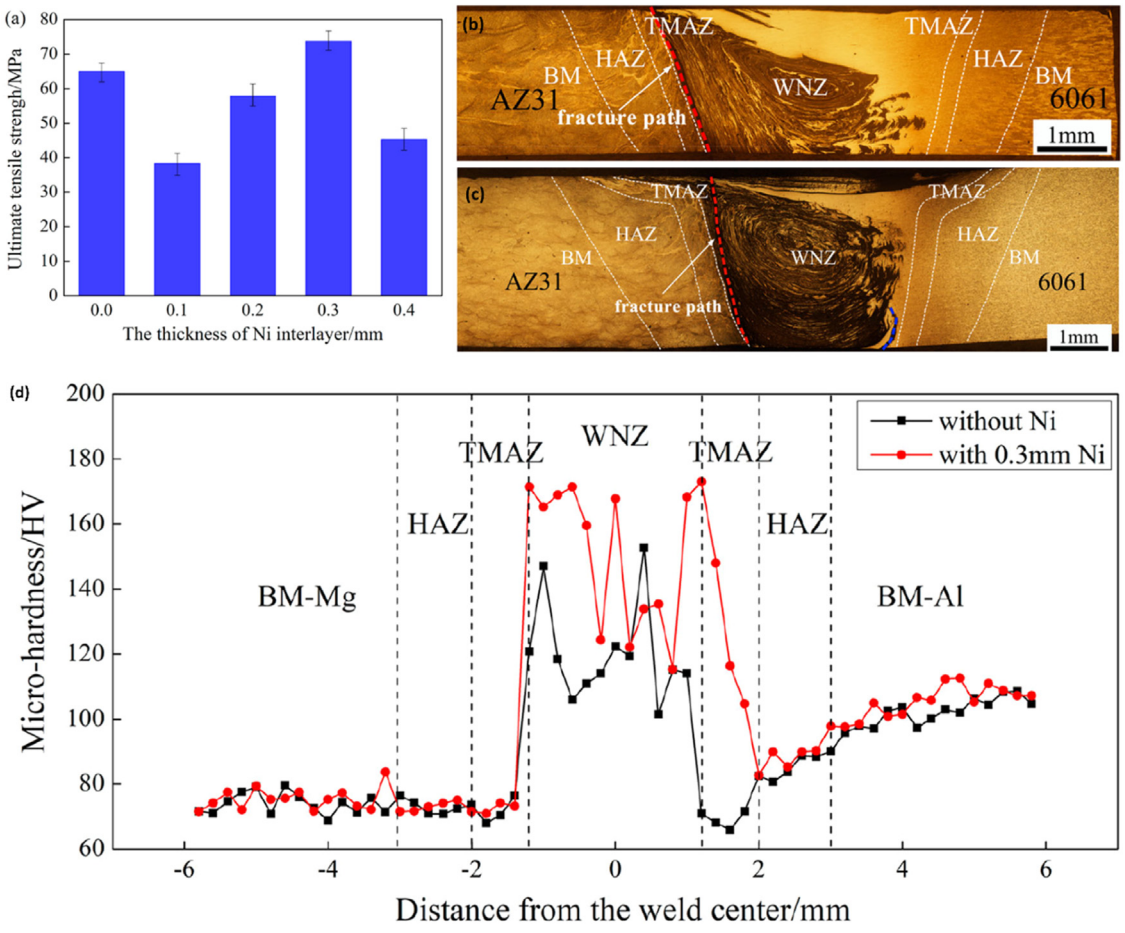

Fig. 44. (a) tensile strength variation with the thickness of Ni interlayer, (b) fracture path of joint without Ni, (c) fracture path of joint with 0.3 mm thickness Ni interlayer and (d) Microhardness profile for the joints with and without Ni interlayer [113].

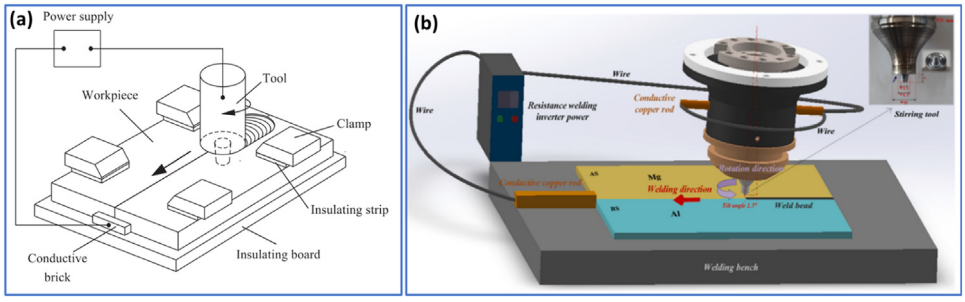

Fig. 45. Schematics of the electric-current assisted FSW (EFSW) (a) [136], (b) [91].

215 MPa at 900 rpm at 500 ampers. In terms of hardness, the use of pulsed current has significantly reduced the hardness in the NG zone due to the elimination of the IMCs.

Although the high heat input is not favored for the dissimilar Mg/Al welding to suppress the IMCs layer formation and improve joint quality, based on the few studies available in this regard, the use of external heating such as laser-assisted FSW (LAFSW) and electric-current assisted FSW (EAFSW) gave quite promising results in terms of improved tensile strength and elimination of defects. On the other hand, it can be noted that the welding parameters used with the conventional FSW have to be reduced to compensate for the heat generated from the external source. For example, Xiaoqing et al. [91] obtained the highest tensile strength of 162 MPa at 1200 rpm and 25 mm/min in the case of FSW. However, the rotation rate of 900 rpm was optimal for obtaining the highest strength of 215 MPa at a current of 500 amperes.

5.3. Controlling heat generation

In addition to these two applications to obtain higher quality welded joints in the Al-Mg system by FSW, suppressing excessive heat generation is another welding strategy that will increase the welding performance as it will reduce the for-

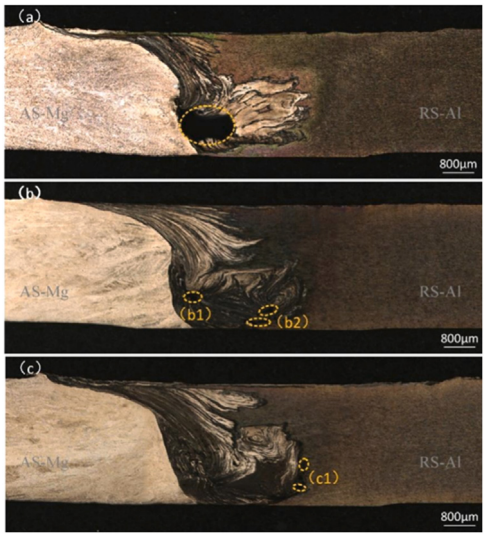

Fig. 46. Weld cross-sectional macrographs of FSWed AA6061/AZ31B joints: (a) FSW without pulse current assistance, (b) pulse current: 300 A, and (c) pulse current: 500 A (note reduction in the amount of defects with increasing current) [91].

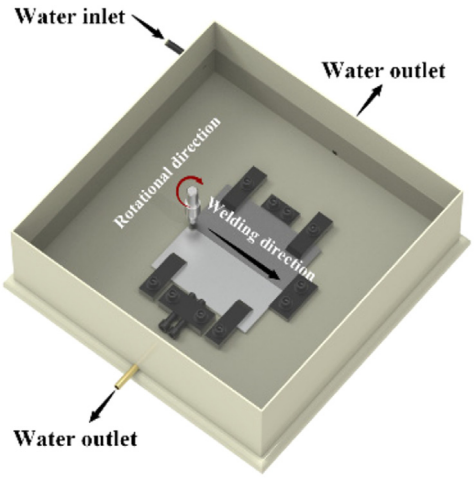

Fig. 47. Schematic illustration of the SFSW process [116].

mation of detrimental brittle intermetallics. Among the approaches that can be applied to prevent excessive heat generation are the use of submerged FSW, stationary shoulder, and external cooling. Submerged FSW is one of the standard methods for the improvement of mechanical properties of dissimilar Al-Mg joint. In submerged friction stir welding (S-FSW) the welding process is conducted in a coolant bath or underwater. Water-submerged FSW is one of the best alternative method for generating fine-grained welds with excellent mechanical properties in dissimilar Al-Mg FSW. Fig. 47 shows the schematic of the SFSW process. External cooling can also applied in a bath of a coolant, such as liquid nitrogen or water [137–139,64]. For instance, Mofid et al. [64] conducted water-submerged friction stir welding (SFSW) to produce dissimilar AA5083 Al-alloy and AZ31C-0 Mg-alloy joints. Peak temperatures of weld during submerged conditions reached up to 387 °C, which is 25 °C lower than the usual welding temperature. They also reported that the formation of intermetallic compounds was suppressed significantly. In addition, grain growth was not noticeable in the stir region due to lower peak temperatures. Chen et al. [137] also claimed that the hardness of the stir zone can be reduced by performing the welding underwater which leads to a reduced intermetallic formation in the stir zone. They clearly demonstrated that with the decreasing of the ambient temperature, the quantities of IMCs reduced gradually, and thus, the least IMCs appeared in the joint fabricated FSW in 60 °C water. This result can be attributed to the decrease of peak time, dwelling time above higher temperatures and increase in cooling rate during the welding process, which restrains the formation of IMCs, i.e. the content of IMCs reduced from about 31.79% to 7.8%. Thus, joint tensile strength increased from 92 MPa to 168 MPa. Similarly, Mehta et al. [138] joined Al and Mg plates by both conventional FSW and underwater FSW with Mg-alloy on the trailing side and a tool offset on the Mg-alloy side using 1070 rpm rotational rate and 70 mm/min traverse speed. The results showed that the welded joint made by underwater FSW has a lower amount of intermetallic phase formation in the stir zone and, therefore, displays higher tensile strength. Similar observations were also claimed by Zhao et al. [139] in underwater FSW of Al–Mg alloys. They reported that AA6063-AZ31 welded joints produced by underwater FSW exhibited higher weld surface quality and higher weld performance as a result of lower intermetallic formation. They also reported that a very thin intermetallic layer was formed at the interface due to the reduced temperature of the weld zone. They achieved a tensile strength of up to 152.3 MPa in the underwater friction stir welded joint, equivalent to 63.3% of AZ31 Mg alloy strength. Huang et al. [116] investigated the interface formation during SFSW of 4 mm thickness AZ31B/AA6061 using different tool rotation rates of 800, 900, and 1000 rpm at a constant welding speed of 70 mm/min. They reported that the SFSW was beneficial in decreasing peak temperature, suppressing the coarsening of IMCs layer, and improving the joint quality (Fig. 48). All the joints (Fig. 48b–d) produced using SFSW were found to be free of defects, while the ones produced using FSW only contained macro-defects (Fig. 48a) as well as microdefects and cavities (Fig. 49a–c). This indicates the effectiveness of SFSW in improving joint quality. In terms of its effect on the IMCs layer, their SEM and EDS investigations presented in Fig. 49 (a–f) where the SEM/EDS of the joint produced using conventional FSW showed coarse IMCs layers Fig. 49 (a–c) and that produced using SFSW showed only fine IMCs Fig. 49 (d–f). Furthermore, a reduction in the IMCs layer thickness from 0.78 μm to 0.59 μm at the shoulder affeacted zone and from 1.31 μm to 1.21 μm at the probe affected zone were noted [116]. They reported an improvement of the joint tensile strength to 171MPa which represent 71% of AZ31B strength. This was attributed to that the SFSW enhanced the thermal cycle, improved dissimilar material interlocking, retraded the IMCs layer formation.

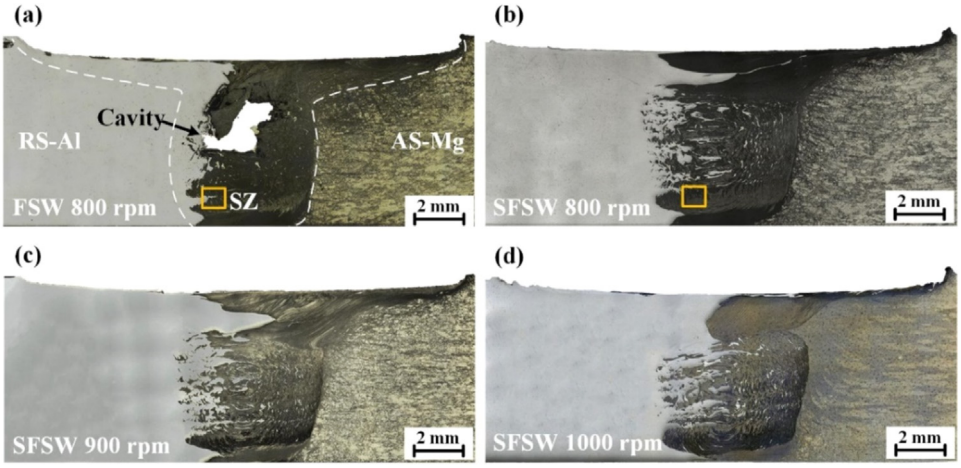

Fig. 48. Transverse cross-section macrographs of FSWed and SFSWed AZ31B/AA6061 at a constant welding speed of 70 mm/min and different tool rotation rates of (a) FSW at 900 rpm, (b) SFSWed 800 rpm, (c) SFSWed 900 rpm, and (d) SFSWed 1000 rpm [116].

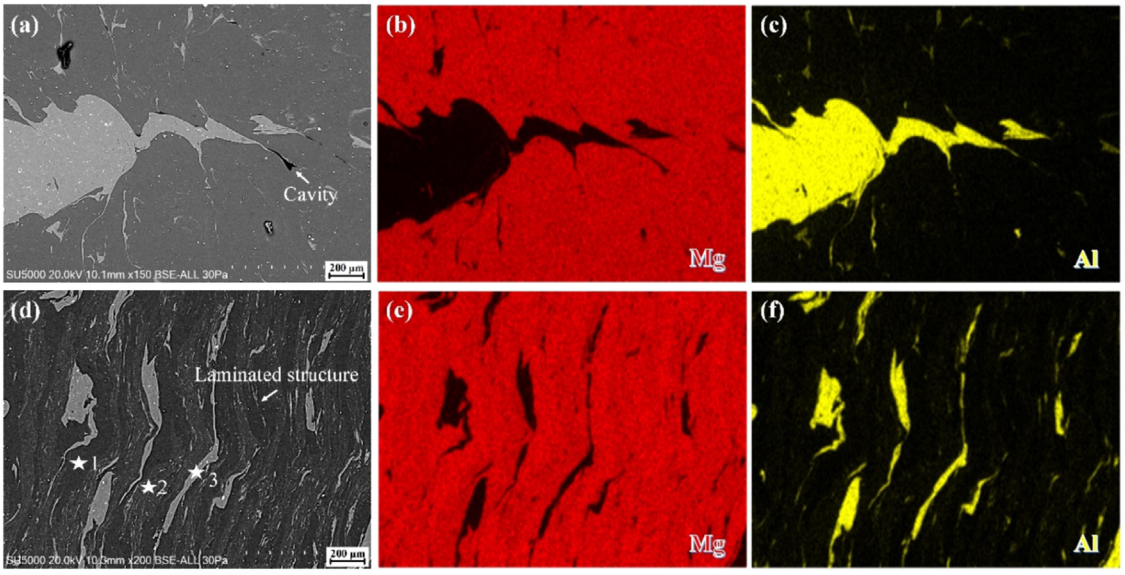

Fig. 49. SEM images and EDS mapping of the microstructure in (a–c) FSW and (d–f) SFSW weld fabricated at 800 rpm [116].

Another way of reducing heat generation during FSW is the use of a stationary shoulder in addition to weld parameter optimization. The static shoulder reduces the amount of heat produced by eliminating the rotating action of the shoulder [105,117,140,141]. For instance, Ji et al. [117] employed stationary shoulder-assisted friction stir welding (SSFSW) to decrease the heat generation during the process and thus reduce the amount of Al-Mg IMCs. They reported that the ultimate tensile strength (UTS) of the SSFSW joint was higher than that of the joint produced by conventional FSW. Similarly, under similar welding conditions, Liu et al. [105] reported that conventional FSW obtained the maximum UTS of 107 MPa, while when the SSFSW technique was used, the maximum UTS increased to 135 MPa [106]. Song et al. [103] also used stationary shoulder friction stir welding with ultrasonic vibration assistance (U-SSFSW) to join the dissimilar alloys of AA6061-T6 Al-alloy and AZ31B Mg-alloy. They observed that various intercalated structures comprised of AZ31B Mg, AA6061-T6 Al and Al-Mg IMCs layers are formed in the stir zone. They further increased the maximum UTS to 158 MPa by the combined effect of using stationary shoulder and ultrasonic vibration. They also pointed out that the diminished IMCs realized by higher welding speed and lower rotating speed and the thinner intercalated structure realized by higher ultrasonic power are the key factors in acquiring higher joint strength.

A further measure that can be taken against excessive heat generation during FSW is external cooling. External cooling is one of the standard methods for the improvement of mechanical properties of dissimilar Al-Mg joints. External cooling during FSW can be done by various coolants, including air stream [142], running water [143,144], and sprayed liquid CO_2 [145,146]. This process is particularly suitable for joining alloys sensitive to overheating during welding [147]. Liq-

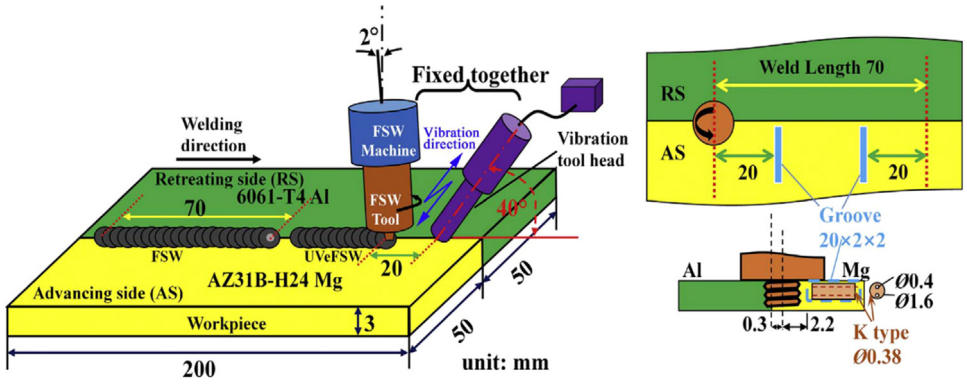

Fig. 50. FSW assembly of Mg/Al alloys with UVaFSW system attached [90].

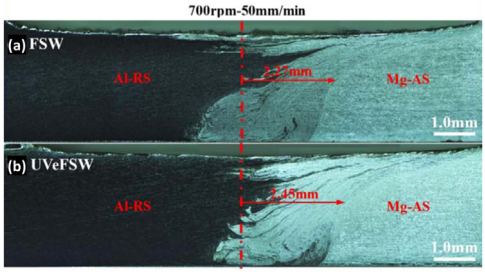

Fig. 51. Transverse cross section macrographs of FSWed AZ31B/AA6061-T4 at 700 rpm and 50mm/min (a) without UVa and (b) with UVa [90].

uid nitrogen and water are the most common cooling mediums. For example, Mofid et al. [148] used liquid nitrogen as a cooling medium to suppress the IMC formation in the weld zone and obtained a maximum peak temperature of 382 °C for welds made under liquid nitrogen, which is 53 °C lower than conventional FSW in air. They achieved finer grains (2.5 μm) and reduced amounts of IMCs in the stir zone, which led to improved joint strength, i.e. 134 MPa (30 MPa higher than conventional FSW). In addition to these, Mofid et al. [148] also stated that the dissimilar AA5083-AZ31 welded joint produced by FSW with external water cooling is of higher quality than conventional the joints obtained by conventional FSW in air as a result of lower peak temperature generated.

Based on the above-summarized literature on the control of heat generation, it can be said that submerged FSW is more effective in controlling heat generation, especially if associated with a system to control the temperature. This can effectively enhance the dissimilar materials' mixing and flow, reduce the intermetallic layer formation, and improve the joint quality. Then, the stationary shoulder FSW can, to some ex-

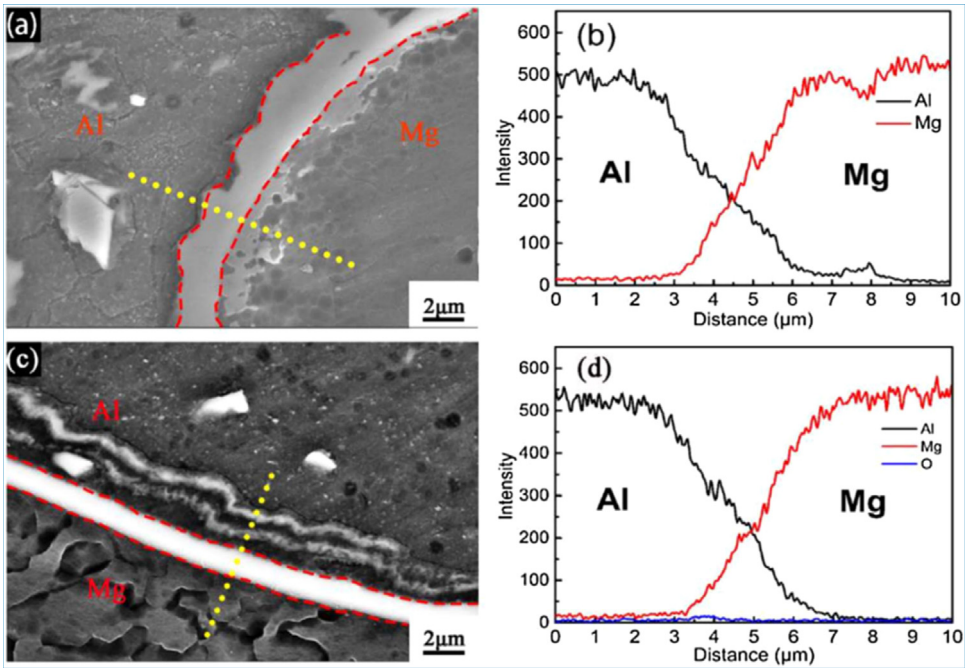

Fig. 52. SEM micrographs and EDS line scan profiles of Al-Mg weld interfaces at 700 rpm and 50 mm/min. (a) and (b) for FSW, (c) and (d) for UVeFS [90].

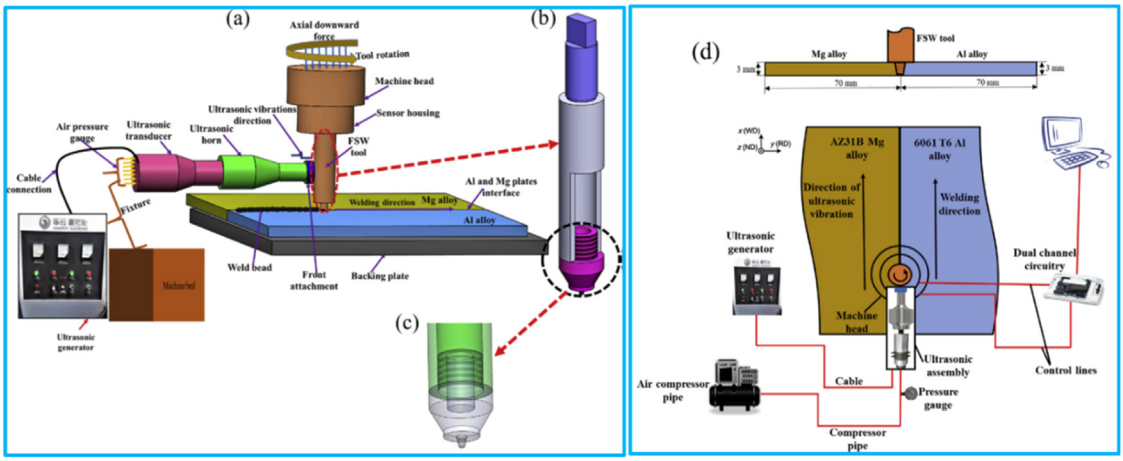

Fig. 53. (a) A UVaFSW assembly and related terminology (b,c) schematic of specially designed FSW tool (d) A schematic diagram showing the ultrasonic process and its attachments [81].

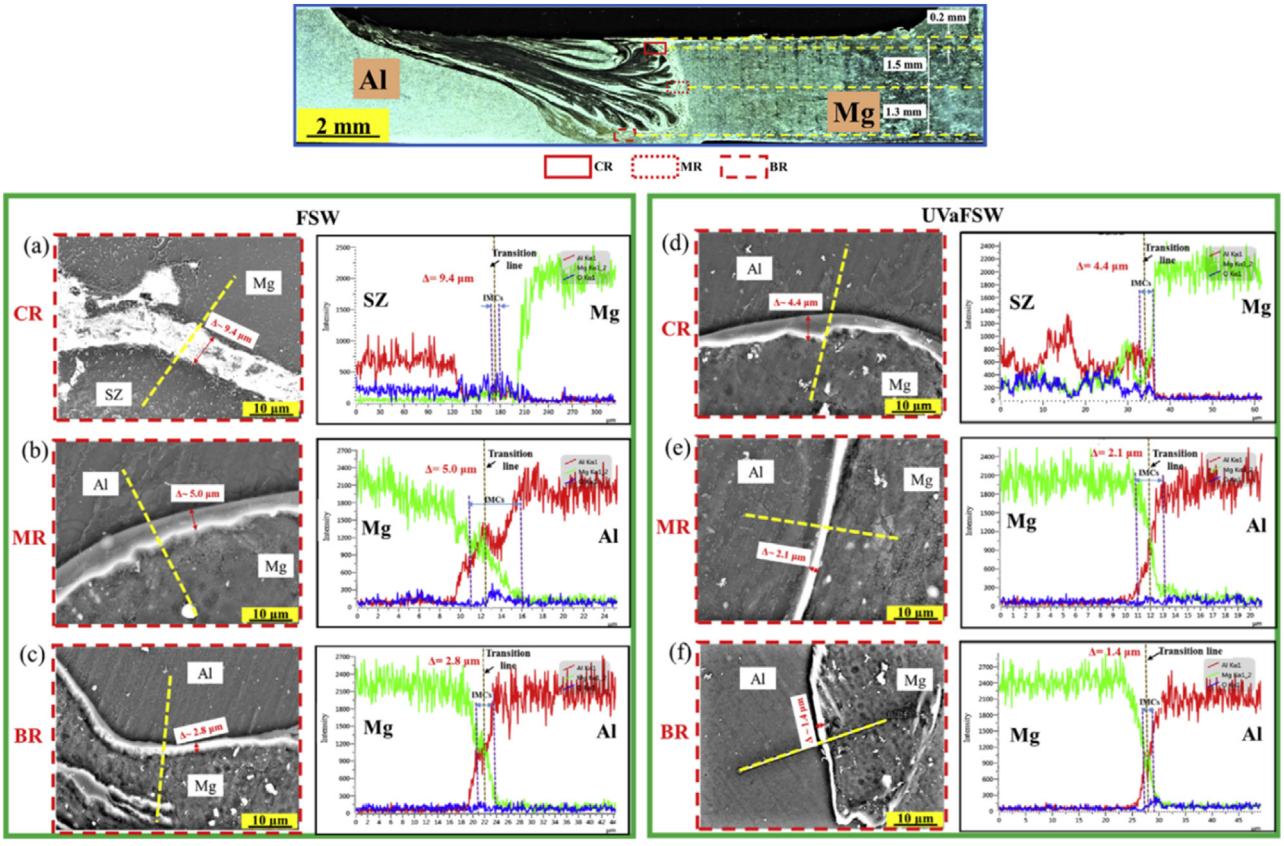

Fig. 54. SEM images and corresponding EDS line scan profiles of AleMg alloys joints made at 800/100 (a,c,e) FSW (d–f) UVaFSW across crown region (CR), mid-region (MR) and bottom region (BR) [81].

tent, contribute to reducing the heat generation by eliminating the heat generation from the shoulder and can be more effective if associated with another strategy, such as ultrasonic and/or additional Zn interlayer. The external cooling can be effective in enhancing grain refining by suppressing the static annealing after FSW; however, in the case of thick section joints, its effect will be limited to the surface layers and can lead to more variation on the microstructure through the thickness of the joint.

5.4. Use of ultrasonic vibrations

Due to the proven effectiveness of the ultrasonic vibrations (UVa) action, it has been employed in a wide range of metal processing such as direct welding (Ultrasonic welding), metal forming, and manufacturing processes [149,81]. Also, it has been used to assist various fusion welding and solid-state welding processes [149,81]. In direct welding of metals, ultrasonic vibration of high-frequency vibrations (in

Table 12
IMCs thickness and corresponding percentage change with ultrasonic assistance under various parameters [81].

Parameters	Regions	IMCs thickness in microns		
		FSW	UVaFSW	% change
400/100	CR	4.6 ± 0.36	2.3 ± 0.11	49.93 ±1.09
	MR	3.3 ± 0.28	1.5 ±0.23	54.86 ± 3.47
	BR	2.1 ± 0.53	1.9 ± 0.3	8.94 ± 3.06
600/100	CR	5.9 ± 0.18	2.8 ± 0.4	52.68 ± 5.56
	MR	4.6 ± 0.38	2.2 ± 0.36	52.38 ± 2.38
	BR	4 ± 0.3	2 ± 0.19	50.09 ± 1.26
800/100	CR	9.4 ± 0.2	4.4 ± 0.40	53.26 ± 3.26
	MR	5 ± 0.2	2.1 ± 0.23	58.09 ± 2.32
	BR	2.8 ± 0.1	1.4 ± 0.3	50.32 ± 8.94
1000/100	CR	19 ± 0.96	8.5 ± 0.67	55.28 ± 0.28
	MR	4.6 ± 0.36	2.4 ± 0.53	48.39 ±8.59
	BR	1.6 ± 0.4	1.2 ± 0.31	24.17 ± 3.33

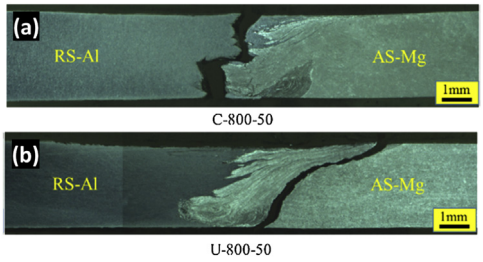

Fig. 55. Transverse cross section after tensile test of the FSWed (a) and UVaFSWed (b) AZ31B-H24 and AA6061-T6 [92].

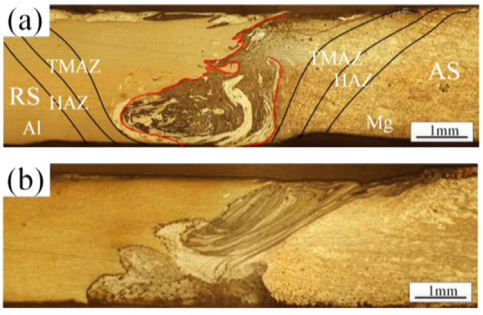

Fig. 56. Cross-sectional images of the weld zone of dissimilar AA6061-AZ31 welded joint fabricated by FSW: (a) ultrasonic vibration assisted-FSW and (b) conventional FSW without ultrasonic vibration [104].

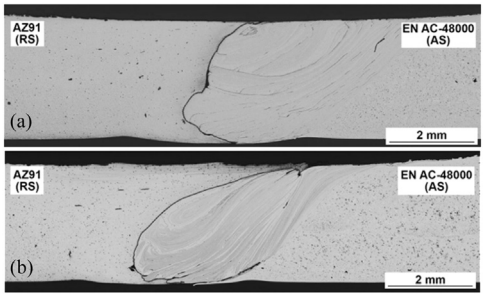

Fig. 57. Cross-sectional images of the weld zone of dissimilar die-cast aluminum alloy EN AC-48000/AZ91 welded joint fabricated by FSW: (a) conventional FSW without ultrasonic vibration and (b) ultrasonic vibration assisted-FSW [159].

the range of 19–22 kHz) and pressure are used to join two materials [149]. Recently UVa has been adopted with friction stir welding and found to be very useful in obtaining sound joints and improving the mechanical properties of similar Al alloys [150,151], dissimilar Al/Cu alloys [152], and Al-Steel alloys [153]. Importantly UVa have been used extensively to assist in dissimilar FSW of Mg/ Al alloys [13,81,90,103,106,109,129,154–156]. UVa has demonstrated that ultrasonic vibration-assisted FSW can also be successfully applied to improve the welding performance of dissimilar Al-Mg welded joints [81,90,92,104–107,109,155,157–159]. UVa applied by Lv et al.[90,160] ahead of the FSW tool to enhance Mg/Al joint strength and reduce the IMCs layer thickness. Similarly, Zhao et al used the same UVaFSW arrangement [92]. Lv et al. [90,160] directly applied the UVa at 20 kHz ahead of the FSW tool with a distance of 20 mm and at an angle of 45° relative to the workpiece, a schematic of the FSW system with the UVaFSW setup is illustrated in Fig. 50. They reported that the mechanical interlocking of the Al-Mg joint is improved by the ultrasonically induced nailing and hooking features at the weld interface, as can be observed in the macrographs in Fig. 51. Also, they noted that IMCs layer became discontinuous and less in thickness (Fig. 52 a–f), which improved the mechanical properties (Fig. 52 g,h).

Kumar et al.[81,93,154,157] have developed an ultrasonic vibration system to assist FSW of Mg/Al dissimilar welding. They consider it a high-power ultrasonic-assisted friction stir welding (UVaFSW) system that aims to induce a thermo-mechanical-acoustic effect in the SZ mainly to improve the plastic deformation of the material in the shear layer. In this UVaFSW system, the axis of the acoustic horn was kept normal to the FSW tool so that ultrasonic vibrations could be transmitted into the SZ along the welding direction [81,157]. The schematic of their UVaFSW system is illustrated in Fig. 53. They conducted a detailed investigation for the FSWed and UVaFSWed AZ31B and AA6061-T6 Al of 3 mm thickness at a range of tool rotation rates from 400–1000 rpm and welding speeds from 50 – 250 mm/min. They analyzed

Table 13
Summary of materials, FSW parameters, and mechanical properties of dissimilar FSWed Mg/Al alloys using UVaFSW.

Alloys (Mg/Al), thickness (mm)	FSW parameters 1. Rotation rate, rpm 2. Welding Speed, mm/min 3. Mg Position 4. Strategy	Properties (Strategy Vs No strategy) Hardness, Hv Tensile strength MPa, % Elongation	Comments	Refs.
AZ31B /AA6061-T6, 3.	1. 400 to 1000 2. 50 – 250 3. RS 4. UVaFSW	I. 174 vs 166 II. 163 vs 130 III. NA	Maximum tensile obtained at 800 rpm and 100 mm/min with joint efficiency of about 70% for UVaFSW joint.	[81,93]
AZ31B/6061-T4, 3	1. 400–800 2. 50 3. AS 4. UVaFSW	I. 85 vs 110 II. 180 vs 160 III. NA	UVaFSW reduced IMCs layer thickness and enhanced tensile at all parameters.	[90]
AZ31B/6061-T4, 3	1. 700 2. 50 3. RS 4. UVaFSW	I. 85 vs 110 II. 180 vs 160 III. NA	The ultrasonic vibration inhibited the formation of intermetallic compounds and reduced the thickness of the intermetallic compound layer by inducing variation of thermal cycles.	[90,160]
AZ31B /6061-T6, 3	1. 1200 2. 40 3. AS 4. U-SSFSW	I. NA II. 120 vs 64 III. 1.5 vs 0.5	The coupling of acoustic and streaming induced by ultrasonic can break partial IMCs into pieces or particles.	[104]
AZ91/Die-cast aluminum alloy ENAC-48000 (AlSi12CuNiMg), 3	1. 300 2. 30 3. RS 4. UVaFSW	I. NA II. 142 vs 64 III. NA	USaFSW reduced the brittle IMCs at the interface and enhanced tensile by about 226%.	[159]
AZ31B-H24/AA6061-T6, 3	1. 800 2. 30 – 80 3. AS 4. UVaFSW	I. NA II. 196 vs 175 III. NA	The highest tensile (196MPa) was obtained for UVaFSW at 800–50, and the upper part of this joint showed the highest tensile of 204 MPa.	Zhao et al. [92]
AZ31B/AA6061-T6, 3	1. 1000 2. 30 3. AS with offset 0.3 to AS 4. U-SSFSW	I. NA II. 115 vs 78 III. 0.6 vs 0.63	UVaFSW effectively smashed the IMCs and dispersed evenely in the SZ.	Meng et al. [107]
AZ31B/ 6061-T6, 3	1. 997 2. 63 3. AS 4. U-SSFSW	I. 120 vs NA II. 161 vs NA III. NA	The Pigeon-inspired optimization (PIO) optimization is an effective way to optimize the U-SSFSW process of Al/Mg dissimilar alloys.	[98]
AZ31B/ 6061-T6, 3	1. 1000 2. 60 3. AS 4. U-SSFSW	I. 95 vs 125 II. 152.4 vs 135 III. 1.9 vs 1.5	UVaFSW changed the fracture location from Mg side interface to Al side interface.	[106]

the IMCs thickness using SEM and EDS analysis at three different levels through the thickness, crown region (CR), mid-region (MR), and bottom region (BR) of the joints, as indicated on the transverse cross-section macrograph in Fig. 54. The SEM micrographs and their corresponding EDS analysis for the FSWed and UVaFSWed joints produced using 800 rpm and 100 mm/min are presented in Fig. 54 as an example of the best tensile properties joint. In terms of the IMCs layer for the FSW joint showed 9.4, 5.0, and 2.8 μm for CR, MR, and BR, respectively. On the other hand, the UVaFSW joint showed IMC layer thickness of about 4.4, 2.1 and 1.4 μm for CR, MR, and BR, respectively, as can be observed from Fig. 54. The main IMCs were found to be Al_3Mg_2 based on the EDS analysis. This results confirm the significant effect of UVaFSW in the suppression of IMC formation and the reduction in its thickness [115]. Table 12 presents the IMC layer thickness for the FSW and UVaFSW joints at different positions through the thickness and the FSW parameters.

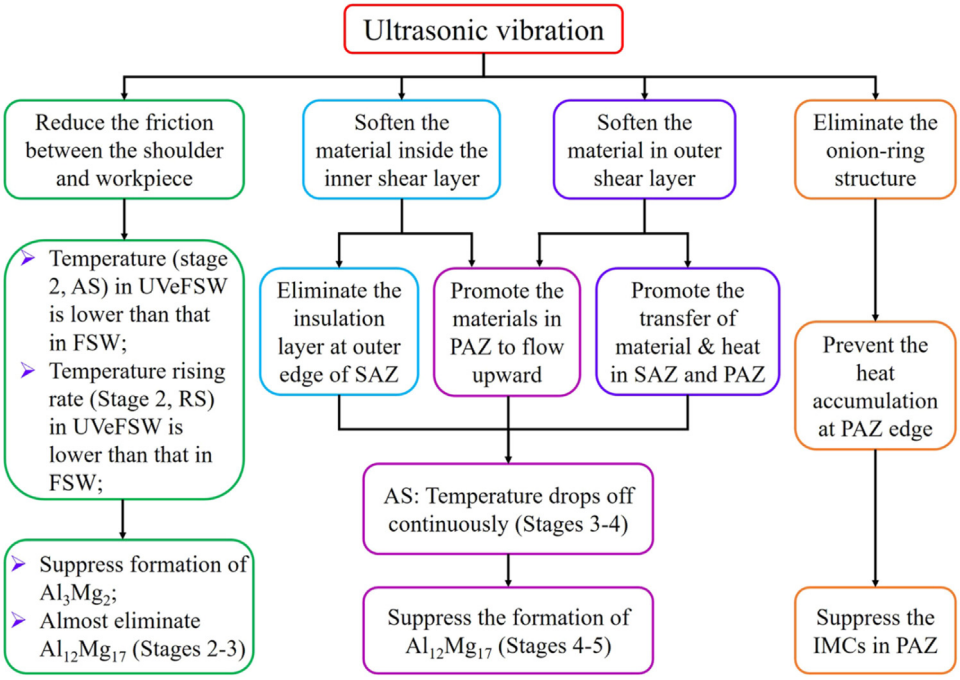

Fig. 58. Schematic of the effects of ultrasonic vibration on the material flow, thermal cycles, and subsequent suppression of IMCs formation [160]. SAZ and PAZ stand for shoulder-affected zone and pin-affected zone, respectively.

Significant reduction in the IMC thickness can be observed at the weld crown and less reduction at the weld bottom. On the other hand, they reported that increasing the rotation rate at constant welding speed increases the IMC layer thickness. Based on this reduction in the IMC layer thickness, the joint strength has increased to 160.5 MPa with a joint efficiency of about 71% compared to 58% in the case of its FSW counterpart. The UVaFSW results in a fragmentation of the IMC layer through the enhancement of material flow and the intermixing of dissimilar alloys across their interfaces [107]. Similar results were reported by Zhao et al. [92] in their investigation of the tensile strength and toughness of the different parts of the AZ31B-H24/AA6061-T6 UVaFSWed joint. They reported that the upper part of the weld had the best strength due to enhanced materials mixing/interlocking and a small amount of IMCs. However, the lower part was the weakest part due to the poor materials mixing/interlocking and a large amount of IMCs. The application of ultrasonic vibration can improve the tensile strength of each part of the welds, but the improvement rate of tensile strength is greater for the upper and middle parts of the welds. The key factor in the application of UVaFSW is the improved material mixing/mechanical interlocking in the welds as a basis for obtaining higher joint strength, and the thinner intermetallic compound layer is the key to the better toughness of the joint [92]. It can be noted that the application of UVaFSW has improved the tensile strength and changed the fracture position from being at the center of the NG zone (Fig. 55 (a)) to the interface between the NG and the Mg base material (Fig. 55 (b)). This implies the fragmentation of the IMCs inside the NG and the improved mixed materials induced by the ultrasonic vibration.

The ultrasonic vibration assistance during FSW provides a better flow and intermixing of base materials and, thus, a more homogeneous intercalated (successive) lamellar structure in the stir zone and significantly reduces the layer thickness of the brittle intermetallic phase formed in this region. For example, Liu et al. [105,106] performed the welding process assisted by ultrasonic vibration in order to prevent or reduce the formation of continuous intermetallic phase in FSW of AA6061 and AZ31 sheets, which adversely affects the welding quality and determined that the ultrasonic vibration led to the breakage and fragmentation of the continuous intermetallic phase within the thermomechanical affected zone (TMAZ). As a result, they reported that the joint produced with the ultrasonic vibration-assisted FSW showed higher tensile strength than the joints produced with conventional FSW.

Similarly, Ji et al. [104] also obtained dissimilar AA6061-AZ31 joints by ultrasonic vibration-assisted FSW, and as can be seen from Fig. 56, better material flow in the weld zone was achieved by the ultrasonic vibration assistance resulting in a better mixing of the two base materials and an onion-ring-shaped intercalated lamellar structure was formed in the stir zone. Gester et al. [159] also successfully joined die-cast aluminum alloy EN AC-48000 (AlSi12CuNiMg) and magnesium alloy AZ91 (MgAl9Zn1) plates with ultrasonic-assisted FSW, and with ultrasonic vibration assistance, both base materials were mixed better in the stir zone (Fig. 57) and they stated that the joint obtained in this way showed higher tensile strength (221% of that of the joint fabricated by conven-

tional FSW). In addition to these, in the study conducted by Lv et al. [155,90], Al_3Mg_2 + $Al_{12}Mg_{17}$ intermetallic phases were formed in the stir zone of Al/Mg joints obtained by conventional FSW without ultrasonic assistance. On the other hand, ultrasonic assistance in conjunction with a tool offset on the Mg-alloy side during FSW resulted in the formation of only thin Al_3Mg_2 intermetallic phase in the stir zone; as a result, the joint strength increased. Table 13 summarizes the materials, FSW parameters, and mechanical properties of dissimilar FSWed Mg/Al alloys using UVaFSW.

These results show that the ultrasonic vibration assistance applied during FSW effectively reduces the thickness of the intermetallic phase formed in the stir zone, improving the mechanical properties of the welded joint. However, it should be considered that any additional process to improve the welding quality, such as underwater FSW, external cooling, or ultrasonic vibration assistance, requires additional welding equipment and inevitably increases the manufacturing cost. Fig. 58 summarizes the effects of UVaFSW on the dissimilar Mg/Al FSW.

6. Conclusions and future research trends

Joining the two lightweight magnesium and aluminum alloys is essential for a wide range of applications. This necessitates achieving high-quality joints. The conventional FSW more likely results in the formation of the brittle intermetallics Al_3Mg_2 and $Al_{12}Mg_{17}$ in thick and continuous layers, severely deteriorating the mechanical properties and resulting in cracking sometimes immediately after FSW. Therefore, plenty of studies have been conducted in applying various assisting strategies over the last decade to achieve sustainable and high-quality Mg/Al dissimilar joints. This review is a trial to summarize and discuss the latest effort in this topic based on the discussed studies, the following conclusions and future trends can be outlined.

6.1. Conclusions

- The FSW parameters are the primary factor for controlling the dissimilar Mg/Al joint quality. The optimization and selection of each parameter are critical as they affect two main processes controlling the Mg/Al joint quality. First is the interdiffusion between Mg and Al, which increases with the increase of rotation rate and the decrease of the welding speed. Second is the material mixing and flow, which are essential for obtaining defect-free joints.
- The Mg/Al plate positions relative to the FSW tool are an important parameter, and based on the discussed results, it has been found that placing the Mg plate at the advancing side (AS) is preferable for reducing the temperature and hence suppressing the IMCs formation, especially if carefully associated with a proper tool offset to the AS.
- Among the metallic interlayer materials summarized in this review, the use of the Zn interlayer is found to be significantly effective in enhancing the dissimilar Mg/Al joint quality through the prevention of Mg/Al interdiffusion, which reduces the formation of the brittle intermetallics (Al_3Mg_2 and $Al_{12}Mg_{17}$) and instead forming the less harmful Mg_2Zn IMCs. This can be considered the most practical strategy in terms of industrial applicability and cost-effectiveness. It can be easily applied for butt welding of a wide range of plate thicknesses.
- The main effect of the Zn interlayer in enhancing the Mg/Al joint quality is based on metallurgical bonding rather than mechanical interlocking. This can probably be attributed to the high solubility of Zn in Al and Mg, especially at high temperatures.
- The use of external heating with electric-current-assisted FSW (EAFSW) gave promising results in improved tensile strength and elimination of defects of Mg/Al joints. On the other hand, the FSW parameters need to be optimized for this strategy. The main advantage of this method can be the ease of applicability.
- Among the generated heat strategies summarized, the submerged FSW (SFSW) effectively controls heat generation. This can effectively enhance the dissimilar materials' mixing and flow, reduce the intermetallic layer formation, and improve the joint quality. However, its applicability is quite limited, especially for industrial-level applications. Its effect is mainly based on lowering the welding temperature to a level that limits the formation of the brittle IMCs.
- Ultrasonic vibration effectively improves the Mg/Al joint quality by enhancing material mixing/mechanical interlocking, reducing the IMCs layer thickness, and fragmentation of IMCs layers and their interruption across dissimilar interfaces. The limitation of this strategy is that it does not eliminate the formation of the brittle IMCs, and its effect in reducing IMC layer thickness is high near the top surface and decreases to the bottom regions.
- The factors for achieving high Mg/Al joint strength and quality are (1) Suppressing the brittle IMCs formation, reducing their thickness, fragmentation, and interruption at the dissimilar interfaces. (2) Obtaining enhanced mixing and mechanical interlocking within a joint free from micro and macro defects.

6.2. Trends for future research

- More research is needed in using machine learning optimization techniques to optimize the FSW parameters and precisely predict mechanical properties. This can save time and effort in obtaining high-quality Mg/Al joints.
- Most available studies using the Zn interlayer are of small plate thicknesses up to 4 mm; its applicability and optimization for thick sections are highly needed and worth investigating.
- Very few studies are available in the literature on the use of EAFSW in dissimilar Mg/Al joining, although the enhancement achieved through EAFSW looks superior to any other strategy. Thus, it is worth more effort and investigation.
- Bobbin tool FSW (BTFSW) is a variant that allows an even heat distribution through the thickness of the joint

and can be a good candidate for FSW of dissimilar Mg/Al alloys. However, BTFSW parameters optimization is critical, especially since the process has two shoulders, and this can result in excessive heat generation.

- It is evident that the dissimilar FSW of Mg and Al alloys has reached a mature status by applying one or two of the assisting strategies. Thus, focusing on the developed joints' life cycle in terms of fatigue life and corrosion is essential because of the lack of studies in these areas confirmed with both the scientometric and conventional reviews carried out in this work.

Declaration of competing interest

None.

Acknowledgment

This study was sponsored by the Prince Sattam bin Abdulaziz University via project number 2023/RV/018.

References

[1] M.M.Z. Ahmed, M.M.E. Seleman, D. Fydrych, G. Cam, Materials 16 (2023) 2971 (Basel), doi:10.3390/ma16082971.
[2] G. Çam, V. Javaheri, A. Heidarzadeh, J. Adhes. Sci. Technol. 37 (2) (2023) 162–194, doi:10.1080/01694243.2022.2028073.
[3] S. Shankar, K.P. Mehta, S. Chattopadhyaya, P. Vilaca, Mater. Chem. Phys. 288 (2022), doi:10.1016/j.matchemphys.2022.126371.
[4] N. Kashaev, V. Ventzke, G. Çam, J. Manuf. Process. 36 (November) (2018) 571–600, doi:10.1016/j.jmapro.2018.10.005.
[5] G. Çam, G. İpekoğlu, Int. J. Adv. Manuf. Technol. 91 (5–8) (2017) 1851–1866, doi:10.1007/s00170-016-9861-0.
[6] V.P. Singh, S.K. Patel, A. Ranjan, B. Kuriachen, J. Mater. Res. Technol. 9 (3) (2020) 6217–6256 WE - Science Citation Index Expanded (SCI-EXPANDED), doi:10.1016/j.jmrt.2020.01.008.
[7] A. Heidarzadeh, S. Mironov, R. Kaibyshev, G. Çam, A. Simar, A. Gerlich, et al., Prog. Mater. Sci. 117 (October 2020) (2021) 100752, doi:10.1016/j.pmatsci.2020.100752.
[8] G. Çam, Int. Mater. Rev. 56 (1) (2011) 1–48, doi:10.1179/095066010X12777205875750.
[9] Y.C. Chen, K. Nakata, Mater. Des. 30 (3) (2009) 469–474 Mar., doi:10.1016/j.matdes.2008.06.008.
[10] A. Eyvazian, A. Hamouda, F. Tarlochan, H.A. Derazkola, F. Khodabakhshi, J. Mater. Res. Technol. 9 (3) (2020) 3767–3781, doi:10.1016/j.jmrt.2020.02.003.
[11] S. Ji, X. Cui, L. Ma, H. Liu, Y. Zuo, Z. Zhang, Acta Metall. Sin. (Engl. Lett.) 36 (4) (2023) 552–572, doi:10.1007/s40195-022-01512-5.
[12] A. Ghiasvand, E. Ranjbarnodeh, S.E. Mirsalehi, J. Mater. Res. Technol. 23 (2023) 6023–6038, doi:10.1016/j.jmrt.2023.02.222.
[13] J.J. Zhao, C.S. Wu, L. Shi, H. Su, J. Mater. Sci. Technol. 139 (2023) 31–46 WE - Science Citation Index Expanded (SCI-EXPANDED), doi:10.1016/j.jmst.2022.08.025.
[14] N.A. Muhammad, P.H. Geng, C.S. Wu, N.S. Ma, Int. J. Mach. Tools Manuf. 186 (2023), doi:10.1016/j.ijmachtools.2023.104004.
[15] P.J.L. Kumar, P. Sevvel, T.G. Loganathan, D. Prakash, Mater. Res. Express 10 (2) (2023) WE - Science Citation Index Expanded (SCI-EXPANDED, doi:10.1088/2053-1591/acbbbb.
[16] M. Sajed, J.W.G. Guerrero, H.A. Derazkola, Appl. Sci. 13 (3) (2023) WE - Science Citation Index Expanded (SCI-EXPANDED), doi:10.3390/app13031563.
[17] M.M. Joshi, A. Ubale, 3C Empresa 12 (1) (2023) 346–359 WE - Emerging Sources Citation Index (ESCI), doi:10.17993/3cemp.2023.120151.346-359.
[18] M.J. Tan, C.S. Wu, L. Shi, Materials 16 (1) (2023) (Basel)WE - Science Citation Index Expanded (SCI-EXPANDED), doi:10.3390/ma16010051.
[19] M.J. Tan, C.S. Wu, H. Su, Weld. World 67 (2) (2023) 373–384, doi:10.1007/s40194-022-01429-8.
[20] M.M.Z. Ahmed, M.A.A. Abdul-Maksoud, M.M. El-Sayed Seleman, A.M.A. Mohamed, J. Eng. Res. 9 (2021) 1–2, doi:10.36909/JER.11367.
[21] M.M.Z. Ahmed, N. Jouini, B. Alzahrani, M.M.E.S. Seleman, M. Jhaheen, Metals 11 (2) (2021) (Basel), doi:10.3390/met11020330.
[22] L. Liu, Welding and Joining of Magnesium Alloys to Aluminum Alloys, Woodhead Publishing Limited, 2010 no. 2008, doi:10.1533/9780857090423.1.38.
[23] A. Kirby, Publications 11 (1) (2023) 10.
[24] A. Perianes-Rodriguez, L. Waltman, N.J. Van Eck, J. Informetr. 10 (4) (2016) 1178–1195.
[25] K. Singh, G. Singh, H. Singh, J. Magnes. Alloy. 6 (4) (2018) 399–416, doi:10.1016/j.jma.2018.06.001.
[26] B.R. Sunil, G.P.K. Reddy, A.S.N. Mounika, P.N. Sree, P.R. Pinneswari, I. Ambica, R.A. Babu, P. Amarnadh, J. Magnes. Alloy. 3 (4) (2015) 330–334 WE - Emerging Sources Citation Index (ESCI), doi:10.1016/j.jma.2015.10.002.
[27] S. Ugender, J. Magnes. Alloy. 6 (2) (2018) 205–213, doi:10.1016/j.jma.2018.05.001.
[28] K. Singh, G. Singh, H. Singh, J. Magnes. Alloy. 6 (3) (2018) 292–298, doi:10.1016/j.jma.2018.05.004.
[29] K. Mroczka, S. Dymek, W. Aleksandra, C. Hamilton, Materials 16 (2023) 3953 (Basel).
[30] S. Mironov, T. Onuma, Y.S. Sato, H. Kokawa, Acta Mater. 100 (2015) 301–312, doi:10.1016/j.actamat.2015.08.066.
[31] U.F.H.R. Suhuddin, S. Mironov, Y.S. Sato, H. Kokawa, C. Lee, Acta Mater. 57 (18) (2009) 5406–5418, doi:10.1016/j.actamat.2009.07.041.
[32] F. Badkoobeh, H. Mostaan, M. Rafiei, H.R. Bakhsheshi-Rad, F. Berto, Materials 14 (21) (2021) 15–17 (Basel), doi:10.3390/ma14216726.
[33] L. Xie, X. Zhu, Y. Fan, W. Sun, P. Wang, C. Jiang, X. Xiao, S. Yang, Y. Song, Materials 15 (1) (2022) 1–16 (Basel), doi:10.3390/ma15010023.
[34] U.K. Singh, A.K. Dubey, Mater. Corros. (February) (2023) 1217–1232, doi:10.1002/maco.202313798.
[35] M.N. Borse, R. Bauri, S. Shankar, Mater. Sci. Eng. A 879 (December 2022) (2023) 145274, doi:10.1016/j.msea.2023.145274.
[36] Y.S. Khan, M.H. Abidi, W. Malik, N.F. Lone, M.K. Aboudaif, M.K. Mohammed, Materials 16 (14) (2023) (Basel), doi:10.3390/ma16144902.
[37] K. Moiduddin, A.N. Siddiquee, M.H. Abidi, S.H. Mian, M.K. Mohammed, Materials 14 (22) (2021) 1–11 (Basel), doi:10.3390/ma14226924.
[38] Z. Mengran, S. Yufeng, M. Yoshiaki, U. Kohsaku, F. Hidetoshi, J. Magnes. Alloy. 8 (4) (2020) 1071–1083, doi:10.1016/j.jma.2020.05.015.
[39] A. Heidarzadeh, S. Mironov, R. Kaibyshev, G. Çam, A. Simar, A. Gerlich, et al., Prog. Mater. Sci. 117 (September 2020) (2021) 100752, doi:10.1016/j.pmatsci.2020.100752.
[40] J. Zhang, Y. Zhang, X. Chen, Z. Li, G. Huang, F. Pan, Mater. Sci. Eng. A 882 (May) (2023) 145444, doi:10.1016/j.msea.2023.145444.
[41] G. Çam, S. Mistikoglu, J. Mater. Eng. Perform. 23 (6) (2014) 1936–1953, doi:10.1007/s11665-014-0968-x.
[42] P. Dong, F. Lu, J.K. Hong, Z. Cao, Sci. Technol. Weld. Join. 6 (5) (2001) 281–287 Oct., doi:10.1179/136217101101538884.
[43] R.S. Mishra, Z.Y. Ma, Mater. Sci. Eng. R Rep. 50 (1–2) (2005) 1–78, doi:10.1016/j.mser.2005.07.001.
[44] R. Nandan, T. DebRoy, H.K.D.H. Bhadeshia, Prog. Mater. Sci. 53 (6) (2008) 980–1023, doi:10.1016/j.pmatsci.2008.05.001.
[45] P.L. Threadgill, Sci. Technol. Weld. Join. 12 (4) (2007) 357–360.
[46] P. L. Threadgill, A. J. Leonard, H. R. Shercliff, and P. J. Withers, vol. 54, no. 2, pp. 49–93, 2009, doi: 10.1179/174328009X411136.
[47] A. Yazdipour, A. Shafiei M, K. Dehghani, Mater. Sci. Eng. A 527 (1–2) (2009) 192–197, doi:10.1016/j.msea.2009.08.040.

[48] G. İpekoğlu, G. Çam, Metall. Mater. Trans. A Phys. Metall. Mater. Sci. 45 (7) (2014) 3074–3087, doi:10.1007/s11661-014-2248-7.
[49] I. Kalemba-Rec, M. Kopyściański, D. Miara, K. Krasnowski, Int. J. Adv. Manuf. Technol. 97 (5–8) (2018) 2767–2779, doi:10.1007/s00170-018-2147-y.
[50] M.M.Z. Ahmed, S. Ataya, M.M. El-Sayed Seleman, A.M.A. Mahdy, N.A. Alsaleh, E. Ahmed, Metals 11 (1) (2021) 1–20 (Basel), doi:10.3390/met11010068.
[51] J.F. Guo, H.C. Chen, C.N. Sun, G. Bi, Z. Sun, J. Wei, Mater. Des. 56 (2014) 185–192, doi:10.1016/j.matdes.2013.10.082.
[52] J.H. Ouyang, R. Kovacevic, J. Mater. Eng. Perform. 11 (1) (2002) 51–63, doi:10.1361/105994902770344394.
[53] G. Çam, G. Ipekoğlu, H.T. Serindağ, Sci. Technol. Weld. Join. 19 (8) (2014) 715–720, doi:10.1179/1362171814Y.0000000247.
[54] R. Beygi, M. Zarezadeh Mehrizi, A. Akhavan-Safar, S. Mohammadi, L.F.M. da Silva, Lubricants 11 (2) (2023), doi:10.3390/lubricants11020059.
[55] H. Shi, K. Chen, Z.Y. Liang, F.B. Dong, T.W. Yu, X.P. Dong, L.T. Zhang, A.D. Shan, J. Mater. Sci. Technol. 33 (4) (2017) 359–366 WE - Science Citation Index Expanded (SCI-EXPANDED), doi:10.1016/j.jmst.2016.05.006.
[56] Y.S. Sato, S.H.C. Park, M. Michiuchi, H. Kokawa, Scr. Mater. 50 (9) (2004) 1233–1236 WE - Science Citation Index Expanded (SCI-EXPANDED), doi:10.1016/j.scriptamat.2004.02.002.
[57] B.L. Fu, G.L. Qin, F. Li, X.M. Meng, J.Z. Zhang, C.S. Wu, J. Mater. Process. Technol. 218 (2015) 38–47 WE - Science Citation Index Expanded (SCI-EXPANDED), doi:10.1016/j.jmatprotec.2014.11.039.
[58] S.K. Raval, K.B. Judal, Mater. Today Proc. 22 (2020) 2665–2675 no. 2nd International Conference on Materials Manufacturing and Modelling (ICMMM)WE-Conference Proceedings Citation In, doi:10.1016/j.matpr.2020.03.398.
[59] M. Kumar, A. Das, R. Ballav, Mater. Today Proc. 26 (2020) 2123–2129, doi:10.1016/j.matpr.2020.02.458.
[60] L.H. Shah, N.H. Othman, A. Gerlich, Sci. Technol. Weld. Join. 23 (3) (2018) 256–270 WE - Science Citation Index Expanded (SCI-EXPANDED), doi:10.1080/13621718.2017.1370193.
[61] R. Beygi, A.A. Talkhabi, M.Z. Mehrizi, E.A.S. Marques, R.J.C. Carbas, L.F.M. da Silva, Metals 13 (6) (2023) 1027 (Basel), doi:10.3390/met13061027.
[62] V. Firouzdor, S.D. Kou, Metall. Mater. Trans. A Phys. 41A (12) (2010) 3238–3251 WE - Science Citation Index Expanded (SCI-EXPANDED), doi:10.1007/s11661-010-0366-4.
[63] P.Q. Li, G.Q. You, H.Y. Wen, W. Guo, X. Tong, S. Li, J. Mater. Process. Technol. 264 (2019) 55–63 WE - Science Citation Index Expanded (SCI-EXPANDED), doi:10.1016/j.jmatprotec.2018.08.044.
[64] M.A. Mofid, A. Abdollah-zadeh, F.M. Ghaini, Mater. Des. 36 (2012) 161–167 WE - Science Citation Index Expanded (SCI-EXPANDED), doi:10.1016/j.matdes.2011.11.004.
[65] Coelho, R. S., A. Kostka, H. Pinto, A. Rothkirch, and J. Pyzalla, A. R., Dos Santos, Adv. X-Ray Anal., vol. 52, pp. 360–367..
[66] Y.J. Kwon, I. Shigematsu, N. Saito, Mater. Lett. 62 (23) (2008) 3827–3829 WE - Science Citation Index Expanded (SCI-EXPANDED), doi:10.1016/j.matlet.2008.04.080.
[67] N. Yamamoto, J.S. Liao, S. Watanabe, K. Nakata, Mater. Trans. 50 (12) (2009) 2833–2838 WE - Science Citation Index Expanded (SCI-EXPANDED), doi:10.2320/matertrans.M2009289.
[68] B.L. Prasad, G. Neelaiah, M.G. Krishna, S.V.V. Ramana, K.S. Prakash, G. Sarika, G.P.K. Reddy, R. Dumpala, B.R. Sunil, J. Magnes. Alloy. 6 (1) (2018) 71–76 WE - Science Citation Index Expanded (SCI-EXPANDED), doi:10.1016/j.jma.2017.12.004.
[69] P. Venkateswaran, A.P. Reynolds, Mater. Sci. Eng. A Struct. Mater. Prop. Microstruct. Process. 545 (2012) 26–37 WE - Science Citation Index Expanded (SCI-EXPANDED), doi:10.1016/j.msea.2012.02.069.
[70] K. Torabi, R. Beygi, G. Eisaabadi Bozchaloei, L.F.M. da Silva, Appl. Sci. 13 (12) (2023) 7133, doi:10.3390/app13127133.
[71] R. Beygi, H. Pouraliakbar, K. Torabi, B.G. Eisaabadi, V. Fallah, S.K. Kim, R. Shi, L.F.M. da Silva, J. Manuf. Process. 70 (2021) 152–162, doi:10.1016/j.jmapro.2021.08.049.
[72] V. Firouzdor, S. Kou, Metall. Mater. Trans. A Phys. Metall. Mater. Sci. 41A (11) (2010) 2914–2935 WE - Science Citation Index Expanded (SCI-EXPANDED), doi:10.1007/s11661-010-0340-1.
[73] T. Morishige, A. Kawaguchi, M. Tsujikawa, M. Hino, T. Hirata, K. Higashi, Mater. Trans. 49 (5) (2008) 1129–1131 WE - Science Citation Index Expanded (SCI-EXPANDED), doi:10.2320/matertrans.MC200768.
[74] M. Simoncini, A. Forcellese, Mater. Des. 41 (2012) 50–60 WE - Science Citation Index Expanded (SCI-EXPANDED), doi:10.1016/j.matdes.2012.04.057.
[75] P. Pourahmad, M. Abbasi, Trans. Nonferr. Met. Soc. China 23 (5) (2013) 1253–1261 WE - Science Citation Index Expanded (SCI-EXPANDED), doi:10.1016/S1003-6326(13)62590-X.
[76] J. Mohammadi, Y. Behnamian, A. Mostafaei, H. Izadi, T. Saeid, A.H. Kokabi, A.P. Gerlich, Mater. Charact. 101 (2015) 189–207 WE - Science Citation Index Expanded (SCI-EXPANDED), doi:10.1016/j.matchar.2015.01.008.
[77] A. A. Mclean, G. L. F. Powell, I. H. Brown, V. M. Linton, G. L. F. Powell, I. H. Brown, V. M. L. Friction, A. A. Mclean, G. L. F. Powell, I. H. Brown, and V. M. Linton, vol. 1718, pp. 4–7, 2013, doi: 10.1179/136217103225009134.
[78] A. Kostka, R.S. Coelho, J. dos Santos, A.R. Pyzalla, Scr. Mater. 60 (11) (2009) 953–956 WE - Science Citation Index Expanded (SCI-EXPANDED), doi:10.1016/j.scriptamat.2009.02.020.
[79] J.C. Yan, Z.W. Xu, Z.Y. Li, L. Li, S.Q. Yang, Scr. Mater. 53 (5) (2005) 585–589 WE - Science Citation Index Expanded (SCI-EXPANDED), doi:10.1016/j.scriptamat.2005.04.022.
[80] Y. Xu, L. Ke, Y. Mao, J. Sun, Y. Duan, L. Yu, J. Magnes. Alloy. (xxxx) (2022), doi:10.1016/j.jma.2022.01.007.
[81] S. Kumar, C.S. Wu, J. Alloys Compd. 827 (2020) WE - Science Citation Index Expanded (SCI-EXPANDED), doi:10.1016/j.jallcom.2020.154343.
[82] S.A. Khodir, T. Shibayanagi, Mater. Trans. 48 (9) (2007) 2501–2505 WE - Science Citation Index Expanded (SCI-EXPANDED), doi:10.2320/matertrans.MRA2007093.
[83] A. Dorbane, B. Mansoor, G. Ayoub, V.C. Shunmugasamy, A. Imad, Mater. Sci. Eng. A Struct. Mater. Prop. Microstruct. Process. 651 (2016) 720–733 WE - Science Citation Index Expanded (SCI-EXPANDED), doi:10.1016/j.msea.2015.11.019.
[84] V. Paradiso, F. Rubino, P. Carlone, G.S. Palazzo, in: Proceedings of the 17th International Conference on Sheet Metal (SHEMET17), 183, SA, Italy, Univ Salerno, Dept Ind Engn DIIN, 2017, pp. 239–244, doi:10.1016/j.proeng.2017.04.028. I-84084 FiscianoWE - Conference Proceedings Citation Index - Science (CPCI-S).
[85] Y. Yan, D.T. Zhang, C. Qiu, W. Zhang, Trans. Nonferr. Met. Soc. China 20 (SUPPL 2) (2010) S619–S623 WE-Science Citation Index Expanded (S,, doi:10.1016/S1003-6326(10)60550-X.
[86] M.D. Sameer, A.K. Birru, J. Magnes. Alloy. 7 (2) (2019) 264–271 WE - Science Citation Index Expanded (SCI-EXPANDED), doi:10.1016/j.jma.2018.09.004.
[87] A. Masoudian, A. Tahaei, A. Shakiba, F. Sharifianjazi, J.A. Mohandesi, Trans. Nonferr. Met. Soc. China 24 (5) (2014) 1317–1322 WE - Science Citation Index Expanded (SCI-EXPANDED, doi:10.1016/S1003-6326(14)63194-0.
[88] S. Malarvizhi, V. Balasubramanian, Mater. Des. 40 (2012) 453–460 WE - Science Citation Index Expanded (SCI-EXPANDED), doi:10.1016/j.matdes.2012.04.008.
[89] Z.Y. Liang, K. Chen, X.N. Wang, J.S. Yao, Q. Yang, L.T. Zhang, A.D. Shan, Metall. Mater. Trans. A Phys. Metall. Mater. Sci. 44A (8) (2013) 3721–3731 WE - Science Citation Index Expanded (SCI-EXPANDED), doi:10.1007/s11661-013-1700-4.
[90] X.Q. Lv, C.S. Wu, C.L. Yang, G.K. Padhy, J. Mater. Process. Technol. 254 (2018) 145–157 WE - Science Citation Index Expanded (SCI-EXPANDED), doi:10.1016/j.jmatprotec.2017.11.031.
[91] J. Xiaoqing, L. Yongyong, Y. Tao, C. Shujun, W. Lei, J. Wang, J. Manuf. Process. 76 (2022) 123–137, doi:10.1016/j.jmapro.2022.02.007.

[92] J.J. Zhao, C.S. Wu, H. Su, J. Manuf. Process. 65 (2021) 328–341, doi:10.1016/j.jmapro.2021.03.057.
[93] S. Kumar, C.S. Wu, S. Gao, Metall. Mater. Trans. A Phys. Metall. Mater. Sci. 51 (6) (2020) 2863–2881, doi:10.1007/s11661-020-05716-1.
[94] K.P.V Kumar, M. Balasubramanian, Mater. Today Proc. 22 (2020) 2883–2889 no. 2nd International Conference on Materials Manufacturing and Modelling (ICMMM). Anna Univ, Ctr Res, Chennai, Tamil Nadu, IndiaWE-Conference Proceedings Citation In.
[95] M. Regev, M. El Mehtedi, M. Cabibbo, G. Quercetti, D. Ciccarelli, S. Spigarelli, M. El Mehtedi, M. Cabibbo, G. Quercetti, D. Ciccarelli, S. Spigarelli, Metall. Mater. Trans. A Phys. Metall. Mater. Sci. 45A (2) (2014) 752–764 WE - Science Citation Index Expanded (SCI-EXPANDED), doi:10.1007/s11661-013-2034-y.
[96] M. Azizieh, A.S. Alavijeh, M. Abbasi, Z. Balak, H.S. Kim, Mater. Chem. Phys. 170 (2016) 251–260 WE - Science Citation Index Expanded (SCI-EXPANDED), doi:10.1016/j.matchemphys.2015.12.046.
[97] A.H. Elsheikh, Eng. Appl. Artif. Intell. 121 (June 2022) (2023) 105961, doi:10.1016/j.engappai.2023.105961.
[98] W. Hu, Z.W. Ma, S.D. Ji, Q. Song, M.F. Chen, W.H. Jiang, J. Mater. Sci. Technol. 53 (2020) 41–52 WE - Science Citation Index Expanded (SCI-EXPANDED), doi:10.1016/j.jmst.2020.01.069.
[99] S. Dharmalingam, K. Lenin, D. Srinivasan, Bull. Pol. Acad. Sci. Sci. 70 (1) (2022) WE - Science Citation Index Expanded (SCI-EXPANDED), doi:10.24425/bpasts.2022.140098.
[100] A.R.S. Essa, M.M.Z. Ahmed, A.R.K. Aboud, R. Alyamani, T.A. Sebaey, Materials 16 (10) (2023) (Basel), doi:10.3390/ma16103777.
[101] M.M. Krishnan, J. Maniraj, R. Deepak, K. Anganan, Mater. Today Proc. 5 (2018) 716–723 no. International Conference on Processing of Materials, Minerals and Energy (PMME). Kalaignar Karunanidhi Inst Technol, Coimbatore 641402, Tamil Nadu, IndiaWE - Conference Proceedings Citation Index - Science (CPCI-S), doi:10.1016/j.matpr.2017.11.138.
[102] A. D'Orazio, A. Forcellese, M. Simoncini, Neural Comput. Appl. 31 (11) (2019) 7211–7226 WE - Science Citation Index Expanded (SCI-EXPANDED), doi:10.1007/s00521-018-3562-6.
[103] Q. Song, H.R. Wang, S.D. Ji, Z.W. Ma, W.H. Jiang, M.F. Chen, J. Manuf. Process. 59 (2020) 750–759 WE - Science Citation Index Expanded (SCI-EXPANDED), doi:10.1016/j.jmapro.2020.10.037.
[104] S.D. Ji, X.C. Meng, Z.L. Liu, R.F. Huang, Z.W. Li, Mater. Lett. 201 (2017) 173–176 WE - Science Citation Index Expanded (SCI-EXPANDED), doi:10.1016/j.matlet.2017.05.011.
[105] Z.L. Liu, S.D. Ji, X.C. Meng, Int. J. Adv. Manuf. Technol. 97 (9–12) (2018) 4127–4136 WE - Science Citation Index Expanded (SCI-EXPANDED), doi:10.1007/s00170-018-2255-8.
[106] Z.L. Liu, X.C. Meng, S.D. Ji, Z.W. Li, L. Wang, J. Manuf. Process. 31 (2018) 552–559 WE - Science Citation Index Expanded (SCI-EXPANDED), doi:10.1016/j.jmapro.2017.12.022.
[107] X.C. Meng, Y.Y. Jin, S.D. Ji, D.J. Yan, J. Mater. Sci. Technol. 34 (10) (2018) 1817–1822 WE - Science Citation Index Expanded (SCI-EXPANDED), doi:10.1016/j.jmst.2018.02.022.
[108] M. Kumar, A. Das, R. Ballav, Mater. Today Commun. 35 (January) (2023) 105509, doi:10.1016/j.mtcomm.2023.105509.
[109] J.J. Zhao, C.S. Wu, L. Shi, J. Mater. Res. Technol. 17 (2022) 1–21, doi:10.1016/j.jmrt.2021.12.133.
[110] A. Abdollahzadeh, A. Shokuhfar, J.M. Cabrera, A.P. Zhilyaev, H. Omidvar, J. Manuf. Process. 34 (2018) 18–30 WE - Science Citation Index Expanded (SCI-EXPANDED), doi:10.1016/j.jmapro.2018.05.029.
[111] X.L. Zhong, Y. Zhao, J.H. Pu, K. Yan, H.M. Liang, S.M. Song, Phys. Met. Metallogr. 121 (13) (2020) 1309–1318 WE - Science Citation Index Expanded (SCI-EXPANDED), doi:10.1134/S0031918X20130190.
[112] S.K. Dewangan, M.K. Tripathi, M.K. Manoj, Met. Mater. Int. 28 (5) (2022) 1169–1183, doi:10.1007/s12540-021-00980-1.
[113] S.K. Dong, S. Lin, H. Zhu, C.J. Wang, Z.L. Cao, Sci. Technol. Weld. Join. 27 (2) (2022) 103–113, doi:10.1080/13621718.2021.2014742.
[114] U. Kumar, U. Acharya, S.C. Saha, B.S. Roy, Mater. Today Proc. 26 (2020) 2083–2088 no. 10th International Conference of Materials Processing and Characterization (ICMPC). Natl Inst Technol Agartala, Barjala 799046, Tripura, IndiaWE - Conference Proceedings Citation Index - Science (CPCI-S), doi:10.1016/j.matpr.2020.02.450.
[115] Y. Xu, L. Ke, Y. Mao, Q. Liu, J. Xie, H. Zeng, Materials 12 (7) (2019) (Basel), doi:10.3390/ma12172661.
[116] T.F. Huang, Z.Y. Zhang, J.L. Liu, S.H. Chen, Y.M. Xie, X.C. Meng, Y.X. Huang, L. Wan, Materials 15 (16) (2022) (Basel)WE - Science Citation Index Expanded (SCI-EXPANDED), doi:10.3390/ma15165520.
[117] S.D. Ji, R.F. Huang, X.C. Meng, L.G. Zhang, Y.X. Huang, J. Mater. Eng. Perform. 26 (5) (2017) 2359–2367 WE - Science Citation Index Expanded (SCI-EXPANDED), doi:10.1007/s11665-017-2640-8.
[118] P. Venkateswaran, Z.H. Xu, X.D. Li, A.P. Reynolds, J. Mater. Sci. 44 (15) (2009) 4140–4147 WE - Science Citation Index Expanded (SCI-EXPANDED), doi:10.1007/s10853-009-3607-4.
[119] K.P. Mehta, R. Patel, H. Vyas, S. Memon, P. Vilaca, Manuf. Lett. 23 (2020) 67–70 WE - Emerging Sources Citation Index (ESCI), doi:10.1016/j.mfglet.2020.01.002.
[120] T. Jiang, C.S. Wu, L. Shi, J. Manuf. Process. 74 (2022) 112–122, doi:10.1016/j.jmapro.2021.12.008.
[121] J. Verma, R.V Taiwade, C. Reddy, R.K. Khatirkar, Mater. Manuf. Process. 33 (3) (2018) 308–314 WE - Science Citation Index Expanded (SCI-EXPANDED), doi:10.1080/10426914.2017.1291957.
[122] G. Buffa, D. Baffari, A. Di Caro, L. Fratini, Sci. Technol. Weld. Join. 20 (4) (2015) 271–279 WE - Science Citation Index Expanded (SCI-EXPANDED), doi:10.1179/1362171815Y.0000000016.
[123] A.A. McLean, G.L.F. Powell, I.H. Brown, V.M. Linton, Sci. Technol. Weld. Join. 8 (6) (2003) 462–464 WE - Science Citation Index Expanded (SCI-EXPANDED), doi:10.1179/136217103225009134.
[124] A.C. Somasekharan, L.E. Murr, Mater. Charact. 52 (1) (2004) 49–64 WE - Science Citation Index Expanded (SCI-EXPANDED), doi:10.1016/j.matchar.2004.03.005.
[125] V. Firouzdor, S. Kou, Weld. J. 88 (11) (2009) 213S–224S WE-Science Citation Index Expanded (S.
[126] Z.L. Liu, S.D. Ji, X.C. Meng, J. Mater. Eng. Perform. 27 (3) (2018) 1404–1413 WE - Science Citation Index Expanded (SCI-EXPANDED), doi:10.1007/s11665-018-3216-y.
[127] B. Zheng, X.B. Hu, Q.Q. Lv, L. Zhao, D. Cai, S.J. Dong, Mater. Lett. 261 (2020) WE - Science Citation Index Expanded (SCI-EXPANDED), doi:10.1016/j.matlet.2019.127138.
[128] H.K. Sharma, K. Bhatt, K. Shah, U. Joshi, in: Proceedings of the 3rd International Conference on Innovations in Automation and Mechatronics Engineering (ICIAME), New Vv Nagar 388121, India, AD Patel Insitute Technol, Dept Mech Engn, 2016, pp. 566–572, doi:10.1016/j.protcy.2016.03.064. WE - Conference Proceedings Citation Index - Science (CPCI-S).
[129] S. Kumar, C.S. Wu, J. Mater. Res. Technol. 15 (2021) 4353–4369, doi:10.1016/j.jmrt.2021.10.065.
[130] S.K. Dewangan, P.N. Banjare, M.K. Tripathi, M.K. Manoj, Int. J. Adv. Manuf. Technol. 126 (9–10) (2023) 1–22, doi:10.1007/s00170-023-11348-7.
[131] N. Sharifi Asl, S.E. Mirsalehi, K. Dehghani, N.S. Asl, S.E. Mirsalehi, K. Dehghani, J. Manuf. Process. 38 (2019) 338–354, doi:10.1016/j.jmapro.2019.01.023.
[132] M. Tabasi, M. Farahani, M.K.B. Givi, M. Farzami, A. Moharami, Int. J. Adv. Manuf. Technol. 86 (1–4) (2016) 705–715 WE - Science Citation Index Expanded (SCI-EXPANDED), doi:10.1007/s00170-015-8211-y.
[133] A. Abdollahzadeh, A. Shokuhfar, J.M. Cabrera, A.P. Zhilyaev, H. Omidvar, J. Mater. Process. Technol. 263 (2019) 296–307 WE - Science Citation Index Expanded (SCI-EXPANDED), doi:10.1016/j.jmatprotec.2018.08.025.
[134] G.K. Padhy, C.S. Wu, S. Gao, Sci. Technol. Weld. Join. 20 (8) (2015) 631–649, doi:10.1179/1362171815Y.0000000048.
[135] W.S. Chang, S.R. Rajesh, C.K. Chun, H.J. Kim, J. Mater. Sci. Technol. 27 (3) (2011) 199–204 WE - Science Citation Index Expanded (SCI-EXPANDED), doi:10.1016/S1005-0302(11)60049-2.
[136] J. Luo, W. Chen, G. Fu, J. Mater. Process. Technol. 214 (12) (2014) 3002–3012, doi:10.1016/j.jmatprotec.2014.07.005.
[137] W. Chen, W.X. Wang, Z.P. Liu, X. Zhai, G.B. Bian, T.T. Zhang,

P. Dong, J. Alloys Compd. 861 (2021), doi:10.1016/j.jallcom.2020.157942.
[138] K.P. Mehta, P. Carlone, A. Astarita, F. Scherillo, F. Rubino, P. Vora, Mater. Sci. Eng. A Struct. Mater. Prop. Microstruct. Process. 759 (May) (2019) 252–261 WE - Science Citation Index Expanded (SCI-EXPANDED), doi:10.1016/j.msea.2019.04.120.
[139] Y. Zhao, S. Jiang, S.F. Yang, Z.P. Lu, K. Yan, Int. J. Adv. Manuf. Technol. 83 (1–4) (2016) 673–679 WE - Science Citation Index Expanded (SCI-EXPANDED), doi:10.1007/s00170-015-7624-y.
[140] A.S. Hammad, M.M.Z. Ahmed, H. Lu, A.B. El-Shabasy, B. Alzahrani, M.M. El-Sayed Seleman, Y. Zhang, A. El Megharbel, Proc. Inst. Mech. Eng. Part C J. Mech. Eng. Sci. 236 (12) (2022) 6665–6676, doi:10.1177/09544062211070716.
[141] M.M.Z. Ahmed, B.P. Wynne, W.M. Rainforth, P.L. Threadgill, Scr. Mater. 64 (2011) 45–48, doi:10.1016/j.scriptamat.2010.08.060.
[142] P. Mohamed Nishath, K. Sekar, Mater. Today Proc. 22 (2019) 1517–1523, doi:10.1016/j.matpr.2020.02.069.
[143] H. Lin, Y. Wu, S. Liu, X. Zhou, Mater. Charact. 141 (February) (2018) 74–85, doi:10.1016/j.matchar.2018.04.029.
[144] N.P. Patel, P. Parlikar, R. Singh Dhari, K. Mehta, M. Pandya, J. Manuf. Process. 47 (October) (2019) 98–109, doi:10.1016/j.jmapro.2019.09.020.
[145] N. Xu, Q.N. Song, Y.F. Bao, J. Alloys Compd. 834 (2020) 155052, doi:10.1016/j.jallcom.2020.155052.
[146] N. Xu, R. Ueji, Y. Morisada, H. Fujii, Mater. Des. 56 (2014) 20–25, doi:10.1016/j.matdes.2013.10.076.
[147] F. Rui-dong, S. Zeng-qiang, S. Rui-cheng, L. Ying, L. Hui-Jie, L. Lei, Mater. Des. 32 (10) (2011) 4825–4831, doi:10.1016/j.matdes.2011.06.021.
[148] M.A. Mofid, A. Abdollah-zadeh, C.H. Gur, Int. J. Adv. Manuf. Technol. 71 (5–8) (2014) 1493–1499 WE - Science Citation Index Expanded (SCI-EXPANDED), doi:10.1007/s00170-013-5565-x.
[149] S. Kumar, C. Wu, J. Harbin Inst. Technol. (New Ser.) 24 (6) (2017), doi:10.11916/j.ISSN. 105-9113.17065.
[150] L. Shi, J. Chen, C.S. Wu, L. Fu, Sci. Technol. Weld. Join. 26 (5) (2021) 363–370 Jul., doi:10.1080/13621718.2021.1917748.
[151] Y. Hu, H. Liu, S. Du, Mater. Sci. Eng. A 804 (2021) 140587, doi:10.1016/j.msea.2020.140587.
[152] J. You, Y. Zhao, C. Dong, Y. Su, J. Mater. Process. Technol. 311 (August 2022) (2023) 117812, doi:10.1016/j.jmatprotec.2022.117812.
[153] T. Liu, S. Gao, W. Ye, L. Shi, S. Kumar, J. Qiao, J. Mater. Res. Technol. 25 (2023) 5096–5109, doi:10.1016/j.jmrt.2023.06.251.
[154] S. Kumar, W. Ding, Z. Sun, and C. S. Wu, pp. 1269–1284, 2018.
[155] X.Q. Lv, C.S. Wu, G.K. Padhy, Mater. Lett. 203 (2017) 81–84 WE - Science Citation Index Expanded (SCI-EXPANDED), doi:10.1016/j.matlet.2017.05.090.
[156] T. Wang, C.S. Wu, L. Shi, Sci. Technol. Weld. Join. 27 (5) (2022) 398–405, doi:10.1080/13621718.2022.2055291.
[157] S. Kumar, C.S. Wu, Mater. Today Proc. 5 (2018) 18142–18151 no. 8th International Conference on Materials Processing and Characterization (ICMPC). Shandong Univ, MOE Key Lab Liquid Solid Struct Evolut & Mat Proc, Inst Mat Joining, Jinan 250061, Shandong, Peoples R ChinaWE - Conference Proceedings Citation Index - Science (CPCI-S), doi:10.1016/j.matpr.2018.06.150.
[158] B. Strass, G. Wagner, C. Conrad, B. Wolter, S. Benfer, W. Fuerbeth, Adv. Mater. Res. 966–967 (2014) 521–535, doi:10.4028/www.scientific.net/AMR.966-967.521.
[159] A. Gester, M. Thoma, G. Wagner, B. Strass, B. Wolter, S. Benfer, W. Furbeth, Weld. World 63 (5) (2019) 1173–1186 WE - Science Citation Index Expanded (SCI-EXPANDED), doi:10.1007/s40194-019-00767-4.
[160] X.Q. Lv, C.S. Wu, Z. Sun, Metall. Mater. Trans. A Phys. 53 (4) (2022) 1572–1584, doi:10.1007/s11661-022-06621-5.